Transition Metal and Main Group Complexes Stabilized by Dispersion Energy Donor (DED) Ligand Derivatives of 1-bromo-2,4,6-tricyclohexylbenzene
AND
Ni(I) and Ni(II) Bis(trimethylsilyl)amides Obtained in Pursuit of the Elusive Structure of $Ni\{N(SiMe_3)_2\}_2$

By

CONNOR P. MC LOUGHLIN
DISSERTATION

Submitted in partial satisfaction of the requirements for the degree of

DOCTOR OF PHILOSOPHY

in

CHEMISTRY

in the

OFFICE OF GRADUATE STUDIES

of the

UNIVERSITY OF CALIFORNIA

DAVIS

Approved:

Philip P. Power, Chair

Jesús M. Velázquez

Louise A. Berben

Committee in Charge
2024

Table of Contents

Acknowledgement iii
Abstract iv
Chapter 1. General Introduction 1
Chapter 2. Mn(II), Fe(II), and Co(II) Aryloxides: Steric and Dispersion Effects and the Thermal Rearrangement of a Cobalt Aryloxide to a Co(II) Semiquinone Complex 4
- **2.1** Abstract 4
- **2.2** Introduction 5
- **2.3** Experimental 7
- **2.4** Results and Discussion 12
- **2.5** Conclusion 25

Chapter 3. Rearrangement of a Ge(II) aryloxide to yield a new Ge(II) oxo-cluster $[Ge_6(\mu_3\text{-}O)_4(\mu_2\text{-}OC_6H_2\text{-}2,4,6\text{-}Cy_3)_4](NH3)_{0.5}$: main group aryloxides of Ge(II), Sn(II), and Pb(II) $[M(OC_6H_2\text{-}2,4,6\text{-}Cy_3)_2]_2$ (Cy = cyclohexyl) 35
- **3.1** Abstract 35
- **3.2** Introduction 36
- **3.3** Results and Discussion 37
- **3.4** Conclusion 51
- **3.5** Experimental 51

Chapter 4. Dispersion Energy Donor Ligand Supports the Isolation of Ge(II), Sn(II), and Lewis-Base Free Pb(II) Arylthiolate Dimers $\{M(SC_6H_2\text{-}2,4,6\text{-}Cy_3)_2\}_2$ (M = Ge, Sn, Pb; Cy = cyclohexyl) 64
- **4.1** Abstract 64
- **4.2** Introduction 65
- **4.3** Results and Discussion 67
- **4.4** Conclusion 82
- **4.5** Experimental 83

Chapter 5. Ni(I) and Ni(II) Bis(trimethylsilyl)amides Obtained in Pursuit of the Elusive Structure of $Ni\{N(SiMe_3)_2\}_2$ 98
- **5.1** Abstract 98
- **5.2** Introduction 99
- **5.3** Experimental 100
- **5.4** Results and Discussion 105
- **5.5** Conclusion 120

ACKNOWLEDGEMENT

First, I would like to thank my advisor, Dr. Philip P. Power. Go raibh maith agat as ucht do tacaíocht, do foighne, agus do cairdeas. It was an honor to work under your tutelage and I cannot thank you enough for the wealth of knowledge you shared in even the simplest conversations throughout my time in your lab. This dissertation would not be possible without your consistent encouragement during the many challenges that arose throughout the years, both personal and professional. I would also like to thank Dr. James C. Fettinger for teaching me the intricacies of small molecule X-ray crystallography and my extended doctoral thesis committee members, Dr. Jesús M. Velázquez, and Dr. Louise A. Berben. I would be remiss if I did not thank Dr. Eugenijus Urnezius, who encouraged me to attend graduate school and who has been one of my strongest supporters. Thank you for encouraging me to step out of my comfort zone and attend U.C. Davis. To all my friends, thank you for always listening after a long day and reminding me of the importance of enjoying the simple things in life. To Nicole, thank you for standing beside me through every challenge I have faced. I will forever cherish your words of encouragement, your patience, and our time together. To my sister, Darby, thank you for being there for me when it matters most. I am so proud of you and all you have accomplished, and I cannot wait to see where life takes you. Finally, I thank my parents, Kevin and Melissa, for always being available regardless of the day or time. Your prayers and support are invaluable, and I thank you for coming to visit me as often as you could. I can never repay you for all you have given me, and I am blessed to have you as my family.

In memory of John Walter Mc Loughlin and John Leslie Darby

ABSTRACT

The purpose of the first part of this thesis is to describe how dispersion energy donor ligands derived from 1-bromo-2,4,6-tricyclohexylbenzene (BrC_6H_2-2,4,6-Cy_3) can effect the stabilization of low-valent transition metal and main group compounds. Thus, reactions of 2,4,6-tricyclohexylphenol with $[M\{N(SiMe_3)_2\}_2]_2$ (M = Mn(II), Fe(II), Co(II)) at room temperature in hexanes afforded the dimeric species $[M(OC_6H_2$-2,4,6-$Cy_3)_2]_2$ (M= Mn(II), Fe(II), Co(II)) in high yield as crystalline species. Use of the sterically similar ligand HOC_6H_3-2,6-Pr^i_2 (Pr^i = isopropyl) gave trimeric species $[M(OC_6H_3$-2,6-$Pr^i_2)_2]_3$ (M = Fe(II), Co(II)) and implicates the dispersion energy donor capabilities of the phenol HOC_6H_2-2,4,6-Cy_3 as the driving force for the formation of dimeric rather than trimeric species. While the Mn(II) and Fe(II) aryloxides are thermally stable, the corresponding Co(II) derivative rearranges to form a dimeric Co(II) semiquinone complex when heated under dynamic vacuum to temperatures above ca. 180 ^oC. Analogous reactions of HOC_6H_2-2,4,6-Cy_3 with main group bis(trimethylsilyl)amides $M\{N(SiMe_3)_2\}_2$ (M = Ge(II), Sn(II), and Pb(II)) gave the dimeric tetrel(II) aryloxides $[M(OC_6H_2$-2,4,6-$Cy_3)_2]_2$. For Ge(II), stirring the reaction for longer than ca. 30 minutes at room temperature in hexane allows the isolation of the rearranged Ge_6O_8 cluster $[Ge_6(\mu_3$-$O)_4(\mu_2$-OC_6H_2-2,4,6-$Cy_3)_4](NH_3)_{0.5}$ which traps *in situ* generated ammonia in non-coordinating positions through the dispersion energy donor interactions provided by the cyclohexyl groups of -OC_6H_2-2,4,6-Cy_3.

The arylthiolates $[M(SC_6H_2$-2,4,6-$Cy_3)_2]_2$ (M = Ge(II), Sn(II), Pb(II)) were synthesized in an analogous manner to the tetrel(II) aryloxides by the addition of HSC_6H_2-2,4,6-Cy_3 to the M(II) bis(trimethylsilyl)amides. They are the first examples of dimeric M(II) arylthiolates of Ge(II) and Sn(II). Also, the Pb(II) species is the first arylthiolate isolable in the absence of donor

ligands or Lewis bases. Previous attempts to obtain a Ge(II) arylthiolate using the thiol HSC_6H_2-2,4,6-Pr^i_3 gave the Ge(IV) hydride $HGe(SC_6H_2\text{-}2,4,6\text{-}Pr^i_3)_3$. DFT calculations revealed that an increase in the dispersion energy stabilization provided by -SC_6H_2-2,4,6-Cy_3 in the species $[Ge(SC_6H_2\text{-}2,4,6\text{-}Cy_3)_2]_2$ prevents the formation of a Ge(IV) hydride analogous to that observed when the thiolato ligand -SC_6H_2-2,4,6-Pr^i_3 was used. A concentration dependent monomer-dimer equilibrium is evident in benzene solutions of $[Ge(SC_6H_2\text{-}2,4,6\text{-}Cy_3)_2]_2$, despite the large increase in dispersion energy stabilization. The Ge(II) and Sn(II) arylthiolates are not isostructural with their aryloxo congeners and have a *cis* arrangement of the ligands in the solid state. In contrast, the Pb(II) thiolate is isostructural with the Pb(II) aryloxo congener and crystallizes with a *trans* arrangement of the -SC_6H_2-2,4,6-Cy_3 ligands.

The final section of this thesis provides detail on the synthesis and isolation of Ni(I) and Ni(II) bis(trimethylsilyl)amides that were isolated during pursuit of the solid-state structure of the highly unstable species $Ni\{N(SiMe_3)_2\}_2$. The use of the bis(trimethylsilyl)amide $K\{N(SiMe_3)_2\}$ as transfer agent was reported to give intractable solids when reacted with $NiCl_2$ in diethyl ether. This prompted a reinvestigation of the use of this transfer agent in the synthesis and isolation of new Ni(II) bis(trimethylsilyl)amides. The reaction of $K\{N(SiMe_3)_2\}$ with NiI_2 in Et_2O gave the three new complexes $[K][Ni\{N(SiMe_3)_2\}_3]$, $[K][Ni\{N(SiMe_3)_2\}_2]$, and $[K(THF)_2][Ni\{N(SiMe_3)_2\}_3]$. The use of $NiCl_2$(DME) (DME = 1,2-dimethoxyethane) instead of NiI_2 as the nickel source gave $[K(DME)][Ni_2\{N(SiMe_3)_2\}_3]$. The isolation of the Ni(I) complexes $[K][Ni\{N(SiMe_3)_2\}_2]$ and $[K(DME)][Ni_2\{N(SiMe_3)_2\}_3]$ highlights both the tendency for $K\{N(SiMe_3)_2\}$ to function as a reducing agent and the sensitivity and unpredictable nature of the Ni(II) bis(trimethylsilyl)amido derivatives. Introduction of adventitious O_2 to solutions of $[K][Ni\{N(SiMe_3)_2\}_2]$ gave the first nickel inverse crown ether (ICE) species

$[K_2][O(Ni\{N(SiMe_3)_2\}_2)_2]$, which is one of just four known ICE complexes of the 3d metals. While the Ni(I) species can be isolated as crystalline solids from the disproportionation of the Ni(II) species, the corresponding Ni(III) products were not readily isolable under the employed reaction conditions.

CHAPTER 1. GENERAL INTRODUCTION

Recent attempts to isolate low-valent transition metal and main group compounds have often relied on the use of sterically encumbering terphenyl ligands. However, the importance of dispersion energy donor (DED) characteristics in the stabilization of these species has been shown by dispersion modified DFT calculations.[1-5] The DED stabilizations principally arise from interligand H···H close contacts which can provide metastability to unusual species, such as the iron(IV) cyclohexyl complex,[3] "$FeCy_4$," of Fürstner and coworkers. In 2018, Schreiner and coworkers quantified the DED stabilization provided by methyl, isopropyl, *t*-butyl, phenyl, cyclohexyl, and adamantyl groups in trityl radicals.[4] They determined that increasing the number of -CH moieties available for interligand H···H close contacts correlates to an increase in DED stabilization, and their findings have been corroborated throughout the literature.[1-5] While the sterically encumbering terphenyl ligands, such as -C_6H_3-2,6-(C_6H_2-2,4,6-Me_3)$_2$, -C_6H_3-2,6-(C_6H_2-2,4,6-Pr^i_3)$_2$, and -C_6H_2-3,5-Pr^i_2-2,6-(C_6H_2-2,4,6-Pr^i_3)$_2$ feature many -CH moieties for interligand C-H···H-C close-contacts, their syntheses are often laborious.[1,6] The compound 1,3,5-tricyclohexylbenzene was chosen as a new DED ligand due to the more numerous -CH groups provided by the cyclohexyl residues. In contrast to the terphenyl ligand syntheses, the compound 1,3,5-tricyclohexylbenzene can be synthesized in just 4 hours via Friedel-Crafts alkylation from inexpensive starting materials, namely benzene and cyclohexyl bromide. Bromination of 1,3,5-tricyclohexylbenzene with Br_2 (*l*) affords BrC_6H_2-2,4,6-Cy_3 in high yield.[7] The Grignard reagent is readily accessible,[8] but the lithiation of BrC_6H_2-2,4,6-Cy_3 with *t*-BuLi in diethyl ether to give 2,4,6-$Cy_3C_6H_2Li(Et_2O)$[9] affords greater versatility of the aryl moiety -C_6H_2-2,4,6-Cy_3. Thus, the chalcogenide derivatives of the aryl group -C_6H_2-2,4,6-Cy_3 are readily accessible and comprise 2,4,6-tricyclohexylphenol, 2,4,6-tricyclohexylphenylthiol,[8,9] and the diselenide bis(2,4,6-

tricyclohexylphenyl)diselenide. The phenol ligand 2,4,6-tricyclohexylphenol (HOC_6H_2-2,4,6-Cy_3) is commercially available and can also be synthesized via literature procedures.[10] In contrast, the thiol HSC_6H_2-2,4,6-Cy_3 and the diselenide $Se_2(C_6H_2$-2,4,6-$Cy_3)_2$ are unavailable commercially. The new thiol was synthesized by standard means[9] and is stable under aerobic conditions as a pale-yellow crystalline solid, but the selenol 2,4,6-tricyclohexylphenylselenol is unstable. Organic workup under ambient conditions[9] of concentrated ethyl acetate solutions of this selenol afford the diselenide as dark orange crystals.

REFERENCES

[1] Liptrot, D. J.; Power, P. P. London Dispersion Forces in Sterically Crowded Inorganic and Organometallic Molecules. *Nat. Rev. Chem.* **2017**, 1-12.

[2] Grimme, S.; Djukic, J. P. The Crucial Role of Dispersion in the Cohesion of Nonbridged Binuclear Os→Cr and Os→W Adducts. *Inorg. Chem*. **2010**, *49*, 2911−2919.

[3] Casitas, A.; Rees, J. A.; Goddard, R.; Bill, E.; DeBeer, S.; Fürstner, A. Two Exceptional Homoleptic Iron(IV) Tetraalkyl Complexes. *Angew. Chem., Int. Ed*. **2017**, 56, 10108−10113.

[4] Rosel, S.; Becker, J.; Allen, W.D.; Schreiner, P.R. Probing the Delicate Balance between Pauli Repulsion and London Dispersion with Triphenylmethyl Derivatives. *J. Am. Chem. Soc*. **2018**, 140, 14421−14432.

[5] Li, H.; Hu, Y.; Wan, D.; Zhang, Z.; Fan, Q.; King, R.B.; Schaefer, H.F. Dispersion Effects in Stabilizing Organometallic Compounds: Tetra-1-norbornyl Derivatives of the First-Row Transition Metals as Exceptional Examples. *J. Phys. Chem. A*. **2019**, *123*, 9514−9519.

[6] Barnett, B. R.; Mokhtarzadeh, C. C.; Figueroa, J. S.; Lummis, P.; Wang, S.; Queen, J. D.; Gavenonis, J.; Schüwer, N.; Tilley, T. D.; Boynton, J. N.; Power, P. P.; Ditri, T. B.; Weidemann, N.; Agnew, D. W.; Smith, P. W.; Carpenter, A. E.; Pratt, J. K.; Mendelson, N. D.; Figueroa, J. S.; Terphenyl Ligands and Complexes. *Inorg. Synth*. **2018**, *37*, 85−122.

[7] Salvi L.; Davis, N. R.; Ali, S. Z.; Buchwald, S. L. A New Biarylphosphine Ligand for the Pd-Catalyzed Synthesis of Diaryl Ethers under Mild Conditions. *Org. Lett*. **2012**, *14*, 170–173.

[8] Wong, M. L. J.; Sterling, A. J.; Mousseau, J. J.; Duarte, F.; Anderson, E. A. Direct Catalytic Asymmetric Synthesis of α-chiral Bicyclo[1.1.1]pentanes. *Nat. Commun.* **2021**, *12*, 1–9.

[9] McLoughlin, C.P.; Witt, A.J.; Nelson, J.P.D.; Tuononen, H.M.; Power. P.P. Dispersion Energy Donor Ligand Supports the Isolation of Ge(II), Sn(II), and Lewis-Base Free Pb(II) Arylthiolate Dimers $\{M(SC_6H_2\text{-}2,4,6\text{-}Cy_3)_2\}_2$ (M = Ge, Sn, Pb; Cy = cyclohexyl) *Polyhedron*, **2024**, *252*, 116877.

[10] Stanciu, C.; Olmstead, M. M.; Phillips, A. D.; Stender, M.; Power, P. P. Synthesis and Characterization of the Very Bulky Phenols Ar*OH and Ar'OH (Ar* = C_6H_3-2,6-$Trip_2$, Trip = C_6H_2-2,4,6-*i*Pr_3; Ar' = C_6H_3-2,6-$Dipp_2$, Dipp = C_6H_2-2,6-*i*Pr_2) and Their Lithium and Sodium Derivatives $(LiOAr')_2$ and $(NaOAr^*)_2$. *Eur. J. Inorg. Chem*. **2003**, 3495-3500.

CHAPTER 2. Mn(II), Fe(II), and Co(II) Aryloxides: Steric and Dispersion Effects and the Thermal Rearrangement of a Cobalt Aryloxide to a Co(II) Semiquinone Complex

Mn(II), Fe(II), and Co(II) Aryloxides: Steric and Dispersion Effects and the Thermal Rearrangement of a Cobalt Aryloxide to a Co(II) Semiquinone Complex

Citation: C.P. McLoughlin, J.C. Fettinger, P.P. Power. *Inorg. Chem.* **2023**, *62*, 10131−10140.

2.1. ABSTRACT

A series of Mn(II), Fe(II), and Co(II) bisaryloxide dimers ($[M(OC_6H_2\text{-}2,4,6\text{-}Cy_3)_2]_2$ {M = Mn (**1**), Fe (**2**), and Co (**3**)} were synthesized by the addition of 2,4,6-tricyclohexylphenol ($HOC_6H_2\text{-}2,4,6\text{-}Cy_3$) to the silyl amido dimers $[M(N(SiMe_3)_2)_2]_2$ (M = Mn, Fe, Co; Cy = cyclohexyl). An unexpected and unique Co(II) phenoxide derivative (**4**), $[Co(OC_6H_2\text{-}2,4,6\text{-}Cy_3)(O_2C_6H\text{-}3,5,6\text{-}Cy_3)]_2$, was obtained via ligand rearrangement of **3** at ca. 180 °C. This yielded **4** in which there are two unchanged, bridging phenoxide ligands as well as a terminal bidentate semiquinone ligand bound to each cobalt. Complexes **1** and **2** did not undergo such a rearrangement under the same conditions; both are thermally stable to temperatures exceeding 250 °C and feature numerous short-contact (<2.5 Å) H···H interactions consistent with the presence of dispersion stabilization. Use of the aryloxide ligand $-OC_6H_3\text{-}2,6\text{-}Pr^i_2$ (Pr^i = isopropyl), which is sterically similar to $-OC_6H_2\text{-}2,4,6\text{-}Cy_3$ but produces fewer close H···H interactions, gave the trimeric species $[M(OC_6H_3\text{-}2,6\text{-}Pr^i_2)_2]_3$ {M = Fe (**5**) or Co (**6**)} which feature a linear array of three metal atoms bridged by aryloxides. The higher association number in **5** and **6** in comparison to those

of **1–3** is due to the lower dispersion energy donor properties of the $-OC_6H_3$-2,6-Pr^i_2 ligand and the lower stabilization it produces.

2.2. INTRODUCTION

First synthesized by Bürger and Wannagat in 1963, the transition metal bissilylamides $[M(N(SiMe_3)_2)_2]_2$ (M=Mn, Co, Ni) have been crucial for the development of low-coordinate (coordination numbers 2 or 3) open shell transition metal complexes. These compounds are important as convenient synthons for numerous other low-coordinate metal complexes under mild conditions.[1,2] Their iron(II) bissilylamido congener $[Fe(N(SiMe_3)_2)_2]_2$, synthesized in 1988, was shown to have a similar structure and behavior to its Mn and Co analogs.[3] However, in 1978 it emerged that the original syntheses[1,2] of $[M(N(SiMe_3)_2)_2]_2$ (M=Mn, Co, Ni) by Bürger and Wannagat had actually described the tetrahydrofuran complexes, $M(N(SiMe_3)_2)_2(THF)$ (M=Mn, Co), rather than the THF-free metal bissilylamides as reported originally.[4] Similarly, $Fe(N(SiMe_3)_2)_2(THF)$ was isolated when the silylamide was prepared in THF.[5] However, the use of diethyl ether instead of THF as a solvent afforded the THF-free complexes $[M(N(SiMe_3)_2)_2]_2$ (M=Mn, Fe, Co, Ni) due to the lower donor properties of Et_2O and its greater steric demand in precluding its coordination.[3,4,6-11] Nonetheless, it was not until 2013 that a clear distinction between the dichroic red/olive $[Co(N(SiMe_3)_2)_2]_2$ and the bright green $Co(N(SiMe_3)_2)_2(THF)$ complex was recognized.[8,9] One of the more important features of these silylamides arises from the pKa (25.8)[12] of 1,1,1,3,3,3-hexamethyldisilazane (HMDS) which facilitates protonolysis reactions with alkyl or aryl alcohols. For example, reactions of $[M(N(SiMe_3)_2)_2]_2$ (M=Mn, Fe, Co) with 2,4,6-tri-t-butylphenol, $HOC(C_6H_{11})_3$, $HOC(4\text{-}MeC_6H_4)_3$, or $HOSiPh_3$ yielded the corresponding neutral, dimeric metal phenoxides or siloxides, while the use of trityl alcohol produced mononuclear, distorted tetrahedral metal coordination in the presence of Lewis

bases.[13,14] Further examples using boryloxides (-OBR_2) as ligands also yielded products with M_2O_2 core structures.[15] Additionally, use of adamantyl-substituted aryloxides afforded monomeric products,[16] and substituted di-*t*-butylphenols formed dimers unless coordinated by ethereal solvents or ammonia.[17] In parallel work, the reaction of $[Co(N(SiMe_3)_2)_2]_2$ with 3,5-di-tert-butylcatechol resulted in the formation of a tetrameric Co(II) catecholate, featuring a cubane-like Co_4O_4 core which was spectroscopically and structurally characterized.[18]

The importance of dispersion energies in the stabilization of unusual coordination numbers, bonding types, or oxidation states in several transition metal species[19,20] has been shown by dispersion modified DFT calculations. For example, the close interligand H···H contacts in the transition metal (IV) norbornyls, originally reported by Bower and Tennent in 1972 are key for their stability.[21-23] Further calculations[24] revealed that dispersion energy stabilization in these sterically crowded complexes can range from a few kcal mol^{-1} to above 35 kcal mol^{-1}. Fürstner and coworkers also showed that the homoleptic iron(IV) cyclohexyl complex, "$FeCy_4$," which featured extensive H···H contacts between the four cyclohexyl groups conferred metastability on this unique species.[25] In 2018, Schreiner and coworkers provided a cogent illustration of the importance of dispersion energies for stability, when they showed that the stability of trityl radicals increases with substitution by alkyl groups due to increasing interligand dispersion interactions.[26] Low-coordinate metal complexes were also isolated using highly sterically encumbering terphenyl ligands, but their syntheses are often laborious.[27-30] Thus, we sought to employ a new dispersion energy donor ligand that is not as sterically encumbering as those used in previously reported metal(II) aryloxides, but features substituents that produce extensive interligand H···H contacts. The substituent 2,4,6-tricyclohexylphenol has numerous C-H moieties available for potential dispersion interactions. Consequently, we decided to investigate

its ligand characteristics, including its dispersion effects.[24] From a steric perspective, the 2,4,6-tricyclohexylphenoxy substituent most closely resembles the related 2,4,6-tri-isopropylphenoxy or 2,6-di-isopropylphenoxy species.[31,32] In passing, we note that no homoleptic 2,4,6-tri-isopropylphenol or 2,6-di-isopropylphenol complexes of the metals Mn(II), Fe(II), and Co(II) have been characterized. In fact just ca. 10 compounds of the type $[M(OR)_2]_n$ (M=Mn, Fe, Co, n=2,3) of any kind have been structurally characterized, although a larger number of such complexes stabilized by σ-donor Lewis bases or solvent molecules such as ether, pyridine, ammonia, or THF are known.[13-17] Herein we report the synthesis and characterization of six neutral metal(II) aryloxides (M=Mn, Fe, Co) synthesized from 2,4,6-tricyclohexylphenol or 2,6-di-isopropylphenol and the respective bissilylamides $[M(N(SiMe_3)_2)_2]_2$ (M=Mn, Fe, Co) as synthons to demonstrate how dispersion energy donor stabilization affects physical properties and structures.

2.3. EXPERIMENTAL SECTION

General Considerations

All manipulations were carried out under anaerobic and anhydrous conditions by using standard Schlenk techniques or in a Vacuum Atmospheres OMNI-Lab drybox under an atmosphere of dry argon or nitrogen. Solvents were dried by the method of Grubbs[33] and co-workers, stored over potassium or sodium, and then degassed by the freeze−pump−thaw method. All physical measurements were made under strictly anaerobic and anhydrous conditions. NMR spectra were recorded on a Varian Inova 600 MHz spectrometer or a Bruker 400 MHz Avance III HD Nanobay spectrometer, and the ^{1}H NMR spectra were referenced to the residual solvent signals in deuterated benzene. Melting points of samples in flame-sealed capillaries were determined using a Meltemp

II apparatus equipped with a partial immersion thermometer. Magnetic susceptibility data were collected at room temperature by the Evans' method[34] using the indicated deuterated solvent and were corrected using the appropriate diamagnetic constants.[35] IR spectra were recorded as Nujol mulls between CsI plates on a PerkinElmer 1430 spectrometer. UV−vis spectra were recorded as dilute hexane or toluene solutions in 3.5 mL quartz cuvettes using an Olis 17 modernized Cary 14 UV−vis−near-IR spectrophotometer. Unless otherwise stated, all materials were obtained from commercial sources and used as received. The ligand 2,4,6-tricyclohexylphenol is commercially available in large quantities but was donated by Toray Industries, Inc. and used without further purification. The ligand 2,6-di-isopropylphenol was purchased from Alfa Aesar and purified by distillation. The metal(II) bissilylamides $[M(N(SiMe_3)_2)_2]_2$ (M=Mn, Fe, Co) were prepared as described in reference 36.

$[Mn(OC_6H_2\text{-}2,4,6\text{-}Cy_3)_2]_2$ (**1**). $[Mn(N(SiMe_3)_2)_2]_2$ (0.417 g, 0.555 mmol) was added to a Schlenk tube containing 0.756 g (2.220 mmol) of 2,4,6-tricyclohexylphenol. The flask was briefly placed under dynamic vacuum, sealed, and heated with stirring to ca. 60 ^{0}C for ca. five minutes. The flask was removed from the heat source and immediately placed under dynamic vacuum for a further five minutes to remove the volatile materials. This left a green residue which was dissolved in benzene (15 mL) and placed in a ca. 8 ^{0}C refrigerator to give 0.365 g (80.2%) of **1** as pale green rectangular blocks upon cooling for 24 h., mp >250 ^{o}C, μ_{eff}: 5.9 μ_B (25 ^{o}C). ^{1}H NMR (600 MHz, benzene-d_6) δ 7.29, 7.03, 4.33, 3.28, 3.09, 2.76, 2.11, 1.99, 1.96, 1.93, 1.91, 1.79, 1.76, 1.74, 1.68, 1.53, 1.49, 1.47, 1.43, 1.35, 1.31, 1.25, 0.89, 0.30, 0.22. UV-vis λ/nm (ε/$M^{-1}cm^{-1}$) 234 (15,000), 281 (7,700). IR (Nujol; $\tilde{\nu}/cm^{-1}$) 2930s, 2860s, 1580w, 1460s, 1450s, 1378m, 1365m, 1355m, 1300w, 1260s, 1190w, 1180w, 1150w, 1120w, 1090m, 1020s, 950w, 862w, 800s, 675w, 535w, 455w.

[Fe(OC$_6$H$_2$-2,4,6-Cy$_3$)$_2$]$_2$ (**2**). [Fe(N(SiMe$_3$)$_2$)$_2$]$_2$ (0.389 g, 0.517 mmol) was added to a Schlenk tube containing 0.704 g (2.068 mmol) of 2,4,6-tricyclohexylphenol. The flask was briefly placed under dynamic vacuum, then sealed, and heated to ca. 50 ^{0}C with stirring for ca. five minutes. The flask was removed from the heat source and immediately subjected to dynamic vacuum for five min. to remove volatile materials. This resulted in a solid yellow residue which was dissolved in ca. 15 mL benzene. Cooling in a ca. 8 ^{0}C refrigerator for 24 h. gave 0.321 g (75.5%) of **2** as yellow rectangular blocks, mp >250 ^{o}C, μ_{eff}: 3.9 μ_B (25 ^{o}C). ^{1}H NMR (600 MHz, benzene-d$_6$) δ 78.14, 40.64, 36.85, 27.37, 18.08, 14.48, 13.27, 10.67, 9.30, 8.29, 6.08, 2.12, 1.30, 1.03, -0.15, -0.34, -2.01, -3.52, 3.82, -6.60, -8.58, -9.61, -15.33, -17.18, -22.19. UV-vis λ/nm (ε/M^{-1}cm^{-1}) 282 nm (11,000), 310 nm (4,100). IR (Nujol; ṽ/cm^{-1})2930s, 2850s, 2680w, 1590w, 1445s, 1372m, 1352m, 1345m, 1290m, 1281m, 1260m, 1251m, 1200w, 1171w, 1148w, 1115w, 1035w, 952w, 860m, 807w, 753w, 726w, 690w, 655w, 525w, 460w.

[Co(OC$_6$H$_2$-2,4,6-Cy$_3$)$_2$]$_2$ (**3**). [Co(N(SiMe$_3$)$_2$)$_2$]$_2$ (0.799 g, 1.052 mmol) was added to a Schlenk tube along with 1.433 g (4.208 mmol) of 2,4,6-tricyclohexylphenol. The flask was cooled to 0 ^{o}C and ca. 60 mL of hexane were added. The solution immediately assumed a dark red color and was warmed to room temperature. The mixture was stirred for 2 hours and the solvent was removed under dynamic vacuum to yield a red residue. This was gently heated to ca. 40 ^{o}C for fifteen minutes to remove all volatile materials. The resulting red solid was dissolved in ca. 30 mL benzene and placed in a ca. 8 ^{0}C refrigerator. Red rectangular blocks of **3** formed from this concentrated benzene solution after 24 h. to give 0.786 g (90.2%) of **3**, mp >250 ^{o}C, μ_{eff}: 5.4 μ_B (25 ^{o}C). ^{1}H NMR (600 MHz, benzene-d$_6$) δ 143.93, 77.54, 71.67, 36.16, 34.51, 22.97, 21.78, 19.39, 15.57, 7.12, 7.03, 6.99, 4.31, 2.73, 2.10, 1.91, 1.75, 1.67, 1.47, 1.32, 1.20, 0.30, -0.03, -1.97, -5.72, -6.86, -10.02, -10.44, -16.065, -19.78, -22.11, -50.80, -59.64. UV-vis λ/nm (ε/M^{-1}cm^{-1}) 276

(7,800), 499 (1,500). IR (Nujol; $\tilde{\nu}/cm^{-1}$) 2940s, 2860s, 1635w, 1585m, 1460s, 1450s, 1380m, 1350m, 1300m, 1280m, 1260s, 1240m, 1200m, 1170m, 1150m, 1100s, 1020s, 950w, 890w, 865m, 800s, 730w, 695w, 670w, 540w, 465w, 390w.

[Co(OC$_6$H$_2$-2,4,6-Cy$_3$)(O$_2$C$_6$H-3,5,6-Cy$_3$)]$_2$ (**4**). [Co(N(SiMe$_3$)$_2$)$_2$]$_2$ (0.331 g, 0.436 mmol) was added to a Schlenk tube with 0.594 g (1.743 mmol) 2,4,6-tricyclohexylphenol. The flask was placed briefly under dynamic vacuum, sealed, and heated to ca. 90 ºC with stirring for five minutes. The temperature was increased to ca. 180 ºC to melt the remaining unreacted material. The flask was removed from heat and immediately placed under dynamic vacuum for five minutes to remove the volatile materials, which left a red solid residue. The solid was dissolved in ca. 30 mL hexanes and placed in an 8 ^{0}C refrigerator. A mixture of red crystals of **3** and **4** formed after 24 hours to yield a total of 0.094 g of red crystals. Complex **4** was manually separated under a microscope as dark red square crystals to give an overall yield of 0.001 g (2.14%), mp >250 ºC.

[Fe(OC$_6$H$_3$-2,6-Pr$^i_2$)$_2$]$_3$ (**5**). [Fe(N(SiMe$_3$)$_2$)$_2$]$_2$ (0.498 g, 0.661 mmol) was added to a Schlenk tube containing 0.472 g (2.648 mmol) of 2,6-di-isopropylphenol. The flask was briefly placed under dynamic vacuum, then sealed, and heated to ca. 50 ^{0}C with stirring for ca. five minutes. The flask was removed from the heat source and immediately subjected to dynamic vacuum for ca. ten min. to remove the volatile materials. This resulted in a solid green residue which was redissolved in ca. 5 mL benzene. The solution was filtered, and cooled in a ca. 8 ^{0}C refrigerator for ca. 48 h. to give 0.187 g (37.9%) of **5** as emerald green rectangular blocks, mp >250 ºC, μ_{eff}: 8.1 μ_B (25 ºC). ^{1}H NMR (400 MHz, benzene-d$_6$) δ 97.10, 90.60, 36.49, 35.02, 30.93, 21.92, 7.04, 7.02, 4.49, 4.16, 3.35, 1.27, 1.19, 1.17, 1.02, 0.95, 0.91, 0.43, 0.25, -9.47, -11.35, -41.93, -49.41, -54.48, -73.99, -96.64. UV-vis λ/nm (ε/$M^{-1}cm^{-1}$) 282 nm (22,550), 305 nm (10,090), 367 nm (5,760). IR (Nujol; $\tilde{\nu}/cm^{-1}$), 3060m, 2950s, 2920s, 2840s, 1920w, 1880w, 1850w, 1830w, 1790w, 1690w, 1640w,

1585s, 1460s, 1375s, 1325m, 1255s, 1200m, 1170m, 1105s, 1090s, 1055m, 1040s, 955w, 930m, 900m, 880m, 830m, 800m, 790s, 745s, 710m, 680m, 600w, 560m, 465m, 400m, 285w.

[Co(OC$_6$H$_3$-2,6-Pr$^i_2$)$_2$]$_3$ (**6**). [Co(N(SiMe$_3$)$_2$)$_2$]$_2$ (0.670 g, 0.882 mmol) was added to a Schlenk tube along with 0.629 g (3.528 mmol) of 2,6-di-isopropylphenol. The flask was placed briefly under dynamic vacuum, sealed, and heated to ca. 90 ºC with stirring for five minutes. The flask was removed from the heat source and immediately subjected to dynamic vacuum for ca. ten min. to remove volatile materials. This resulted in a red solid material which was dissolved in ca. 30 mL of hot hexane and placed in a ca. 8 ^{0}C refrigerator. Ruby red rectangular plates of **6** formed after 24 h. to give 0.099 g (14.8%) of **6**, mp >234-235 ºC, μ_{eff}: 7.4 μ_B (25 ºC). ^{1}H NMR (400 MHz, benzene-d$_6$) δ96.97, 86.14, 21.79, 4.59, 3.08, 1.89, 1.18, 0.83, 0.52, -9.45, -80.87, -85.25, -122.34. UV-vis λ/nm (ε/M^{-1}cm^{-1}) 277 (12,350), 282 (14,040), 472 (3,100). IR (Nujol; $\tilde{\nu}$/cm^{-1}) 3450s, 3100s, 2910, 2710w, 1910w, 1845w, 1785w, 1690w, 1650w, 1585m, 1450s, 1375s, 1360s, 1310s, 1250s, 1200m, 1180s, 1155m, 1105s, 1090s, 1055m, 1040s, 955w, 930m, 895m, 880m, 865m, 830s, 800s, 790s, 750s, 745s, 700m, 680s, 600m, 570w, 550m, 485m, 400m, 330w, 280w.

X-ray Crystallographic Studies

Crystals of **1**-**4** suitable for X-ray crystallographic studies were obtained from concentrated benzene solutions of **1** and **2**, or a toluene solution of **3**, and a hexane solution of **4**, at ca. 5 ºC after 24 hours. Crystals of **5** and **6** suitable for X-ray crystallographic studies were obtained from concentrated benzene and hexane solutions, respectively, at ca. 8 ºC after 24 hours. Single crystals were removed from the Schlenk tube and immediately covered with a layer of hydrocarbon oil. Suitable crystals were selected, mounted on a nylon cryoloop, and then placed in the cold nitrogen stream of the diffractometer. Data for **1**, **2**, and **4** were collected at 190(2) K with Cu Kα_1 radiation

(λ = 1.5418 Å) and data for **3** and **6** were collected at 129(2) K and 190(2) K, respectively, with Mo $K\alpha_1$ radiation (λ = 0.71073 Å) using a Bruker D8 Venture dual source diffractometer in conjunction with a CCD detector. Data for **5** were collected at 90(2) K with Mo $K\alpha_1$ radiation (λ = 0.71073 Å) using a Bruker APEX II Mo diffractometer in conjunction with a CCD detector. The collected reflections were corrected for Lorentz and polarization effects and for absorption by using Blessing's method as incorporated into the program SADABS.[37,38] The structures were solved by direct methods and refined with the SHELXTL (2012, version 6.1) or SHELXTL (2013) software packages.[39] Refinement was by full-matrix least-squares procedures, with all carbon-bound hydrogen atoms included in calculated positions and treated as riding atoms. The thermal ellipsoid plots were drawn using OLEX2 software.[40]

2.4. RESULTS AND DISCUSSION

Complex **1** was prepared by combining $[Mn(N(SiMe_3)_2)_2]_2$ and HOC_6H_2-2,4,6-Cy_3 in a Schlenk flask and heating in an oil bath at the melting point of $[Mn(N(SiMe_3)_2)_2]_2$, i.e. at ca. 58 °C (Scheme 1). The melting point of 2,4,6-tricyclohexylphenol is similar (ca. 50 °C),[36] and the reaction proceeds quickly as soon as either reagent liquifies. Extraction of the resultant pale green solid with benzene produced, upon standing, pale green crystals of **1** that were suitable for single crystal X-Ray diffraction studies (Figure 1). The structure of **1** proved to consist of dimeric molecules with bridging aryloxide ligands and a slight pyramidalization of the three coordinate geometry at each Mn(II) center.

Scheme 1. Solvent-free protonolysis of $[M(N(SiMe_3)_2)_2]_2$ (M=Mn, Fe) with 2,4,6-tricyclohexylphenol (HOC_6H_2-2,4,6-Cy_3) to form $[M(OC_6H_2$-2,4,6-$Cy_3)_2]_2$ (M=Mn (**1**), Fe (**2**)).

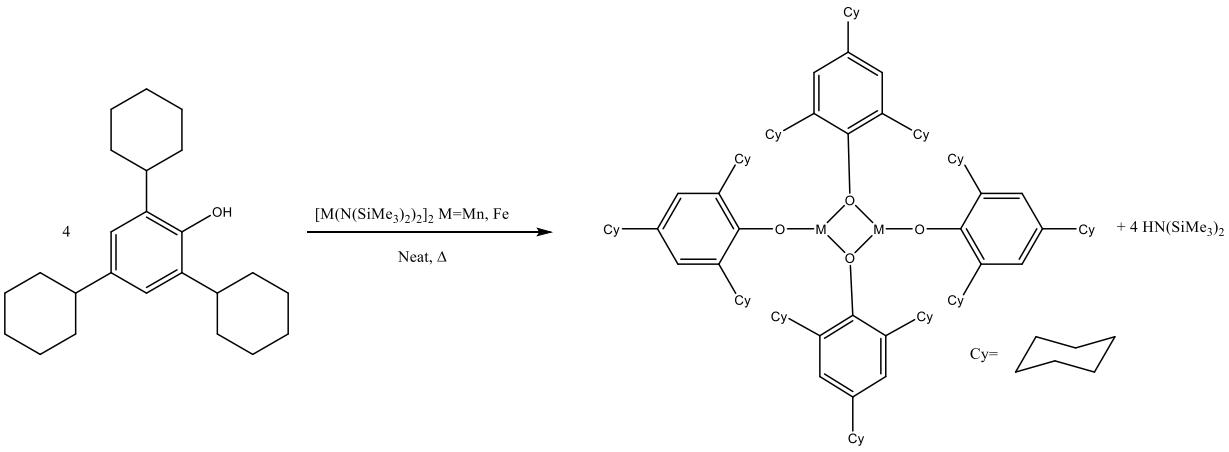

The terminal and bridging Mn-O distances in **1** are longer than those in the previously reported pyridine chelated aryloxide $[Mn_2(3,5\text{-}t\text{-}Bu_2C_6H_2O_2)_2(py)_6]$ (py=pyridine).[13] The large variation in the terminal C-O distances is due to disorder at the terminal ligands from molecular librations. The Mn···Mn distance in complex **1** is shorter than that in the related dimer $[Mn(OC_6H_2\text{-}2,4,6\text{-}Bu^t_3)_2]_2$[13] by ca. 0.07 Å, while the average distance for both terminal and bridging Mn-O bonds in complex **1** are ca. 0.03 Å shorter than those in $[Mn(OC_6H_2\text{-}2,4,6\text{-}Bu^t_3)_2]_2$ (Table 1).

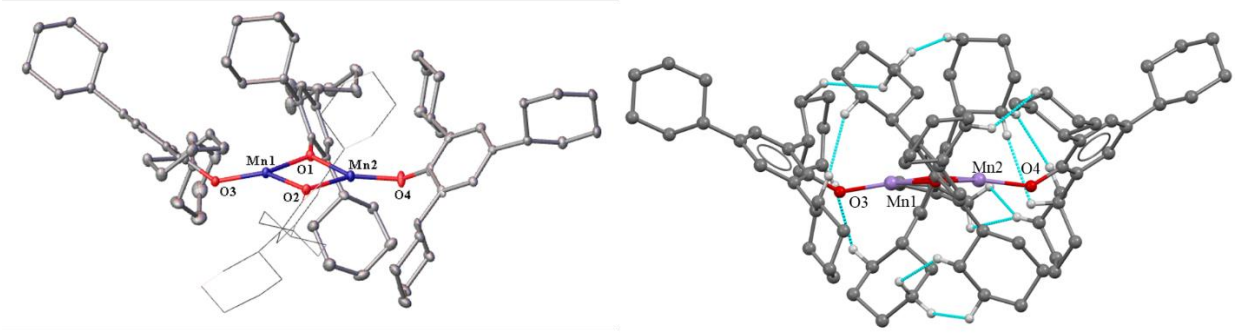

Figure 1. Left: Crystal structure of **1** with thermal ellipsoids shown at 30% probability. Hydrogen atoms are not shown. Important distances and angles: Mn1···Mn2 3.085(4) Å. Terminal Mn-O (avg.) 1.859(5) Å. Bridging Mn-O (avg.) 2.017(11) Å. Terminal C-O (avg.) 1.373(28) Å. Bridging C-O (avg.) 1.371(1) Å. Sum of angles at Mn1: 359.25(10). Sum of angles at Mn2: 359.64(17). R_1:

0.054. Right: Molecular model showing interligand close contacts (≤ 2.5 Å) in **1** depicted in blue, only hydrogen atoms participating in these close contacts are shown.

The UV-Vis spectrum in hexanes is featureless above 300 nm with two LMCT bands observable with maxima at 234 (ε=15,000) and 281 nm (ε=7,700) due to the d^5 electron configuration. The IR spectrum in Nujol shows the characteristic Mn-O bands of equal intensity at 455 and 535 cm^{-1}. A magnetic moment of 5.9 μ_B is consistent with strong anti-ferromagnetic coupling between the two Mn(II) nuclei. In contrast, the spin-only value without coupling for two distinct, non-interacting d^5 Mn^{2+} nuclei is calculated to be 11.84 μ_B.[41] Complex **1** remains unchanged up to temperatures greater than 250 °C and there are 12 interligand close (≤ 2.5 Å) H···H contacts observed, presumably generating dispersion energies and a stability that are comparable to those of previously reported 3-coordinate homoleptic Mn(II) dimers featuring bulkier alkyl (i.e. Bu^t) groups on the central aryl ring.[13,42]

Table 1. Selected average distances in **1**-**3** and related complexes.

Compound	M···M (Å)	Terminal M-O (Å)	Bridging M-O (Å)	Terminal C-O (Å)	Bridging C-O (Å)
1 (Mn)	3.085(4)	1.859(5)	2.017(11)	1.373(28)	1.371(1)
[Mn(OC_6H_2-2,4,6-Bu^t_3)$_2$]$_2$[13]	3.156(2)	1.873(4)	2.050(8)	1.353(10)	1.387(9)
2 (Fe)	2.973(9)	1.806(39)	1.957(4)	1.360(37)	1.388(1)
[Fe(OC_6H_2-2,4,6-Bu^t_3)$_2$]$_2$[13]	3.126(2)	1.822(5)	2.016(8)	1.365(18)	1.399(14)
[Fe(OC_6H_3-2,6-Bu^t_2)$_2$]$_2$[17]	3.099(12)	1.813(4)	2.020(20)	1.342(3)	1.386(2)
3 (Co)	2.925(19)	1.795(5)	1.937(11)	1.370(5)	1.407(16)

The synthesis of complex **2** was accomplished in a similar manner to that of **1** by combining the solid reagents in the Schlenk flask and placing them in an oil bath above the melting point of

$[Fe(N(SiMe_3)_2)_2]_2$, ca. 36 ºC (Scheme 1).[36] An alternative synthetic route to **1** and **2** is via combination of the solids in a Schlenk flask and adding hexanes (80 mL) as a solvent at ca. 0 ºC.

When the reaction is carried out in hexanes at room temperature, the solution became dark yellow almost immediately. The ice bath was then removed and stirring was continued for 1 hour at room temperature. The solvent was pumped off along with eliminated $HN(SiMe_3)_2$ with gentle heating to ca. 35 ºC. Complex **2** was then completely redissolved in hot (ca. 60ºC) benzene and bright yellow crystals of **2** were grown from this concentrated benzene (ca. 1.09 g in ca. 15 mL) solution in ca. 75% yield. These proved suitable for X-Ray crystallographic studies (Figure 2). The structure consists of dimeric molecules with two bridging and two terminal aryloxide ligands, creating two 3-coordinate Fe(II) atoms.

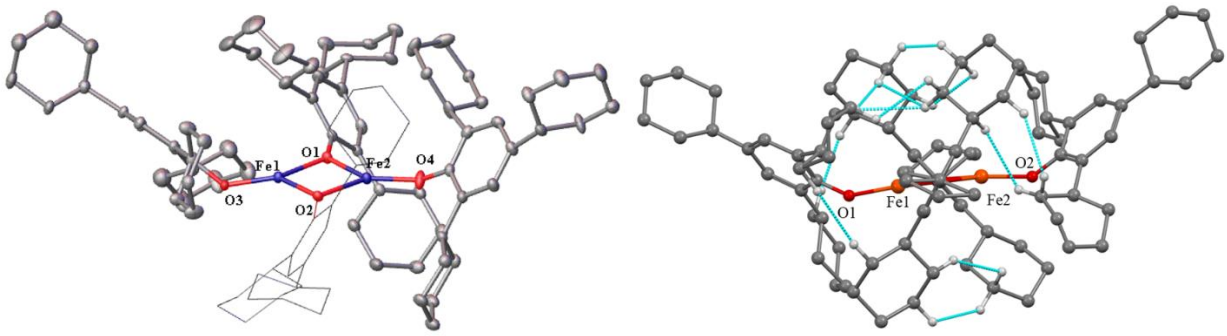

Figure 2. Left: Crystal structure of $[Fe(OC_6H_2\text{-}2,4,6\text{-}Cy_3)_2]_2$ (**2**) with thermal ellipsoids shown at 30% probability, hydrogen atoms are not shown; R_1: 0.096. Right: Molecular model showing interligand close contacts (≤ 2.5 Å) in **2** depicted in blue, hydrogen atoms participating in these close contacts shown in white.

The Fe_2O_4 core unit deviates from planarity as indicated by the interligand bond angles at each metal which do not quite sum to 360º, although the coordination is nearly planar at Fe2 (Table 2). The bridging μ^2-O-Fe bond lengths are 0.119-0.183 Å longer than those of the terminal Fe-O

bonds, with a significant range of distances reflecting the disorder in the structure. In addition, there are 12 relatively close contact (≤ 2.5 Å) interactions between the hydrogens of the cyclohexyl substituents as shown in Figure 1 (right). The predicted bond length for a Fe-O single bond is 1.79 Å,[43] and the distances observed for the terminal Fe-O bonds (av. 1.81(39) Å) match known 2-coordinate Fe(II) aryloxide monomers[13,17] and dimers while the bridging Fe-O bonds (av. 1.96(4) Å) are shorter than those in recently reported Fe(II) aryloxide dimers using similar ligands, such as 2,6-di-*t*-butylphenol (Table 1).[17] The sum of the bond angles around each metal atom are similar in **1** and **2**. The Fe···Fe distance and Fe-O bonds are the shortest in iron aryloxide dimeric species (Table 2), consistent with the presence of dispersion stabilization in **1**. The distances are also consistent with the larger covalent radius of Mn (1.19 Å) in comparison to that of Fe (1.16 Å) (Table 1).[43]

A qualitative indication of the dispersion energy stabilization present in **2** is evident in its high stability. The UV-Vis spectrum features a LMCT band at 282 nm and a d-d transition at 310 nm. IR spectroscopy in Nujol mulls shows two bands that can be assigned to the O-Fe and μ^2-O-Fe stretching modes at 525 and 460 cm^{-1}, respectively, consistent with previously reported data for iron(II) phenoxide dimers.[13,17] A magnetic moment of 3.9 μ_B was obtained via the Evans' method and indicates strong anti-ferromagnetic coupling between the irons in **2**, in contrast to the predicted spin-only moment of two non-interacting nuclei of 9.80 μ_B.[41] The magnetic moment of **1** is notably higher than that of **2**, consistent with the greater number of unpaired electrons in the Mn(II) species.

Table 2. Selected average distances and angles for **2** and average distances and angles in related complexes.

Complex	Fe1···Fe2 (Å)	Terminal Fe-O (Å)	Bridging Fe-O (Å)	Σ Angles Fe1 (°)	Σ Angles Fe2 (°)
$[Fe(OC_6H_2\text{-}2,4,6\text{-}Cy_3)_2]_2$ (**2**)	2.973(9)	1.806(39)	1.957(4)	358.77(25)	359.84(25)
$[Fe(OC_6H_2\text{-}2,4,6\text{-}Bu^t_3)_2]_2$[13]	3.126(2)	1.822(5)	2.016(8)	360.00(5)	359.90(5)
$[Fe(OC_6H_3\text{-}2,6\text{-}Bu^t_2)_2]_2$[17]	3.099(12)	1.813(4)	2.020(20)	359.93(10)	359.98(10)
$[Fe(OC_6H_2\text{-}2,6\text{-}Bu^t_2\text{-}4\text{-}Me)_2]_2$[17]	3.044(5)	1.817(14)	2.004(28)	359.84(7)	359.89(7)
$[Fe\{N(SiMe_3)_2\}\{OC_6H_2\text{-}2,4,6\text{-}Bu^t_3\}]_2$[13]	3.147(2)	1.905(2)	N/A	360.00(2)	360.00(2)

While **3** can be obtained by performing the reaction without solvent, as in the case of **1** and **2**, pure **3** can only be isolated via the reaction of the metal bisamide with the phenol at 0 °C in hexanes (Figure 3). If the reaction is carried out with neat reagents and at a sufficiently high temperature to form a melt, (>170°C) the product is not the expected dimer **3**, but a mixture of two Co(II) phenoxides, compounds **3** and **4**. Unlike its Mn(II) and Fe(II) congeners, the structure of **3** displays only 4 interligand H···H contacts either equal to, or less than, 2.5 Å after modeling the disorder surrounding the cyclohexyl substituent orientations. However, the number of contacts increases to 10 within an H···H separation of 2.6 Å. Despite the lower number of interligand H···H contacts in **3** compared to **1** and **2**, it still displays remarkable stability to temperatures greater than 250 °C.

The structure of **4** (Figure 4) features two bidentate o-dioxolene ligands, each bound to a single cobalt atom, in which two additional oxygens are coordinated to two carbons in the central rings ortho to each phenolic bond, consistent with a 2,3-cyclohexyl ring shift and elimination of hydrogen from a meta position. In contrast, the bridging μ^2-oxygen-cobalt bonds are unchanged

in comparison to **3**. Both **3** and **4** are stable to temperatures beyond 250 °C. While **3** can be isolated in nearly 90% crystalline yield from a solution-phase reaction, **4** is only obtainable via mechanical separation under a microscope in quantities sufficient to calculate a yield and determine the melting point, as the color of **3** and **4** are nearly identical and they can only be visually distinguished by their morphology. Complex **3** crystallizes as red, rectangular plates whereas **4** crystallizes as dark red, square blocks.

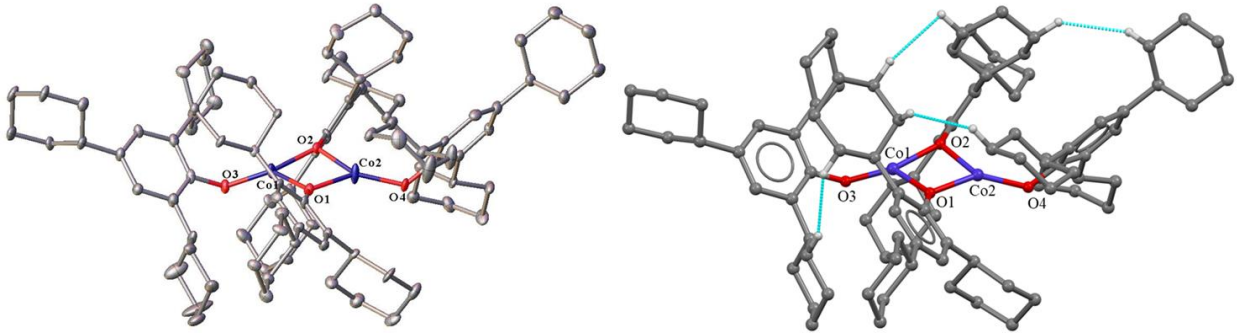

Figure 3. Left: Crystal structure of **3** with thermal ellipsoids shown at 30% probability. Hydrogen atoms are not shown. Important distances and angles: Co1···Co2 2.925(19) Å. Terminal Co-O (avg.) 1.795(5) Å. Bridging Co-O (avg.) 1.937(11) Å. Terminal C-O (avg.) 1.370(5) Å. Bridging C-O (avg.) 1.407(16) Å. Sum of angles around Co1: 354.10(5)°. Sum of angles around Co2: 358.00(5). R_1: 0.067. Right: Molecular model showing interligand close contacts (≤ 2.5 Å) in **3** depicted in blue, hydrogen atoms participating in close contacts shown in white.

Both reactions were carried out in a 4:1 ligand to metal stoichiometry. While there is literature precedent[44] for aryl α-carbon cleavage of phenolics by cobalt Schiff-base complexes to produce quinones, such reactions are typically carried out in the presence of O_2 rather than anaerobically.[45] Furthermore, an "alkyl-walking" mechanism was recently reported for a cobalt catalyzed reaction

in which a 1,4-shift and 1,2-shift of an alkyl group was observed via cobalt-nitrenoid insertion into alkyl substituted arenes.[46]

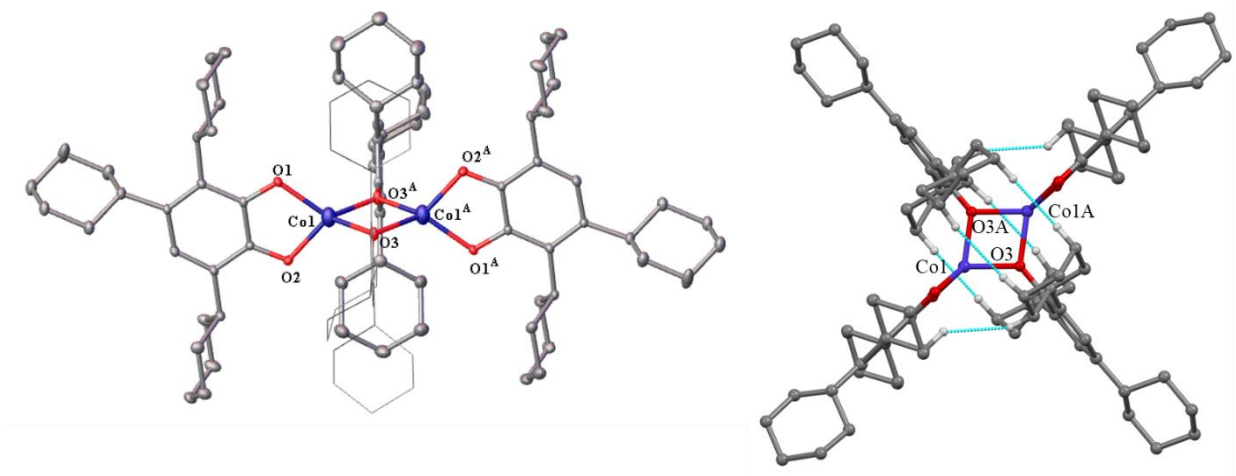

Figure 4. Left: Crystal structure of **4** with thermal ellipsoids shown at 30% probability, hydrogen atoms are not shown. Important distances and angles: Co1···Co1A 2.942(6) Å. Co1-O1 1.947(2) Å. Co1-O2 1.944(3) Å. Co1-O3 1.945(16) Å. Co1-O3A 1.951(16) Å. C1-C2 1.457(4) Å. O1-Co1-O2 84.59(14)°. O3-Co1-O3A 81.93(7)°. Co1-O3-Co1A 98.07(7)°. R_1: 0.066. Right: Molecular model showing interligand close contacts (≤ 2.5 Å) in **4** depicted in blue, hydrogen atoms participating in close contacts shown.

To check if the conversion of **3** to **4** occurs as a result of oxygen contamination,[47] pure **3** was placed under an atmosphere of dried oxygen (1 atm) in an ampule. The solution immediately changed from dark red to brown, followed by green after 10 minutes. From this solution, 2,4,6-tricyclohexylphenol can be recovered and is the only organic product as evidenced by ^{1}H-NMR spectroscopy. Attempts to produce **4** from $[Co(N(SiMe_3)_2)_2]_2$ in quantitative yield using an initial 6:1 ligand to metal ratio were unsuccessful at all temperatures. Furthermore, **4** was only observable

under a microscope in a small quantity upon reacting pure **3** with 2 additional equivalents of 2,4,6-tricyclohexylphenol by combining the solids in a Schlenk flask and heating externally under dynamic vacuum until the products melted together (>170 ^{o}C). Further investigations of the isolation of **4** in quantitative yield are currently underway.

A comparison of the bond lengths in **4** to those in **1**-**3** suggest that the aromaticity of the aryl rings in the bidentate ligands has been disrupted, since the carbon-carbon bond lengths lie between the values of standard single (1.53 Å) and double bonds (1.32 Å) (Table 3).[48] The bond lengths to the terminal chelating rings in **4** resemble those in Co(II) semiquinone complexes and suggest that the phenolic ligands have undergone oxidation from a phenol to a semiquinone, with preservation of the oxidation state of each cobalt atom as Co(II). Modeling of **4** to lower final residual values from ca. 8.4% to 6.6% gives bond distances that lie between the idealized and pre-disorder models. Nonetheless, the bond lengths in the idealized structure and pre-disorder model maintain distances that resemble those in Co(II) semiquinones. Non-bridging carbon-oxygen distances for catecholate complexes fall in the range 1.35-1.37 Å while those of the semiquinones are shorter, between 1.28-1.31 Å.[18,49-51] Two dioxolene ligands bearing isopropyl and cyclohexyl groups were used to characterize Co(II) and Co(III) semiquinone complexes sharing structurally similar parameters in the chelate rings to **4** (cf. Table 3).[52] The eclipsing of the cyclohexyl rings of the ligands in **4** further demonstrates the importance of dispersion forces in the stability of the complex.

Table 3. Comparison of selected chelate ring bond lengths (average) in **4** to those of published Co(II)/Co(III) semiquinone (SQ) and catecholate (Cat) structures.

Complex	M-O Bonds (Å)	C-O Bonds (Å)	C-C (Å)	Type
$[Co_4(DBCat)_4(THF)_{5.5}]$[18]	1.92(14) (term.) 2.11(11) (bridging)	1.34(2) (term.) 1.41(2) (bridging)	1.37(2)	Cat
Co_4(3,5-DBSQ)$_8$ [49]	2.05(4)	1.28(7)	1.45(9)	SQ
Co(3,5-DBCat)(3,5-DBSQ)-(bipy) [50]	1.90(6)	1.30(9)	1.45(11)	SQ
Co(3,5-DBCat)(3,5-DBSQ)-(bipy) [50]	1.87(6)	1.36(10)	1.38(12)	Cat
Co(bpy)(C_6H_2-3,6-di^{i}Pr)$_2$(THF)[52]	1.92(18)	1.29(3)	1.45(4)	SQ
Co(bpy)(C_6H_2-3,6-diCy)$_2$(THF)[52]	2.07(21)	1.29(24)	1.45(23)	SQ
[Co(OC_6H_2-2,4,6-Cy_3)(O_2C_6H-2,4,6-Cy_3)]$_2$ (**4**)	1.95(2)	1.29(3)	1.46(4)	SQ
Reported Range of Catecholate C-O Distances[49]	-	1.35-1.37	1.37-1.41	Cat
Reported Range of Semiquinone C-O Distances[49]	-	1.28-1.31	1.43-1.45	SQ

DBCat: di-*tert*-butylcatecholate; DBSQ: di-*tert*-butylsemiquinone

No homoleptic transition metal derivatives of the sterically similar and commercially available ligand HOC_6H_3-2,6-Pr^i_2 have been reported. The iron and cobalt -OC_6H_3-2,6-Pr^i_2 complexes **5** and **6** were synthesized similarly to **1** and **2** by conducting the reaction neat at the melting point of the metal bissilylamides (Scheme 1). These reactions proceed rapidly in comparison to those of **1** and **2** since 2,6-di-isopropylphenol is a colorless liquid at room temperature that begins solubilizing the metal bissilylamide upon combination of the reactants in the flask. In comparison, combination of 2,4,6-tricyclohexylphenol with the metal bissilylamides to give **1**-**3** requires the formation of a melt before any reactivity is observed. Complex **5** (Figure 5) is an iron(II) aryloxide trimer that crystallizes as large emerald green blocks from benzene at ca. 8 °C. The trimeric structure is similar to $[Mn(Mes)_2]_3$ (Mes=Mesityl), while the use of Trip (-C_6H_2-2,4,6-Pr^i_3) gives the dimer $[Mn(Trip)_2]$.[53,54] Complex **5** crystallizes with two crystallographically distinct molecules per asymmetric unit that includes multiple solvent molecules. The ^{1}H-NMR spectrum (400 MHz, C_6D_6, 25°C) is consistent with a paramagnetic complex with resonances

appearing between +100 and -100 ppm. A magnetic moment of 8.1 μ_B measured via the Evans' method[34] demonstrates strong antiferromagnetic coupling between the three Fe^{2+} ions in the linear Fe_3 array. The UV-Vis spectrum shows three absorbances at 282 nm (22,550), 305 nm (10,000), and 367 nm (5,800) while the IR spectrum shares similar features to **2** with the O-Fe and μ^2-O-Fe stretching modes at 560 and 465 cm^{-1}, respectively. Complex **5** does not melt or decay up to temperatures greater than 250 °C, with the emerald, green crystals maintaining their vibrant hue up to the same temperature.

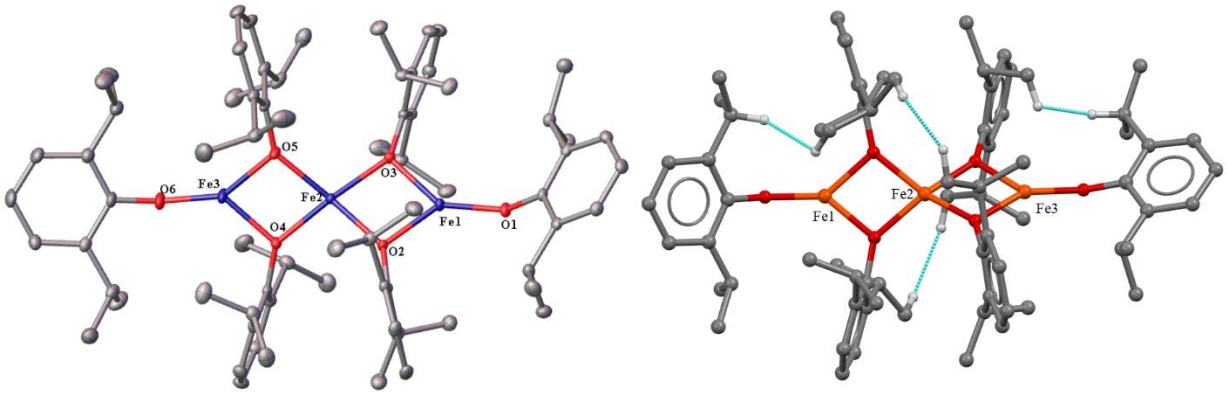

Figure 5. Left: Crystal structure of **5** with thermal ellipsoids shown at 30% probability, hydrogen atoms are not shown, with one of the two crystallographically distinct molecules shown. Important distances and angles: Average Fe···Fe 2.989(9) Å. Terminal Fe-O (ave.) 1.795(16) Å. Bridging Fe-O (ave.) 1.970(19) Å. Terminal C-O (ave.) 1.353(7) Å. Bridging C-O (ave.) 1.391(2) Å. O(2)-Fe(1)-O(3) 82.17(6)°. O(3)-Fe(2)-O(2) 80.22(6)°. O(4)-Fe(2)-O(5) 80.54(6)°. O(5)-Fe(3)-O(4) 81.99(6)°. R_1: 0.047. Right: Molecular model showing interligand close contacts (≤ 2.5 Å) in **5** depicted in blue, hydrogen atoms participating in close contacts shown.

The average Fe···Fe distance in $[Fe(OC_6H_3\text{-}2,6\text{-}Pr^i_2)_2]_3$ (**5**) is slightly longer (by ca. 0.02 Å) than that observed in $[Fe(OC_6H_2\text{-}2,4,6\text{-}Cy_3)_2]_2$ (**2**), but the average terminal Fe-O distances are

similar (1.795 Å in **5** vs. 1.806 Å in **2**). This is presumably due to a combination of the reduced dispersion energy donor capability of -OC_6H_3-2,6-Pr^i_2 in comparison to -OC_6H_2-2,4,6-Cy_3 as well as the presence of a 4-coordinate Fe(II) atom in the center of the linear array. The bridging Fe-O distances around Fe2 are substantially longer than those of the terminal Fe atoms in the linear array, with an average Fe2-O distance of 1.987(8) Å vs. an average distance of 1.953(3) Å to Fe1 and Fe3, with the latter distance mirroring those of complex **2** (1.957(4) Å). The lengthening of the Fe2-O distances in comparison to Fe1 and Fe3 is expected as they are all bridging μ^2-O-Fe2 bonds. The terminal C-O bonds in **5** (1.353(7) Å) are shorter than those of **2** (1.360(37) Å) while the bridging C-O distances in **5** are nearly identical.

In contrast to **5**, complex **6** crystallizes from hexane with one trimer and no solvent molecules per asymmetric unit. Complex **6** (Figure 6) is structurally analogous to **5** and features a trimeric Co(II) array with six aryloxide ligands in the periphery. The ^{1}H-NMR spectrum (400 MHz, C_6D_6, 25°C) is similar to that of **5** and features a broader range of resonances, stretching from -125 ppm to +100 ppm. Complex **6** shows three absorbances in the UV-Vis at 277 nm (12,350), 282 nm (14,040), and 472 nm (3,100), however two are below 300 nm in contrast to the iron analog. While **5** is stable to 250 °C, [Co(OC_6H_3-2,6-Pr^i_2)$_2$]$_3$ melts at 234-235 °C, but does not decompose.

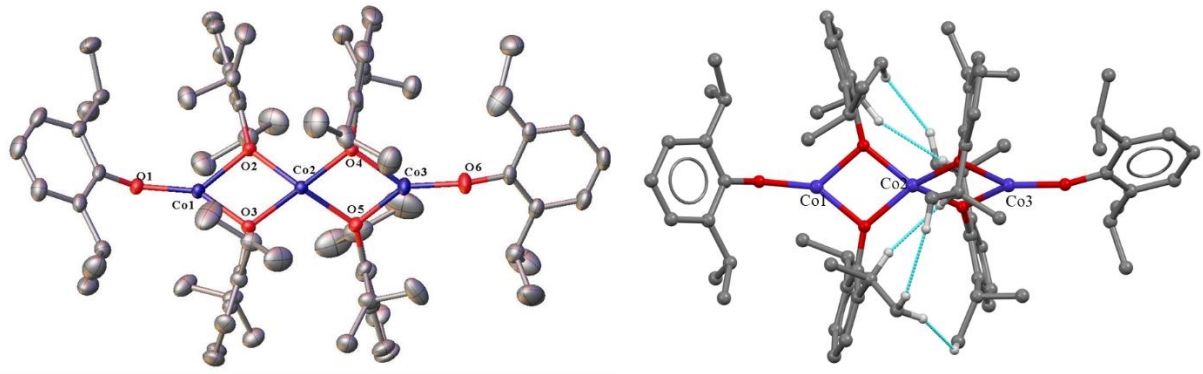

Figure 6. Left: Crystal structure of **6** with thermal ellipsoids shown at 30% probability, hydrogen atoms are not shown. Important distances and angles: Average Co···Co 2.970(3) Å. Terminal Co-O (ave.) 1.769(15) Å. Bridging Co-O (ave.) 1.945(16) Å. Terminal C-O (ave.) 1.346(8) Å. Bridging C-O (ave.) 1.384(1) Å. O(3)-Co(1)-O(2) 80.68(5)°. O(2)-Co(2)-O(3) 79.67(5)°. O(4)-Co(2)-O(5) 79.55(5)°. O(5)-Co(3)-O(4) 81.36(5)°. R_1: 0.036. Right: Molecular model showing interligand close contacts (≤ 2.5 Å) in **6** depicted in blue, hydrogen atoms participating in close contacts shown.

The average Co···Co distance is longer in **6** than that in complex **3** by approximately 0.05 Å while the terminal Co-O distances are shorter by nearly 0.03 Å. While the average bridging Co-O distances are longer in $[Co(OC_6H_3\text{-}2,6\text{-}Pr^i_2)_2]_3$ (**6**) than $[Co(OC_6H_2\text{-}2,4,6\text{-}Cy_3)_2]_2$ (**3**) as a whole, the bridging Co-O distances at each terminal cobalt atom (Co1 and Co3) are shorter in **6** (1.930(5) Å) than **3** (1.937(11) Å), while the central Co2-O distances are significantly longer, averaging 1.959(8) Å. This lengthening is analogous to that of **5** as each Co-O bond is a bridging μ^2-O-Co2 interaction that forms a 4-coordinate Co atom between two terminal 3-coordinate Co atoms. The internal O-Co-O angles are similar in **3** and **6**, owing to the sterically similar isopropyl and cyclohexyl groups on the aryl ring, with those of **6** being slightly more acute in every instance but one by less than a degree.

While the similarity in the bond angles and distances in **5** and **6** to the 2,4,6-tricyclohexylaryloxo congeners demonstrates the structural similarities between 2,6-di-isopropylphenol and 2,4,6-tricyclohexylphenol, disparities arise when comparing their interligand H···H contacts within 2.5 Å and their overall structure. Complex **5** features only 4 H···H close contacts while its 2,4,6-tricyclohexylphenoxo analog features 12. While an analysis of H···H close contacts in complex **3** only returns 4 results ≤ 2.5 Å because of modeling the disorder around the ligands, the number of close contacts increases to 10 within 2.6 Å. In comparison, complex **6** features 5 within or equal to 2.5 Å, and 8 within 2.6 Å. We posit that as the isopropyl groups have less -CH_2 moieties that can participate in H···H close-contact interactions, the formation of trimeric rather than dimeric structures are observed, demonstrating the importance of dispersion energy interactions for the formation of the dimeric complexes **1**-**3**.

2.5. CONCLUSION

Three examples of homoleptic Mn(II), Fe(II), and Co(II) aryloxide dimers were synthesized using 2,4,6-tricyclohexylphenolate as a dispersion energy donor ligand. An additional Co(II) complex, **4**, was isolated as a result of an alkyl-walking shift on the central aryl ring which formed a bidentate chelate ring at the terminal positions with unchanged bridging ligands. It is highly probable that dispersion stabilization energies from interligand H···H contacts contribute to the observed high stability of complexes **1-4**. These stabilities exceed those of previously reported Mn(II), Fe(II), and Co(II) aryloxides such as the *t*-Bu substituted -OC_6H_2-2,4,6-Bu^t_3 or -OC_6H_3-2,6-Bu^t_2 complexes[13,17] despite the decrease in steric bulk provided by the cyclohexyl flanking rings. A separate, novel Co(II) semiquinone **4** was isolated and characterized by X-Ray crystallography; the mechanism for the formation and quantitative synthesis of **4** will require a separate study and is being actively investigated. To demonstrate the importance of H···H close-

contact interactions that generate dispersion stabilization energies to complexes **1**-**3**, two additional complexes (**5** and **6**) were synthesized using the sterically similar 2,6-di-isopropylphenol ligand. $[Fe(OC_6H_3\text{-}2,6\text{-}Pr^i_2)_2]_3$ (**5**) and $[Co(OC_6H_3\text{-}2,6\text{-}Pr^i_2)_2]_3$ (**6**) are trimeric rather than dimeric and feature a linear array of metal atoms with six aryloxo ligands in the periphery, demonstrating the importance of dispersion energy stabilization in the isolation of the dimeric complexes **1**-**3**.

ASSOCIATED CONTENT

Supporting Information.

The following files are available free of charge.

^{1}H-NMR, IR, and UV-Vis spectra for **1**-**3** and **5**-**6**, crystallographic data for **1**-**6** (PDF).

Accession Codes

CCDC 2226833-2226835, 2227111, 2242704-2242705 contain the supplementary crystallographic data for this paper. These data can be obtained free of charge via www.ccdc.cam.ac.uk/data_request/cif, or by emailing data_request@ccdc.cam.ac.uk, or by contacting The Cambridge Crystallographic Data Centre, 12 Union Road, Cambridge CB2 1EZ, UK; fax: +44 1223 336033.

AUTHOR INFORMATION

Corresponding Author

***Philip P. Power** – *Department of Chemistry, University of California, Davis, California 95616, United States;* orcid.org/0000-0002-6262-3209; Email: pppower@ucdavis.edu

Authors

Connor P. McLoughlin – *Department of Chemistry, University of California, Davis, California 95616, United States;* orcid.org/0000-0002-4707-1135

James C. Fettinger – *Department of Chemistry, University of California, Davis, California 95616, United States*; orcid.org/0000-0002-6428-4909

Notes

The authors declare no competing financial interest.

ACKNOWLEDGMENT

We thank the U.S. National Science Foundation for funding (Grant No. CHE-2152760). C.P.M. thanks Toray Industries Inc. for their generous donation of 2,4,6-tricyclohexylphenol and Dr. Qihao Zhu for his useful discussions regarding $[Mn(N(SiMe_3)_2)_2]_2$.

ABBREVIATIONS

Cy, cyclohexyl; py, pyridine; ^{i}Pr, isopropyl; bipy, 2,2′-Bipyridine; DBCat, di-*tert*-butylcatecholate; DBSQ, di-*tert*-butylsemiquinone.

REFERENCES

[1] Bürger, H.; Wannagat, U. Silylamido-Derivate von Eisen und Kobalt. *Monatsh. Chem*. **1963**, *94*, 1007–1012.

[2] Bürger, H.; Wannagat, U. Silylamido-Verbindungen von Chrom, Mangan, Nickel und Kupfer. *Monatsh. Chem*. **1964,** *95*, 1099–1102.

[3] Andersen, R. A.; Faegri, K.; Green, J. C.; Haaland, A.; Lappert, M. F.; Leung, W.P.; Rypdal, K. Bis(bis(trimethylsilyl)amido)iron(II). Structure and Bonding in $M(N(SiMe_3)_2)_2$ (M: Mn, Fe, Co): Two-Coordinate Transition-Metal Amides. *Inorg. Chem*. **1988**, *27*, 1782–1786.

[4] Bradley, D. C.; Hursthouse, M. B.; Abdul Malik, K. M.; Möseler, R. The Crystal Molecular Structure of "Bis(hexamethyldisilylamido)manganese." *Transition Met. Chem*. **1978**, *3*, 253–254.

[5] Olmstead, M. M.; Power, P. P.; Shoner, S. C. Three-Coordinate Iron Complexes: X-Ray Structural Characterization of the Iron Amide-Bridged Dimers $[Fe(NR_2)_2]_2$ (R=$SiMe_3$, C_6H_5) and the Adduct $Fe[N(SiMe_3)_2]_2(THF)$ and Determination of the Association Energy of the Monomer $Fe\{N(SiMe_3)_2\}_2$ in Solution. *Inorg. Chem*. **1991**, *30*, 2547–2551.

[6] Eller, P. G.; Bradley, D. C.; Hursthouse, M. B.; Meek, D.W. Three Coordination in Metal Complexes. *Coord. Chem. Rev*. **1977**, *24*, 1–95.

[7] Horvath, B.; Möseler, R.; Horvath, E. G. Manganese (II) silylamides. *Z. Anorg. Allg. Chem*. **1979**, *450*, 165–177.

[8] Bryan, A. M.; Long, G. J.; Grandjean, F.; Power, P. P. Synthesis, Spectroscopic Characterization, and Determination of the Solution Association Energy of the Dimer $[Co\{N(SiMe_3)_2\}_2]_2$: Magnetic Studies of Low-Coordinate Co(II) Silylamides $[Co\{N(SiMe_3)_2\}_2L]$ (L = PMe_3, Pyridine, and THF) and Related Species That Reveal Evidence of Very Large Zero-Field Splittings. *Inorg. Chem*. **2013**, *52*, 12152–12160.

[9] Cormary, B.; Dumestre, F.; Liakakos, N.; Soulantica, K.; Chaudret, B. Organometallic Precursors of Nano-Objects, A Critical View. *Dalton Trans*. **2013**, *42*, 12546– 12553.

[10] Eichhöfer, A.; Lan, Y.; Mereacre, V.; Bodenstein, T.; Weigend, F. Slow Magnetic Relaxation in Trigonal-Planar Mononuclear Fe(II) and Co(II) Bis(trimethylsilyl)amido Complexes-A Comparative Study. *Inorg. Chem*. **2014**, *53*, 1962– 1974.

[11] Faust, M.; Bryan, A. M.; Mansikkamäki, A.; Vasko, P.; Olmstead, M. M.; Tuononen, H. M.; Power. P. P. The Instability of Ni{N(SiMe$_3$)$_2$}$_2$: A Fifty Year Old Transition Metal Silylamide Mystery. *Angew. Chem. Int. Ed*. **2015**, *54*, 12914–12917.

[12] Fraser, R. R.; Mansour, T. S.; Savard, S. Acidity Measurements on Pyridines in Tetrahydrofuran Using Lithiated Silylamines. *J. Org. Chem.* **1985**, *50*, (17), 3232–3234.

[13] Bartlett, R.A.; Ellison, J.J.; Schoner, S.C.; Power, P.P. Synthesis and Characterization of the Homoleptic Aryloxides [M{O(2,4,6-*t*-Bu$_3$C$_6$H$_2$)}$_2$]$_2$ (M = Mn, Fe), the Adducts [Mn(OCPh$_3$)$_2$(py)$_2$] and [Fe(OCPh$_3$)$_2$(THF)$_2$], and the Mixed Complex [Fe{N(SiMe$_3$)$_2$}{μ-O(2,4,6-*t*-Bu$_3$C$_6$H$_2$)}]$_2$: Evidence for Primarily Ionic Metal-Oxygen Bonding. *Inorg. Chem*. **1991**, *30*, 2888-2894.

[14] Sigel, G. A.; Bartlett, R. A.; Decker, D.; Olmstead, M. M.; Power, P. P. Synthesis and Spectroscopic and X-Ray Structural Characterization and Dynamic Solution Behavior of the Neutral Cobalt(II) Alkoxides [Co{OC(C$_6$H$_{11}$)$_3$}$_2$]$_2$·CH$_3$OH·1/2C$_6$H$_{12}$·THF, [Co(OCPh$_3$)$_2$]$_2$·n-C$_6$H$_{14}$, [Co(OSiPh$_3$)$_2$(THF)]$_2$, and Co(OCPh$_3$)$_2$(THF)$_2$. *Inorg. Chem*. **1987**, *26*, 1773-1780.

[15] Chen, H.; Shoner, S. C.; Power, P. P. Synthesis and Spectroscopic and X-ray Structural Characterization of the First Homoleptic Transition-Metal Boryloxides [Mn(OBTrip$_2$)(μ-OBTrip$_2$)]$_2$ and [Fe(OBMes$_2$)(μ-OBMes$_2$)]$_2$. *Inorg. Chem.* **1991**, *30*, 2884–2888.

[16] Hatanaka, T.; Miyake, R.; Ishida, Y.; Kawaguchi. H. Synthesis of Two-Coordinate Iron Aryloxides and Their Reactions with Organic Azide: Intramolecular C–H Bond Amination. *J. Organomet. Chem.* **2011**, *696*, 4046-4050.

[17] Stennett, C.R.; Fettinger, J.C.; Power, P.P. Low-Coordinate Iron Chalcogenolates and Their Complexes with Diethyl Ether and Ammonia. *Inorg. Chem.* **2021** *60* (9), 6712-6720.

[18] Olmstead, M. M.; Sigel, G.A.; Power, P.P. Structural and Spectroscopic Properties of the Cobalt(II) 3,5-Di-*tert*-butylcatecholate Tetramer Having a Distorted Co_4O_4 Cubane Core. *Inorg. Chem*. **1988**, *27*, 580-583.

[19] Grimme, S.; Djukic, J. P. The Crucial Role of Dispersion in the Cohesion of Nonbridged Binuclear Os→Cr and Os→W Adducts. *Inorg. Chem*. **2010**, *49*, 2911−2919.

[20] Cornaton, Y.; Djukic, J. P. Noncovalent Interactions in Organometallic Chemistry: From Cohesion to Reactivity, a New Chapter. *Acc. Chem. Res*. **2021**, *54*, 3828−3840.

[21] Bower, B. K.; Tennent. H.G. Transition Metal Bicyclo[2.2.1]hept-1-yls. *J. Am. Chem. Soc*. **1972**, *94*, 2512−2514.

[22] Byrne, E. K.; Richeson, D. S.; Theopold, K. H. Tetrakis(1-Norbornyl)Cobalt, a Low Spin Tetrahedral Complex of a First Row Transition Metal. *J. Chem. Soc. Ser. Chem. Commun.* **1986**, *0*, 1491− 1492.

[23] Liptrot, D.J.; Guo, J.D.; Nagase, S.; Power, P.P. Dispersion Forces, Disproportionation, and Stable High-Valent Late Transition Metal Alkyls. *Angew. Chem. Int. Ed*. **2016**, *55*, 14766–14769.

[24] Li, H.; Hu, Y.; Wan, D.; Zhang, Z.; Fan, Q.; King, R.B.; Schaefer, H.F. Dispersion Effects in Stabilizing Organometallic Compounds: Tetra-1-norbornyl Derivatives of the First-Row Transition Metals as Exceptional Examples. *J. Phys. Chem. A*. **2019**, *123*, 9514−9519.

[25] Casitas, A.; Rees, J. A.; Goddard, R.; Bill, E.; DeBeer, S.; Fürstner, A. Two Exceptional Homoleptic Iron(IV) Tetraalkyl Complexes. *Angew. Chem., Int. Ed*. **2017**, 56, 10108−10113.

[26] Rosel, S.; Becker, J.; Allen, W.D.; Schreiner, P.R. Probing the Delicate Balance between Pauli Repulsion and London Dispersion with Triphenylmethyl Derivatives. *J. Am. Chem. Soc*. **2018**, 140, 14421−14432.

[27] Liptrot, D.J.; Power, P.P. London Dispersion Forces in Sterically Crowded Inorganic and Organometallic Molecules. *Nat. Rev. Chem.* **2017**, 1-12.

[28] Mears, K.L.; Power, P.P. Beyond Steric Crowding: Dispersion Energy Donor Effects in Large Hydrocarbon Ligands. *Acc. Chem. Res*. **2022**, *55*, 1337−1348.

[29] Barnett, B. R.; Mokhtarzadeh, C. C.; Figueroa, J. S.; Lummis, P.; Wang, S.; Queen, J. D.; Gavenonis, J.; Schüwer, N.; Tilley, T. D.; Boynton, J. N.; Power, P. P.; Ditri, T. B.; Weidemann, N.; Agnew, D. W.; Smith, P. W.; Carpenter, A. E.; Pratt, J. K.; Mendelson, N. D.; Figueroa, J. S.; Terphenyl Ligands and Complexes. *Inorg. Synth*. **2018**, *37*, 85−122.

[30] Noor, A. Recent Developments in Two Coordinate Transition Metal Chemistry. *Coord. Chem. Rev*. **2023**, *476*, 214941.

[31] Charton, M. Steric Effects. I. Esterification and Acid-Catalyzed Hydrolysis of Esters. *J. Am. Chem. Soc.* **1975**, *97*, 1552-1556.

[32] Pinter, B.; Fievez, T.; Bickelhaupt, F.M.; Geerlings, P.; De Proft, F. On the Origin of the Steric Effect. *Phys. Chem. Chem. Phys.* **2012**, *14*, 9846-9854.

[33] Pangborn, A. B.; Giardello, M. A.; Grubbs, R. H.; Rosen, R. K.; Timmers, F. J. Safe and Convenient Procedure for Solvent Purification. *Organometallics* **1996,** *15*, 1518−1520.

[34] Evans, D. F. The Determination of the Paramagnetic Susceptibility of Substances in Solution by Nuclear Magnetic Resonance. *J. Chem. Soc*. **1959**, *No. 0*, 2003−2005.

[35] Bain, G. A.; Berry, J. F. Diamagnetic Corrections and Pascal's Constants. *J. Chem. Educ*. **2008**, *85*, 532.

[36] Andersen, R. A.; Bryan, A.; M. Faust, M.; Power, P. P. Divalent Manganese, Iron, and Cobalt Bis(trimethylsilyl)amido Derivatives and Their Tetrahydrofuran Complexes. *Inorg. Synth*. **2018**, *37*, 1st Ed., Chapter 1, 1−14.

[37] Sheldrick, G. M. *SADABS*, *Siemens Area Detector Absorption Correction*; Göttingen Universitat: Göttingen, Germany, **2008**; p 33.

[38] Blessing, R. H. An Empirical Correction for Absorption Anisotropy. *Acta Cryst. Sect. A: Found. Cryst*. **1995**, *51*, 33−38.

[39] Sheldrick, G. M. *SHELXTL*, Ver. 6.1; Bruker AXS: Madison, WI, 2002.

[40] Dolomanov, O. V.; Bourhis, L. J.; Gildea, R. J.; Howard, J. A. K.; Puschmann, H. OLEX2: A Complete Structure Solution, Refinement and Analysis Program. *J. Appl. Crystallogr*. **2009**, *42*, 339−341.

[41] Drago, R.S. *Physical Methods in Chemistry*. 1st Ed. Saunders: Pennsylvania, **1977**, Chapter 11, 424-425.

[42] Murray, B.D.; Hope, H.; Power, P.P. An Unusual Carbon-Carbon Bond Cleavage in Bulky Metal Alkoxides: Syntheses and X-Ray Crystal Structures of Three-Coordinate Manganese(II) and Chromium(II) Complexes Containing the di-tert-butylmethoxide Ligand. *J. Am. Chem. Soc*. **1985**, *107*, 169-173.

[43] a) Pyykkö, P.; Atsumi, M. Molecular Single-Bond Covalent Radii for Elements 1–118. *Chem. Eur. J.* **2009**, *15*, 186-197. b) Pyykkö, P.; Atsumi, M. Molecular Double-Bond Covalent Radii for Elements Li–E112. *Chem. Eur. J.* **2009**, *15*,12770-12779. c) Pyykkö, P.; Riedel, S.; Patzschke, M. Triple-Bond Covalent Radii. *Chem. Eur. J.* **2005**, *11*, 3511-3520.

[44] Hames, B.R.; Bozell, J.J. Cobalt-Schiff Base Complex Catalyzed Oxidation of Para-Substituted Phenolics. Preparation of Benzoquinones. *J. Org. Chem*. **1995**, *60*, 2398-2404.

[45] Biannic, B.; Bozell, J.J. Efficient Cobalt-Catalyzed Oxidative Conversion of Lignin Models to Benzoquinones. *Organic Letters*. **2013**, *15*, 2730-2733.

[46] Lee, J.; Kang, B.; Kim, D.; Lee, Jia; Chang, S. Cobalt–Nitrenoid Insertion-Mediated Amidative Carbon Rearrangement via Alkyl-Walking on Arenes. *J. Am. Chem. Soc*. **2021**, 143, 18406−18412.

[47] Zhao, P.; Lei, H.; Ni, C.; Guo, J.D.; Kamali, S.; Fettinger, J.C.; Grandjean, F.; Long, G.J.; Nagase, S.; Power, P.P. Quasi-Three-Coordinate Iron and Cobalt Terphenoxide Complexes $\{Ar^{iPr8}OM(\mu\text{-}O)\}_2$ (Ar^{iPr8} = C_6H-2,6-(C_6H_2-2,4,6-$^iPr_3$)$_2$-3,5-$^iPr_2$; M = Fe or Co) with $M(III)_2(\mu\text{-}O)_2$ Core Structures and the Peroxide Dimer of 2-Oxepinoxy Relevant to Benzene Oxidation. *Inorg. Chem.* **2015**, *54*, 8914–8922.

[48] Smith, M.B. *Advanced Organic Chemistry: Reactions, Mechanisms, and Structure*, 8th Ed. Wiley: New Jersey, **2020**, Chapter 1, 25-27.

[49] Pierpont, C.G.; Buchanan, R.M. Transition Metal Complexes of o-Benzoquinone, o-Semiquinone, and Catecholate Ligands. *Coordination Chemistry Reviews.* **1981,** *38,* 45-87.

[50] Buchanan, R.M.; Fitzgerald, B.J.; Pierpont, C.G. Semiquinone Radical Anion Coordination to Divalent Cobalt and Nickel. Structural Features of the Bis(3,5-di-tert-butyl-1,2-semiquinone)cobalt(II) Tetramer. *Inorg. Chem*. **1979**, *18*, (12), 3439–3444.

[51] Buchanan, R.M.; Pierpont, C.G. Tautomeric Catecholate-Semiquinone Interconversion via Metal-Ligand Electron Transfer. Structural, Spectral, and Magnetic Properties of (3,5-di-tert-butylcatecholato)(3,5-di-tert-butylsemiquinone)(bipyridyl)cobalt(III), a Complex Containing Mixed-Valence Organic Ligands *J. Am. Chem. Soc.* **1980**, *102*, 4951–4957.

[52] Zolotukhin, A.A.; Bubnov, M.P.; Skorodumova, N.A.; Kocherova, T.N.; Bogomyakov, A.S.; Kozlova, E.A.; Fukin, G.K.; Cherkasov, V.K. Valence Tautomerism in Cobalt Complexes Based on Isopropyl- and Cyclohexyl-Substituted o-Quinones. *Inorganica Chimica Acta.* **2022**, *534*, 120811.

[53] Kays, D.L. Recent Developments in Transition Metal Diaryl Chemistry. *Dalton Trans*. **2011**, *40*, 769-778.

[54] Kays, D.L. Extremely Bulky Amide Ligands in Main Group Chemistry. *Chem. Soc. Rev.* **2016**, *45*, 1004-1018.

Chapter 3. Rearrangement of a Ge(II) Aryloxide to Yield a New Ge(II) Oxo-Cluster $[Ge_6(\mu_3\text{-}O)_4(\mu_2\text{-}OC_6H_2\text{-}2,4,6\text{-}Cy_3)_4](NH_3)_{0.5}$: Main Group Aryloxides of Ge(II), Sn(II), and Pb(II) $[M(OC_6H_2\text{-}2,4,6\text{-}Cy_3)_2]_2$ (Cy=Cyclohexyl)

Rearrangement of a Ge(II) Aryloxide to Yield a New Ge(II) Oxo-Cluster $[Ge_6(\mu_3\text{-}O)_4(\mu_2\text{-}OC_6H_2\text{-}2,4,6\text{-}Cy_3)_4](NH_3)_{0.5}$: Main Group Aryloxides of Ge(II), Sn(II), and Pb(II) $[M(OC_6H_2\text{-}2,4,6\text{-}Cy_3)_2]_2$ (Cy=Cyclohexyl)

Citation: C.P. McLoughlin, D.C. Kaseman, J.C. Fettinger, P.P. Power. *Dalton Trans.* **2023**, *52*, 9582−9589.

3.1. ABSTRACT

The new Ge(II) cluster $[Ge_6(\mu_3\text{-}O)_4(\mu_2\text{-}OC_6H_2\text{-}2,4,6\text{-}Cy_3)_4](NH_3)_{0.5}$ (**1**) and three divalent Group 14 aryloxide derivatives $[Ge(OC_6H_2\text{-}2,4,6\text{-}Cy_3)_2]_2$ (**2**), $[Sn(OC_6H_2\text{-}2,4,6\text{-}Cy_3)_2]_2$ (**3**), and $[Pb(OC_6H_2\text{-}2,4,6\text{-}Cy_3)_2]_2$ (**4**) of the new tricyclohexylphenoxo ligand, $[\text{-}OC_6H_2\text{-}2,4,6\text{-}Cy_3)_2]_2$ (Cy=cyclohexyl), were synthesized and characterized. Complexes **1-4** were obtained by reaction of the metal bissilylamides $M(N(SiMe_3)_2)_2$ (M=Ge, Sn, Pb) with 2,4,6-tricyclohexylphenol in hexane at room temperature. If the freshly generated reaction mixture for the synthesis of **2** is stirred in solution for 12 h. at room temperature, the cluster $[Ge_6(\mu_3\text{-}O)_4(\mu_2\text{-}OC_6H_2\text{-}2,4,6\text{-}Cy_3)_4](NH_3)_{0.5}$ (**1**) which features a rare Ge_6O_8 core that includes ammonia molecules in non-coordinating positions is formed. Complexes **3** and **4** were also characterized via $^{119}Sn\{^1H\}$ NMR and ^{207}Pb NMR spectroscopy and feature signals at -280.3 ppm ($^{119}Sn\{^1H\}$, 25 ^oC) and 1,541.0 ppm (^{207}Pb, 37 ^oC), respectively. The spectroscopic characterization of **3** and **4** extends known ^{119}Sn parameters for dimeric Sn(II) aryloxides, but data for ^{207}Pb NMR spectra for Pb(II)

aryloxides are rare. We present also a rare VT-NMR study of a homoleptic 3-coordinate Pb(II) aryloxide. The crystal structures of **2, 3,** and **4** feature interligand H···H contacts that are similar in number to those of related transition metal derivatives despite the larger size of the group 14 elements.

3.2. INTRODUCTION

The main group bissilylamides $M(N(SiMe_3)_2)_2$ (M=Ge, Sn, Pb)[1,2] are frequently employed in the synthesis of low oxidation state complexes of Ge(II), Sn(II), and Pb(II) complexes, several of which can act as precursors to nanomaterials.[3-5] Thus, for the Ge nanomaterials, Ge(II) alkoxide and aryloxides have been synthesized as precursors for materials that could potentially replace silicon-based nanomaterials owing to the higher electron and hole mobility[8] and smaller band gap in germanium species in contrast to that of silicon.[9] In comparison to their Sn(II) analogs,[10-19] however, low-coordinate Ge(II) and Pb(II)[12,20-22] complexes are relatively scarce. For example, Ge(II)-oxo dimers $[Ge(OR)_2]_2$, monomers $Ge(OR)_2$, and calixarene complexes have been reported in approximately equal numbers.[6,7,11,14-16] But, there are just three homoleptic germanium complexes of formula $[Ge(OR)_2]_2$ (R= $-C_6H_3$-2,6-Pr^i_2, $-C_6H_2$-2,4,6-Me_3, $-C_6H_3$-2,6-Me_2).[6,23] For lead, only one homoleptic Pb(II) aryloxide $[Pb(OC_6H_3$-2,6-$Ph_2)]_2$ has been characterized, in this case, by Van Zandt, Huffman, and Stewart in 1998.[20] Similarly, Weinert, Guzei, Rheingold, and Sita isolated a heteroleptic Pb(II) trimethylsilanolato dimer in 1997.[21] Extensive compilations of ^{119}Sn NMR parameters for Sn(II) aryloxides can be found in reviews by Wrackmeyer,[24] Weinert,[25] and Takeuchi and Takayama.[26] However, ^{207}Pb NMR and solution-phase ^{73}Ge NMR data especially for two or three-coordinate Pb(II) and Ge(II) aryloxides are very scarce.[12,24-31] We report herein the synthesis and characterization of 3-coordinate, homoleptic aryloxide dimers of Ge(II), Sn(II), and Pb(II), with the tin and lead analogues being characterized by heteronuclear NMR

spectroscopy. Additionally, we detail the isolation and characterization of a rare Ge_6O_8 aryloxo cluster formed from the rearrangement of the Ge(II) aryloxo dimer.

3.3. RESULTS AND DISCUSSION

The synthesis of the compounds in this article involves amine elimination from the divalent group 14 element amides via the reaction with 2,4,6-tricyclohexylphenol (Scheme 1). This produces, in the first instance, the simple divalent aryloxides $M(OC_6H_2\text{-}2,4,6\text{-}Cy_3)_2$ (M=Ge, Sn, and Pb), which crystallize in good yield as the dimers $[M(OC_6H_2\text{-}2,4,6\text{-}Cy_3)_2]_2$ (M=Ge, **2**; Sn, **3**; Pb, **4**). If the solution of complex **2** is stirred overnight at room temperature in hexanes without isolation of the aryloxide, the solution darkens from pale yellow to orange. Removing the solvent under reduced pressure and washing the crude yellow solid residue with cold hexane four times (ca. 5 mL) until the washings become colorless, followed by recrystallization of the remaining solids from ca. 10 mL hot (ca. 100 ºC) toluene, produced colorless rectangular plates of **1** (Figure 1). Complex **1** is a Ge_6O_8 cluster composed of two 4-coordinate Ge(II) "caps" and four 3-coordinate Ge(II) atoms.

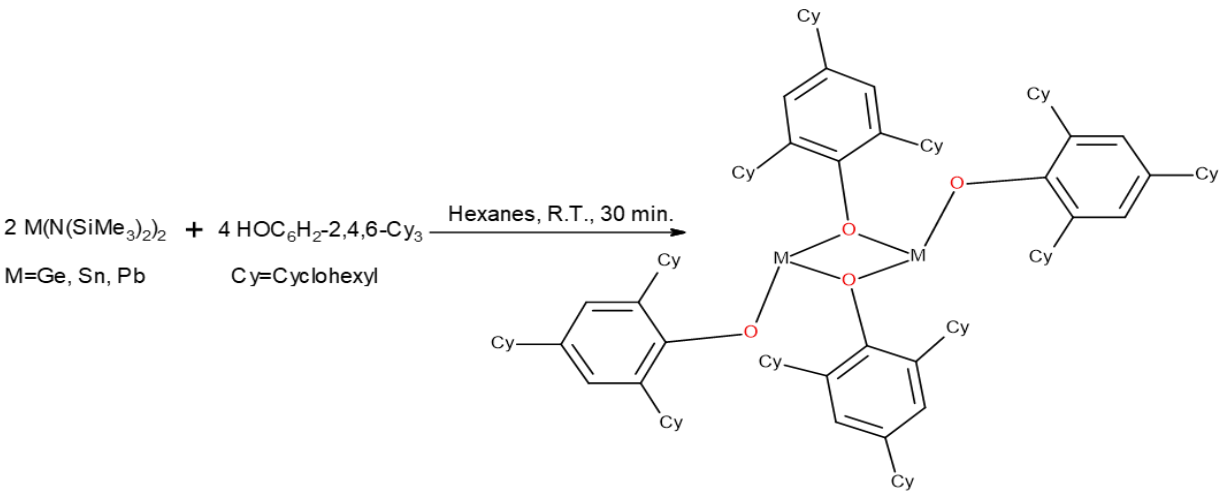

Scheme 1. Synthesis of compounds 2-4.

This arrangement gives alternating faces composed of four Ge_2O_2 rings and four Ge_3O_3 rings (Figure S19). There are four ammonia molecules per unit cell nestled between the radial positions of the ligand in two 25% occupancy general positions. The distance from the nitrogen atoms to the nearest Ge(II) atom is ca. 2.86 Å. This observation is the first of its kind, as ammonia has never been reported in non-coordinating positions in Ge(II) oxo clusters.[32] There are extensive H···H contacts between the ammonia hydrogens and those of the flanking cyclohexyl rings. Placing crystals of cluster 1 under reduced pressure (ca. 0.01 torr) at ambient temperature for 30 min. reveals that the ammonia molecules are tenaciously held between the cyclohexyl substituents of the aryloxo ligands, since an υN-H absorption at 3,610 cm^{-1} is observable in the IR spectrum.

Few instances of Ge(II) dimers rearranging to form "Ge_xO_y" clusters exist in the literature. The first examples, which yielded $[Ge_4(\mu\text{-}O)_2(OC_6H_3\text{-}2\text{-}Bu^t\text{-}4\text{-}Me)_4\cdot NH_3]_2$ and $[Ge_8(\mu_3\text{-}O)_6(OC_6H_3\text{-}2\text{-}Bu^t\text{-}4\text{-}Me)_4]$ were reported by the group of Weinert in 2009.[32] They determined that the driving force for the rearrangement and subsequent generation of similar clusters is a result of the

formation of a silyl ether and ammonia, produced via a side reaction between the substituted phenol and $HN(SiMe_3)_2$.[32]

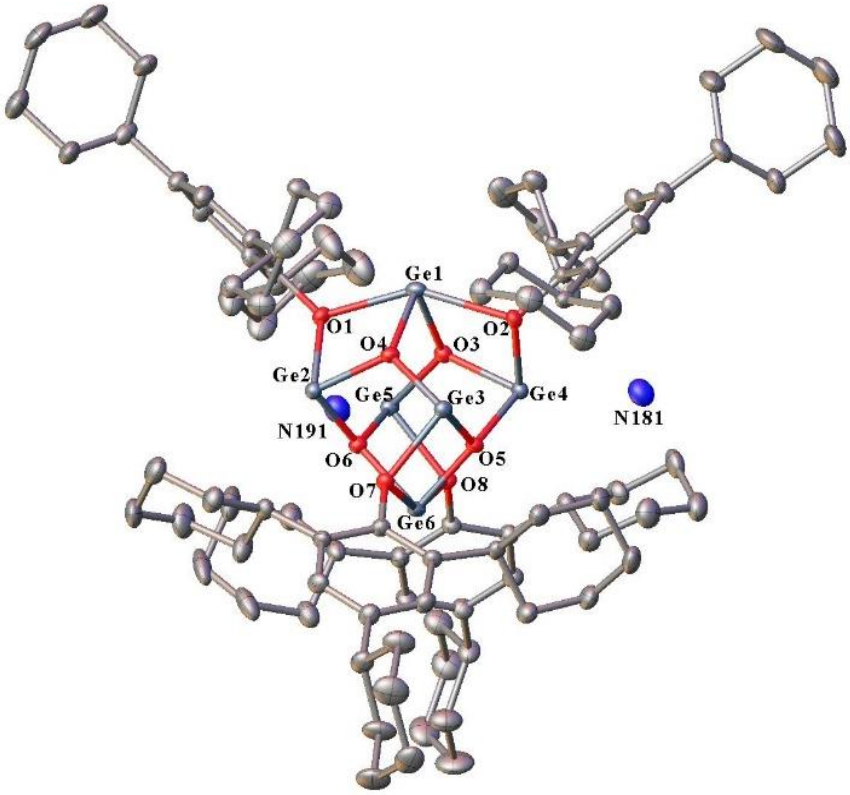

Figure 1. Crystal structure of compound **1** featuring a Ge_6O_8 core with thermal ellipsoids shown at 30%. Co-crystallized solvent molecules (toluene) and hydrogen atoms are not shown. R_1: 0.074.

To check if cluster **1** is formed from the decomposition of **2** (Figure 2) in solution over time or via a similar mechanism to that reported by Weinert,[32] pure **2** was placed in an NMR tube and monitored by ^{1}H NMR spectroscopy over 14 days. These showed that **2** is stable in deuterated toluene at room temperature when protected from air and moisture. The same sample was then exposed to the atmosphere for 24 h. under ambient conditions. Analysis via ^{1}H NMR spectroscopy did not indicate the formation of **1**. The synthesis of complex **1** was repeated in hexane at room

temperature with a 3:4 Ge(II) to phenol ratio, since the aryloxo ligands are also the source of the μ_3-oxo ligands in the cluster,[32] and stirred overnight in a hexane solution which produced crystalline **1**. Notably, previously reported rearrangements occurred with ligands lacking substituents at one or both ortho-positions of the aryl ring.[32] Thus, the formation of **1** challenges the conclusions previously reported, which stated the formation of Ge(II) oxo clusters only occurs if one or both ortho positions of the ligand are lacking a substituent.[32] Only one other Ge_6O_8 cluster, the $[Ge_6(\mu_3\text{-}O)_4(\mu_2\text{-}OC_6H_4\text{-}4\text{-}Bu^t)_4]$ species, has been reported to date. However, it was reported in a Ph.D. dissertation and has not been published in the literature other than in a CCDC submission. It was synthesized from the less sterically encumbering phenol $HOC_6H_4\text{-}4\text{-}Bu^t$ and $Ge(N(SiMe_3)_2)_2$.[33] Notably, there are no NH_3 molecules present, rendering the molecular formula and structure of cluster **1** unique. The average μ_2-O-Ge distances in complex **1** are longer than those in the closely related $[Ge_6(\mu_3\text{-}O)_4(\mu_2\text{-}OC_6H_4\text{-}4\text{-}Bu^t)_4]$[33] cluster by ca. 0.077 Å (Table 1) with a similar variation in the individual distances, while the average μ_3-O-Ge distances are shorter by ca. 0.047 Å with less variation than those observed in $[Ge_6(\mu_3\text{-}O)_4(\mu_2\text{-}OC_6H_4\text{-}4\text{-}Bu^t)_4]$. Likewise, the average C-O distances are longer and have a smaller variation in distance than those in all of the reported clusters, which are in the range of 1.373 Å-1.409 Å.

Table 1. Selected distances and angles in **1** and in other "Ge_xO_y" clusters.

Complex	μ_2-O-Ge (Å) (average)	μ_3-O-Ge (Å) (average)	C-O (Å) (average)
$[Ge_6(\mu_3\text{-}O)_4(\mu_2\text{-}OC_6H_2\text{-}2,4,6\text{-}Cy_3)_4](NH_3)_{0.5}$ (**1**)	2.127(17)	1.923(3)	1.408(5)
$[Ge_6(\mu_3\text{-}O)_4(\mu_2\text{-}OC_6H_4\text{-}4\text{-}Bu^t)_4]$[33]	2.05(16)	1.97(14)	1.375(7)
$[Ge_4(\mu\text{-}O)_2(OC_6H_3\text{-}2\text{-}Bu^t\text{-}4\text{-}Me)_4\cdot NH_3]_2$[32]	1.784(2)	N/A	1.384(4)
$[Ge_8(\mu_3\text{-}O)_6(OC_6H_3\text{-}2\text{-}Bu^t\text{-}4\text{-}Me)_4]$[32]	N/A	1.920(26)	1.392(9)

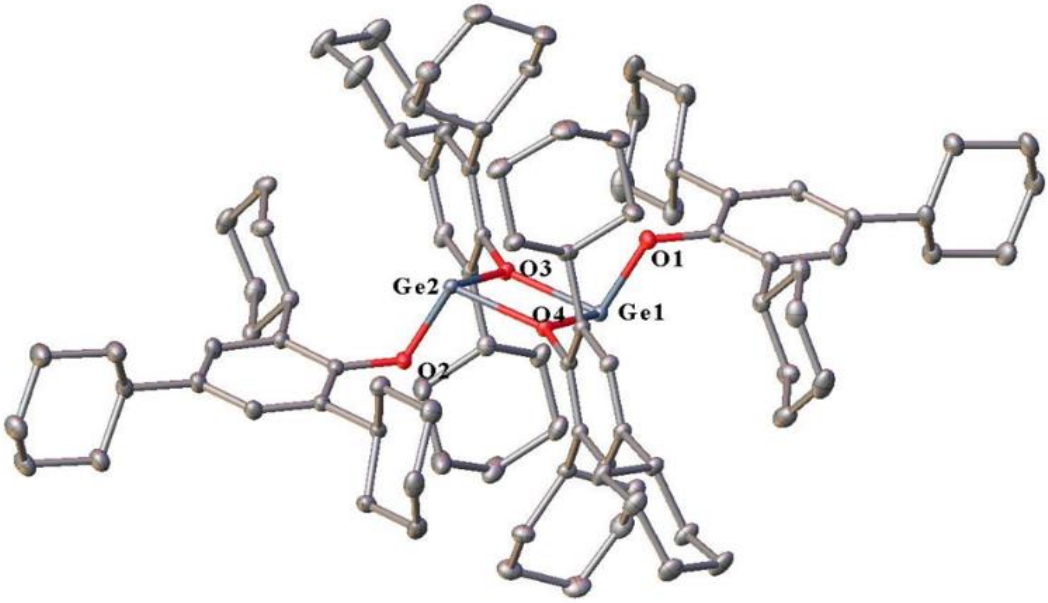

Figure 2. Crystal structure of $[Ge(OC_6H_2\text{-}2,4,6\text{-}Cy_3)_2]_2$ (**2**) with thermal ellipsoids shown at 30%, hydrogen atoms are not indicated. R1: 0.034. Selected distances (Å) and angles (o): Ge···Ge 3.2593(6) Å. Ge1-O1 1.8300(10) Å. Ge1-O3 2.0056(10) Å. Ge1-O4 2.0070(10) Å. Ge2-O2 1.8324(10) Å. Ge2-O3 2.0087(10) Å. Ge2-O4 2.0042(10) Å. O1-Ge1-O3 97.20(4)^o. O1-Ge1-O4 99.01(4)^o. O3-Ge1-O4 71.37(4)^o. O2-Ge2-O3 99.43(4)^o. O2-Ge2-O4 97.13(4)^o. O3-Ge2-O4 71.37(4)^o.

Complex **2** features a dimeric arrangement of two $Ge(OC_6H_2\text{-}2,4,6\text{-}Cy_3)_2$ units in which two bridging and two terminal aryloxide ligands have a trans configuration (Figure 3). The trans arrangement is analogous to those in known dimeric Ge(II) aryloxides (Table 2),[6,23] although such examples remain uncommon despite interest in the application of Ge(II) alkoxy and aryloxy precursors for nanomaterials.[6-8] The terminal Ge-O bond lengths of 1.831(2) Å (ave.) are slightly (ca. 0.009 Å) longer than those in $[Ge(OC_6H_3\text{-}2,6\text{-}Me_2)_2]_2$[6] (av. 1.822(21) Å), while the average bridging Ge-O distance of 2.006(3) Å is slightly longer by ca. 0.022 Å (Table 2). The Ge···Ge separation is also longer by ca. 0.06 Å, likely as a result of the increase in steric pressure on changing from methyl to cyclohexyl substituents.

Table 2. Selected average distances (Å) and angles (°) in **2** and related $[Ge(OR)_2]_2$ dimers.

Complex	Ge···Ge (Å)	Terminal Ge-O (Å)	Bridging μ_2-O-Ge (Å)
$[Ge(OC_6H_2\text{-}2,4,6\text{-}Cy_3)_2]_2$ (**2**)	3.2593(6)	1.831(2)	2.006(2)
$[Ge(OC_6H_3\text{-}2,6\text{-}Pr^i_2)_2]_2$[23]	3.2115(4)	1.824(1)	1.997(15)
$[Ge(OC_6H_2\text{-}2,4,6\text{-}Me_3)_2]_2$[23]	3.2090(8)	1.825(4)	1.984(2)
$[Ge(OC_6H_3\text{-}2,6\text{-}Me_2)_2]_2$[6]	3.1991(12)	1.822(21)	1.984(7)

Similarly, the Ge···Ge distance, terminal Ge-O and bridging μ_2-O-Ge distances are all longer (Table 2) in $[Ge(OC_6H_2\text{-}2,4,6\text{-}Cy_3)_2]_2$ (**2**) than in $[Ge(OC_6H_2\text{-}2,4,6\text{-}Me_3)_2]_2$[23]. A comparison of bond lengths in complex **2** to those in $[Ge(OC_6H_3\text{-}2,6\text{-}Pr^i_2)_2]_2$[23] is consistent with the steric similarity of isopropyl and cyclohexyl substituents.[34,35] The Ge···Ge distance in **2** is ca. 0.048 Å longer than in $[Ge(OC_6H_3\text{-}2,6\text{-}Pr^i_2)_2]_2$ while the average terminal Ge-O distances are similar (ca. 0.007 Å). The average bridging μ_2-O-Ge distances in **2** are slightly longer (ca. 0.009 Å), but this value is misleading as one of the four μ_2-O-Ge bonds in $[Ge(OC_6H_3\text{-}2,6\text{-}Pr^i_2)_2]_2$ is identical (2.008(2) Å), one is longer (2.012(2) Å), and the remaining two are shorter (1.981(2) Å and 1.988(2) Å) than those in **2** (Figure 2). The melting point of **2** is significantly lower (by ca. 12°C)

than those of its heavier congeners Sn and Pb, despite having a similar amount of interligand H···H close contacts between discrete molecules in the solid-state structure. Complex **2** crystallizes as colorless rectangular plates from toluene and hexane, but solutions of **2** are pale yellow in both solvents. Accordingly, the UV-Vis spectrum shows two absorbances, with one in the visible region, at 283 (7863 $\varepsilon/M^{-1}cm^{-1}$) and 338 nm (3200 $\varepsilon/M^{-1}cm^{-1}$). The ^{1}H NMR spectrum shows broadening of various signals in the alkyl region indicative of a dynamic system with potential exchange between terminal and bridging aryloxo ligands as well as inversion of the trans arrangement of the Ge_2O_2 rhomboid center.[23] A comparison of the number of interligand H···H close contacts (≤ 2.4 Å) in $[Ge(OC_6H_3\text{-}2,6\text{-}Pr^i_2)_2]_2$[23] to $[Ge(OC_6H_2\text{-}2,4,6\text{-}Cy_3)_2]_2$ (**2**) demonstrate that despite slight increases in bond lengths, there is a substantial increase in dispersion energy donor[36,37] interactions in the case of **2** (Figure 3). $[Ge(OC_6H_3\text{-}2,6\text{-}Pr^i_2)_2]_2$ features six interligand H···H close contacts, with four of the six contacts originating from a methine hydrogen on the isopropyl substituents. In contrast, $[Ge(OC_6H_2\text{-}2,4,6\text{-}Cy_3)_2]_2$ (**2**) has sixteen interligand H···H close contacts, with three originating from a methine hydrogen on the cyclohexyl groups.

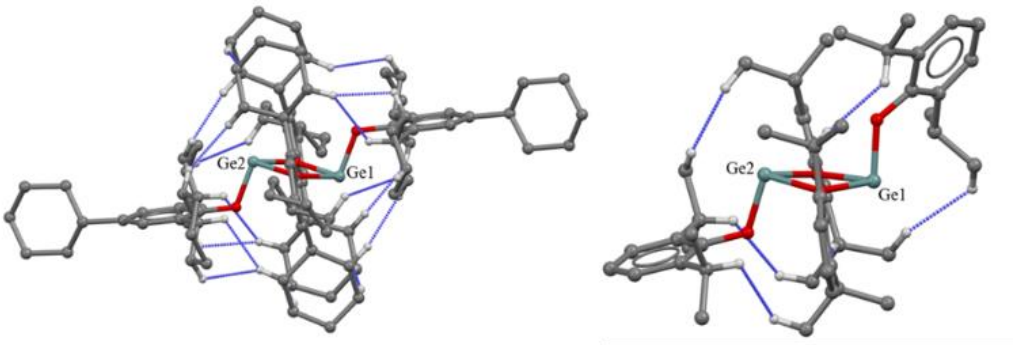

Figure 3. Interligand H···H close (≤ 2.4 Å) contacts in $[Ge(OC_6H_2\text{-}2,4,6\text{-}Cy_3)_2]_2$ (**2**, left) and the sterically related complex $[Ge(OC_6H_3\text{-}2,6\text{-}Pr^i_2)_2]_2$ (right).[23] Interligand H···H close contacts are shown in blue, hydrogen atoms not in close contact are not shown.

The bonding in **3** (Figure 4) and **4** (Figure 5) is analogous to that in **2** since both complexes are dimers with a trans configuration of the ligands. The average terminal (2.030(8) Å) and bridging (2.186(18) Å) Sn-O bond lengths in **3** lie between values reported for monomers,[11-15,17,38] dimers,[18,19] and dinuclear tin(II) calixarenes.[16] The terminal Sn2-O2 distance is ca. 0.011 Å shorter than the terminal Sn1-O1 distance, both distances are similar to the sum of the covalent radii for a Sn-O single bond (2.03 Å).[39] A similar characteristic is observed in the bridging bonds of complex **3** as the Sn1-O4 and Sn2-O3 distances are shorter than the Sn1-O3 and Sn2-O4 distances by ca. 0.03 Å, resulting in the larger standard deviation in the average Sn-O distances for both the terminal and bridging Sn-O bonds.

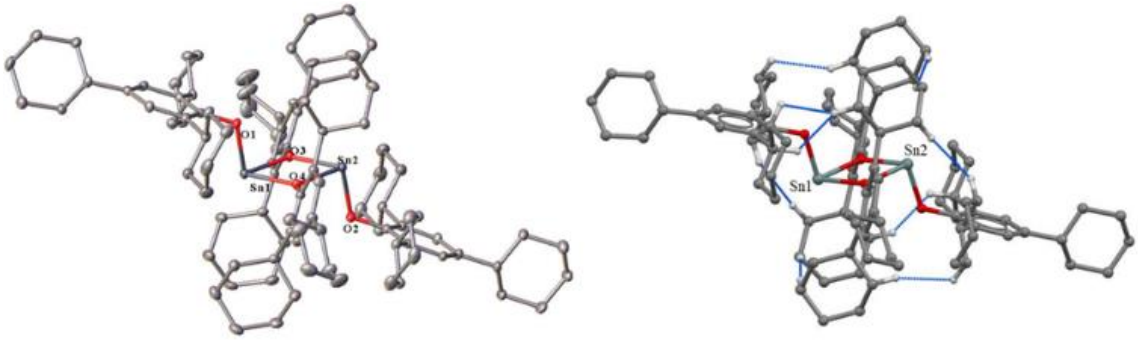

Figure 4. Left: Crystal structure of $[Sn(OC_6H_2\text{-}2,4,6\text{-}Cy_3)_2]_2$ (**3**) with thermal ellipsoids shown at 30%, hydrogen atoms and solvent molecules (toluene) not shown. R_1: 0.044. Sn1-Sn2 3.5907(7) Å. Sn1-O1 2.035(4) Å. Sn1-O3 2.199(4) Å. Sn1-O4 2.166(4) Å. Sn2-O2 2.024(4) Å. Sn2-O3 2.174(3) Å. Sn2-O4 2.203(4) Å. O1-Sn1-O3 95.82(14)°. O1-Sn1-O4 95.74(14)°. O3-Sn1-O4 69.65(12)°. O2-Sn2-O3 96.44(14)°. O2-Sn2-O4 96.45(14)°. O3-Sn2-O4 69.42(13)°. Right: Molecular model of **3** showing interligand H···H close contacts (≤ 2.4 Å) in blue, hydrogen atoms participating in close contacts are shown.

There are nine interligand H···H contacts in $[Sn(OC_6H_2\text{-}2,4,6\text{-}Cy_3)_2]_2$ (**3**) while there are sixteen in $[Ge(OC_6H_2\text{-}2,4,6\text{-}Cy_3)_2]_2$ (**2**). The decrease in the number of H···H close contacts is

likely due to the increase in M-O (M= Ge, Sn) bond distances, since the radii of Ge and Sn differ by 0.19 Å.[39] Multiple heteroleptic Sn(II) aryloxo dimers ligated by similar ligands to 2,4,6-tricyclohexylphenol have been reported,[10,18,19] with the majority of the homoleptic examples existing as monomers[10,11,18] and are stabilized by bulkier terphenyl or calixarene ligands[12-16,38] Reactions of the sterically unencumbering phenol HOC_6H_4-2-Me with $[Sn(NMe_2)_2]_2$ produced a polymeric structure $[Sn(\mu\text{-}OC_6H_4\text{-}2\text{-}Me)_2]_\infty$, while HOC_6H_3-2,6-Me_2 and HOC_6H_3-2,6-Pr^i_2 formed dimers, with the latter ligated by one NMe_2 group at one of the Sn(II) centers.[18] In contrast, the reaction of HOC_6H_3-2,6-Bu^t_2 with $[Sn(NMe_2)_2]_2$ afforded a monomer,[18] which is similar in structure to Lappert and Atwood's $M(OAr)_2$ monomers {M=Ge, Sn, Pb, Ar=-C_6H_2-2,4,6-Bu^t_3 or -C_6H_2-2,6-Bu^t_2-4-Me}.[11]

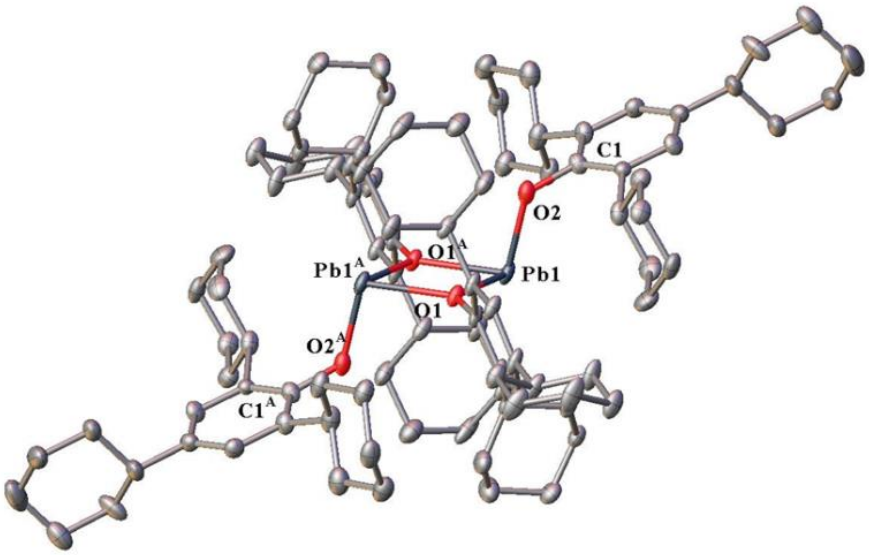

Figure 5. Crystal structure of dimeric $[Pb(OC_6H_2\text{-}2,4,6\text{-}Cy_3)_2]_2$ (**4**) with thermal ellipsoids shown at 30%, with hydrogen atoms and co-crystallized solvent molecules (toluene) not shown. R_1: 0.047. Selected distances (Å) and angles (°): Pb1-Pb1A 3.7725(7). Pb1-O2 2.117(6). Pb1-O1 2.284(4). Pb1-O1A 2.302(4). O1-Pb1-O2 93.87(17). O2-Pb1-O1A 98.65(17). O1-Pb1-O1A 69.34(15).

Available data for both monomeric[12,22,28] and dimeric[20,21] homoleptic Pb(II) aryloxides are limited, with the former representing the majority by a substantial (6:1) margin. A comparison of reported Pb-O bond lengths to those of **4** (Figure 5) shows that the terminal Pb-O bonds (av. 2.128(2) Å) in **4** are shorter than those in $Pb(OC_6H_3\text{-}2,6\text{-}(C_6H_3\text{-}2,6\text{-}Pr^i_2)_2)$,[22] presumably as a result of the steric requirements of the terphenyl ligand in comparison to those of the 2,4,6-tricyclohexylphenoxo ligand. The bond lengths in **4** are also similar to those in the monomeric 2- and 4-coordinate Pb(II) calixarenes [Pb(thiacalix[4]arene$^{t\text{-}Bu}(O)_2(OSi^iPr_3)_2$] and [Pb(thiacalix[4]arene$^{t\text{-}Bu}(O)_2(OBn)_2$] (Bn=benzyl), respectively.[12] The terminal (2.117(6) Å) and bridging (2.293(10) Å) Pb-O bonds in **4** are shorter than those in the dimer $[Pb(OC_6H_3\text{-}2,6\text{-}Ph_2)]_2$.[20]

Table 3. Comparison of selected average bond lengths (Å) in $[Pb(OC_6H_2\text{-}2,4,6\text{-}Cy_3)_2]_2$ (**4**) and $[Pb(OC_6H_3\text{-}2,6\text{-}Ph_2)]_2$.[20]

Complex	Pb···Pb	Terminal Pb-O	Bridging Pb-O	Terminal C-O	Bridging C-O
$[Pb(OC_6H_2\text{-}2,4,6\text{-}Cy_3)_2]_2$	3.7725(7)	2.117(6)	2.293(10)	1.458(9)	1.387(7)
$[Pb(OC_6H_3\text{-}2,6\text{-}Ph_2)]_2$[20]	3.833(8)	2.243(20)	2.347(26)	1.352(13)	1.369(9)

Both terminal and bridging C-O distances in $[Pb(OC_6H_3\text{-}2,6\text{-}Ph_2)]_2$ are shorter than those of complex **4** by ca. 0.11 Å and ca. 0.018 Å, respectively, despite the increase in size of the aryl ring substituents. However, the terminal and bridging Pb-O distances in $Pb(OC_6H_3\text{-}2,6\text{-}Ph_2)]_2$ are significantly longer than those in **4** by ca. 0.13 Å and ca. 0.054 Å, respectively, while the Pb···Pb separation is also longer by ca. 0.061 Å (Table 3). There are eight interligand H···H close (≤ 2.4 Å) contacts in $[Pb(OC_6H_2\text{-}2,4,6\text{-}Cy_3)_2]_2$ (**4**), while there is only one present in $[Pb(OC_6H_3\text{-}2,6\text{-}Ph_2)]_2$ (Figure 6).

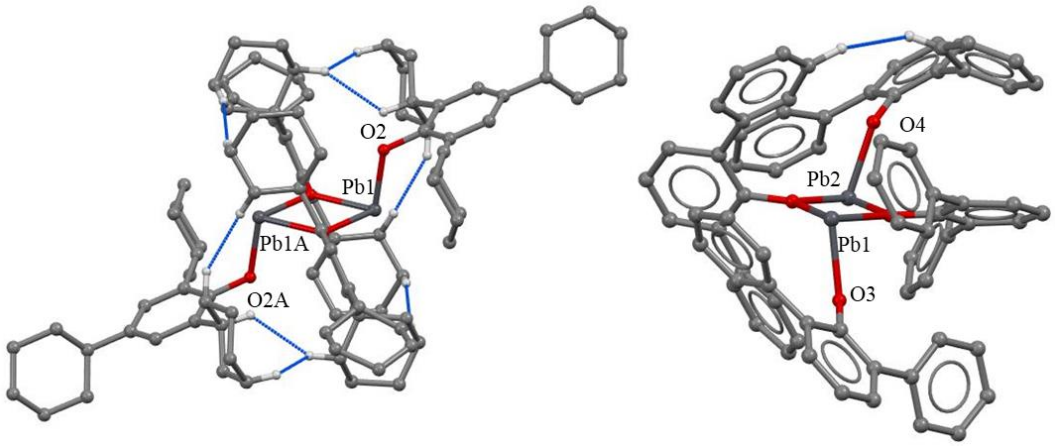

Figure 6. Interligand H···H close (≤ 2.4 Å) contacts in $[Pb(OC_6H_2\text{-}2,4,6\text{-}Cy_3)_2]_2$ (**4**, left) and $[Pb(OC_6H_3\text{-}2,6\text{-}Ph_2)]_2$ (right).[20] Interligand H···H close contacts are shown in blue, hydrogen atoms not in close contact are not shown.

Due to the greater inductive effect of the phenyl residue compared to cyclohexyl, in addition to the π-donating capability of the phenyl group, the expected Pb-O and Pb···Pb distances should be shorter in $[Pb(OC_6H_3\text{-}2,6\text{-}Ph_2)]_2$ than in **4** as a result of greater electrostatic interaction. However, we observe shorter distances in 4, and we propose that the increase in dispersion energy donor interactions upon exchanging the ortho substituents of $[Pb(OC_6H_3\text{-}2,6\text{-}Ph_2)]_2$ for cyclohexyl in $[Pb(OC_6H_2\text{-}2,4,6\text{-}Cy_3)_2]_2$ is responsible for the decrease in Pb-O and Pb···Pb distances, counter to the steric effects. Notably, the $[Pb(OC_6H_3\text{-}2,6\text{-}Ph_2)]_2$[20] complex of Van Zandt is the only other 3-coordinate Pb(II) aryloxide dimer reported in the Cambridge Crystallographic Structural Database.

Analysis of **3** via $^{119}Sn\{^1H\}$ NMR spectroscopy confirms that the structure remains associated in solution at room temperature. Only one ^{119}Sn signal is observed at -280 ppm. From literature values,[10,12,24] the expected shift of **3** should fall in the narrow range of +138 to -350 ppm observed for dimeric, 3-coordinate Sn(II) alkoxides and aryloxides (Table 4). A higher

temperature was not required to observe the ^{119}Sn NMR resonance since the solubility of **3** in deuterated toluene was sufficient to observe a signal at room temperature. Due to the temperature sensitive nature of ^{119}Sn NMR chemical shifts, the sample was not subjected to variable temperature ^{119}Sn{^{1}H} NMR studies.[10,24]

Table 4. ^{119}Sn NMR chemical shifts for two and three coordinate Sn(II) alkoxides and aryloxides. Data were collected at 25 ^{o}C, unless otherwise indicated. A comprehensive list of ^{119}Sn NMR parameters for compounds with Sn-Chalcogen bonds can be found in a reference 24.

Compound*	δ ^{119}Sn NMR (ppm)
[Sn(thiacalix[4]arene$^{t\text{-}Bu}$(O)$_2$(OBn)$_2$][12]	-647.3
[Sn(thiacalix[4]arene$^{t\text{-}Bu}$(O)$_2$(OSi^{i}Pr$_3$)$_2$][12]	-358.8
[Sn(μ-OSiPh$_3$)(OSiPh$_3$)]$_2$[10]	-338
[(DMP)Sn(μ-DMP)]$_2$·tol[18]	-293.5
Sn(OAr^{Dipp})$_2$[13]	-289.7
[Sn(μ-OC$_6$H$_2$-2,4,6-Cy$_3$)(OC$_6$H$_2$-2,4,6-Cy$_3$]$_2$ (**3**)	-280.3
[Sn(μ-O^{i}Pr)(OSiPh$_3$)]$_2$[10]	-246
[Sn(μ-OSiPh$_3$)(Cl)]$_2$[10]	-202
[Sn(μ-OPr^{i})(OPr^{i})]$_2$[10]	-200 (60 ^{o}C)
[Sn(μ-O^{i}Pr)(Cl)]$_2$[10]	-87
[Sn(OSiPh$_3$)(NMe$_2$)]$_2$[10]	-38

*DMP=dimethylpyridine; Ar^{Dipp}= -C$_6$H$_3$-2,6-(C$_6$H$_3$-2,6-Pr$^{i}_2$)$_2$; Bn=Benzyl

Few ^{207}Pb NMR data are available for Pb(II) aryloxides,[12,22,27,28,30,31] and data for 3-coordinate Pb(II) aryloxide dimers were nonexistent. The majority of reported ^{207}Pb NMR chemical shifts concern lead compounds of biological relevance,[29] such as the Calmodulin-type molecules which are bound to lead for toxicological studies. Coordination complexes of Pb(II) bound to EDTA have been heavily investigated.[28] While several complexes with structures similar to **4** have been reported (*vide supra)*, no ^{207}Pb NMR parameters were given. Therefore, we estimated the shift of complex **4** (*vide infra*) based on data for 2-coordinate aryloxides of Pb(II) (Table 5). For 2-coordinate examples, the most relevant structure is Pb(OC$_6$H$_3$-2,6-(C$_6$H$_3$-2,6-Pr$^{i}_2$)$_2$), which featured a

^{207}Pb NMR resonance at +1,070 ppm.[22] Several 4-coordinate Pb(II) calixarenes featured resonances in the range +111 ppm to +1,210 ppm.[12]

Table 5. Selected ^{207}Pb NMR parameters for Pb(II) aryloxides related species.

Compound*	δ ^{207}Pb NMR (ppm)
$[Pb(EDTA)]^{2-}$ [28]	2441
$Pb(EDTA\text{-}N_2)$ [28]	2189
$[Pb(OC_6H_2\text{-}Cy_3)_2]_2$ (**4**)	1541.0 (37 °C)
$[Pb(thiacalix[4]arene^{t\text{-}Bu}(O)_2(OSi^iPr_3)_2]$ [12]	1210
$Pb(OAr^{Dipp})_2$ [22]	1070.3
$Pb(OAr^N)_2$ [30]	141.5
$[Pb(thiacalix[4]arene^{t\text{-}Bu}(O)_2(OBn)_2]$ [12]	111
PbL [31]	-367

*L=(R,R)-(−)-N,N′-bis(3,5-di-tert-butylsalicylidene)-1,2-cyclo-hexanediamine); OAr^{Dipp}=OC_6H_3-2,6-(C_6H_3-2,6-Pr^i_2)$_2$); OAr^N=2,4-di-tert-butyl-6-(1,4,7-trioxa-10-azacyclododec-10-ylmethyl)phenyl); Bn=Benzyl; EDTA=ethylenediamine tetraacetate.

As in the ^{119}Sn NMR spectroscopic studies, ^{207}Pb NMR chemical shifts depend heavily upon coordination number, temperature, and the electronegativity of the ligating atoms.[27] Given that complex **4** has 3-coordinate Pb(II) atoms, we expected to observe the signal between +1,210 ppm and +100 ppm. However, the resonance was located further upfield than that of the two-coordinate complex Pb(OC_6H_3-2,6-(C_6H_3-2,6-Pr^i_2)$_2$) at +1,541 ppm. It should be noted that the signal for **4** was only observable above 37 °C. Complex **4** is dichroic, displaying a yellow color at room temperature and an orange-red color above 100 °C in both the solid state and in solution. The yellow color reappears upon returning to room temperature. A ^{207}Pb VT-NMR study was carried out due to its thermochromism and difficulty in locating the signal at room temperature. We observed the signal first at +1,541 ppm, which shifts further upfield in increments of approximately 6 ppm per 10 °C of temperature change (Figure 7) as the temperature increases.

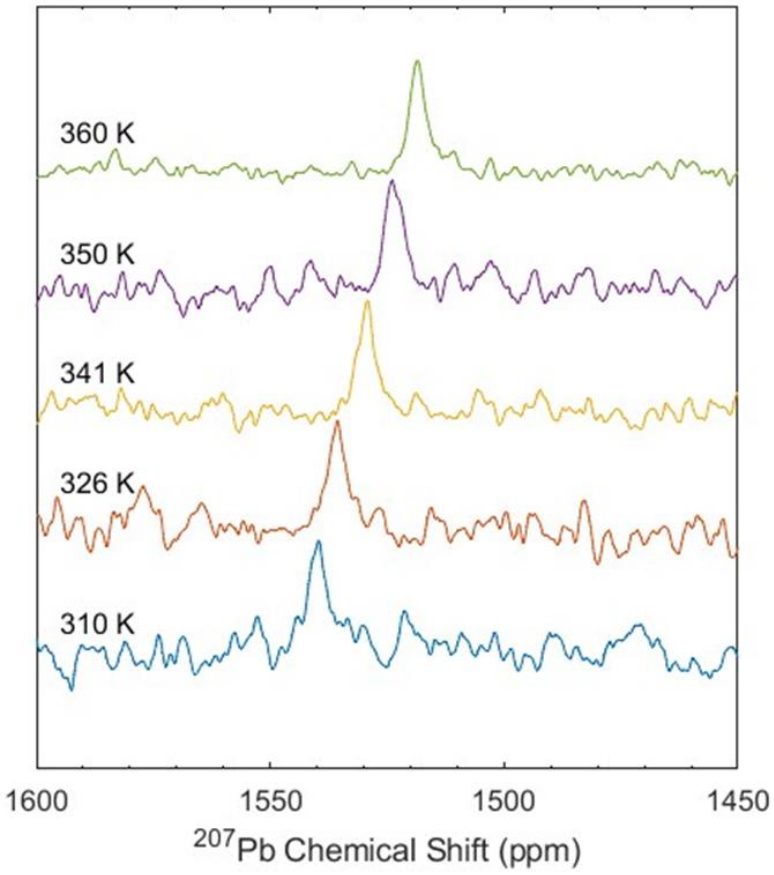

Figure 7. ^{207}Pb Chemical shift (ppm) for **4** as a function of temperature. ^{207}Pb (500 MHz, C_7D_8) (310 K) 1541 ppm, (326 K) 1534 ppm, (341 K) 1529 ppm, (350 K) 1524 ppm, (360 K) 1519 ppm.

Variable temperature UV-Vis studies were carried out in toluene to observe any absorption shifts or new absorptions that appeared over the temperature to range of 25 ^{o}C to 100 ^{o}C. However, no significant changes were observed aside from a decrease in the overall absorption at each data point (Figure S17). The observed thermochromism in compound **4** is similar to that of known Pb(II) aryloxo complexes, although few are known.[20,22]

3.4. CONCLUSION

Three divalent group 14 aryloxide complexes were synthesized via protonolysis of the metal bissilylamides with 2,4,6-tricyclohexylphenol. The complexes were characterized by X-Ray Crystallography, $^{119}Sn\{^{1}H\}$ NMR, and ^{207}Pb NMR spectroscopy. A unique cluster was isolated by stirring a solution of the germanium derivative **2** in the presence of the byproduct of its formation, namely $HN(SiMe_3)_2$, for 24 h. in hexanes. The new complex **1** is a rare Ge_6O_8 aryloxo cluster which is the only example of a Ge_xO_y cluster formed via rearrangement of a dimeric, 3-coordinate Ge(II) aryloxide featuring alkyl substituents in both ortho positions of the ligand aryl rings.

3.5. EXPERIMENTAL SECTION

General Considerations

All manipulations were carried out under anaerobic and anhydrous conditions by using standard Schlenk techniques or in a Vacuum Atmospheres OMNI-Lab drybox under an atmosphere of dry argon or nitrogen. Solvents were dried by the method of Grubbs and co-workers,[40] stored over potassium or sodium, and then degassed by the freeze−pump−thaw method. All physical measurements were made under strictly anaerobic and anhydrous conditions. Melting points of samples in flame-sealed capillaries were determined by using a Meltemp II apparatus equipped with a partial immersion thermometer. IR spectra were recorded as Nujol mulls between CsI plates on a PerkinElmer 1430 spectrometer. UV−vis spectra were recorded as dilute toluene solutions in 3.5 mL quartz cuvettes using an Olis 17 modernized Cary 14 UV−Vis−near-IR spectrophotometer. Unless otherwise stated, all materials were obtained from commercial sources and used as received. The phenol 2,4,6-tricyclohexylphenol was

donated to us by Toray Industries, Inc. The main group silylamides $M(N(SiMe_3)_2)_2$ (M=Ge, Sn, Pb) were synthesized by published procedures.[1,2]

$[Ge_6(\mu_3\text{-}O)_4(\mu_2\text{-}OC_6H_2\text{-}2,4,6\text{-}Cy_3)_4](NH_3)_{0.5}$ (**1**). To a 100 mL Schlenk flask were added 0.541 g (1.375 mmol) of $Ge(N(SiMe_3)_2)_2$ and 0.6242 g (1.833 mmol) of 2,4,6-tricyclohexylphenol at room temperature in ca. 70 mL of hexanes. The yellow solution was stirred for a further 24 h. without separation of the reaction byproducts ($HN(SiMe_3)_2$). The solvent was then removed under reduced pressure to leave a light-yellow residue which was washed with four ca. 5 mL portions of hexanes until the remaining solid had become colorless. The colorless solid was dissolved in ca. 10 mL of hot (ca. 100 ^oC) toluene and cooling in a ca. 5 ^oC refrigerator for 48 h. produced microcrystalline material. The mother liquor was transferred to a separate flask via filter cannula and the microcrystalline solids were redissolved in ca. 3 mL of hot (ca. 100 ^oC) toluene. Upon cooling in a ca. 5 ^oC fridge for 48 h. colorless rectangular blocks of **1** were collected to yield 0.0893 g (20.88%, calc. from Ge), mp 156-158 ^oC. ^{1}H-NMR (400 MHz, C_6D_6, 25 ^oC) 7.19 (2H), 7.14 (1H), 7.09 (1H), 7.07 (1H), 7.05 (2H), 7.03 (1H), 3.57 (1H), 3.17-2.80 (7H), 2.56 (4H), 2.05-1.26 (120H). UV-vis λ/nm ($\varepsilon/M^{-1}cm^{-1}$) 283 (10,300). IR (Nujol; $\tilde{\nu}/cm^{-1}$) 3610m (υN-H), 2950s, 2910s, 2840s, 1600w, 1490w, 1450s, 1370m, 1360m, 1265w, 1255s, 1230w, 1185m, 1165m, 1090s, 1010s, 945w, 890w, 950m, 930w, 800s, 720w, 690w, 650w, 550w, 455w, 380w, 310w.

$[Ge(OC_6H_2\text{-}2,4,6\text{-}Cy_3)_2]_2$ (**2**). To a 100 mL Schlenk flask were added 0.578 g (1.468 mmol) of $Ge(N(SiMe_3)_2)_2$ and 1.001 g (2.940 mmol) of 2,4,6-tricyclohexylphenol at room temperature. Hexanes (ca. 70 mL) were added via cannula and the reaction was stirred for 30 minutes. The solvent was removed under reduced pressure to leave a light-yellow

residue. The flask was heated to ca. 40 °C for 30 minutes to remove the remaining volatile material under reduced pressure. The solid residue was dissolved in ca. 20 mL of hot hexane (temp. ca. 55 °C) and left to stand at room temperature. Colorless crystals of **2** precipitated from the room temperature solution after 12 h. to yield 0.712 g (56.26%). mp 238-239 °C. ^{1}H-NMR (400 MHz, C_7D_8, 25 °C) 7.13-7.07 (8H), 3.49 (1H), 3.10 (6H), 2.52 (4H), 1.97-1.23 (120H). UV-vis λ/nm (ε/$M^{-1}cm^{-1}$) 283 (7863), 338 (3200). IR (Nujol; $\tilde{\nu}/cm^{-1}$) 2970s, 2940s, 2870s, 1460s, 1380s, 1360m, 1350m, 1265s, 1230w, 1190m, 1170m, 1090s, 1020s, 950w, 890w, 865w, 850w, 800s, 770w, 720w, 635w, 600w, 550w, 520w, 490w, 450w, 380w, 360w, 330w, 305w, 295w, 280w.

[Sn(OC$_6$H$_2$-2,4,6-Cy$_3$)$_2$]$_2$ (**3**). Complex **3** was prepared in a similar manner to **2** from 0.654 g (1.488 mmol) of Sn(N(SiMe$_3$)$_2$)$_2$ and 1.014 g (2.976 mmol) of 2,4,6-tricyclohexylphenol at room temperature. Colorless crystals of **3** precipitated from a ca. 30 mL toluene extract standing at room temperature for 12 h. Yield 0.587 g (49.45%). mp>250 °C. ^{1}H-NMR (400 MHz, C_7D_8, 25 °C) 7.11 (2H), 7.08-7.06 (2H), 6.96 (4H), 4.23 (1H), 4.09 (1H), 3.84 (1H), 3.40 (1H), 2.69 (4H), 2.47 (4H), 1.96-1.20 (120H). ^{119}Sn{^{1}H} NMR (400 MHz, C_6D_6) -280.3 ppm. UV-vis λ/nm (ε/$M^{-1}cm^{-1}$) 283 (7,970). IR (Nujol; $\tilde{\nu}/cm^{-1}$) 2960s, 2920s, 2850s, 1460s, 1445s, 1375s, 1360m, 1350m, 1300m, 1290m, 1270m, 1260s, 1230s, 1185s, 1140s, 1105s, 1190s, 1015s, 950w, 890w, 865m, 845m, 810s, 800s, 775m, 765m, 720w, 640w, 630w, 600w, 520w, 500w, 490w, 450w, 380w, 355w, 330w.

[Pb(OC$_6$H$_2$-2,4,6-Cy$_3$)$_2$]$_2$ (**4**). Complex **4** was prepared in a similar manner to **2** and **3** from 0.880 g (1.667 mmol) of Pb(N(SiMe$_3$)$_2$)$_2$ and 1.135 g (3.333 mmol) of 2,4,6-tricyclohexylphenol. Yellow crystals of **4** precipitated from a room temperature toluene

extract (ca. 30 mL) after 3 h. to yield 0.825 g (55.86%) of **4**. mp>250 ^{o}C. ^{1}H-NMR (400 MHz, C_7D_8, 25 ^{o}C) 7.13 (4H), 7.08 (2H), 6.97 (2H), 3.36 (1H), 2.69 (2H), 2.56 (4H), 2.12 (5H), 1.99-1.22 (120H). ^{207}Pb NMR (104.61 MHz, C_7D_8) (37 ^{o}C) 1541 ppm, (53 ^{o}C) 1534 ppm, (68 ^{o}C) 1529 ppm, (77 ^{o}C) 1524 ppm, (87 ^{o}C) 1519 ppm. UV-vis λ/nm ($\varepsilon/M^{-1}cm^{-1}$, 25 ^{o}C) 283 (15,511), 392 (2,559). IR (Nujol; $\tilde{\nu}/cm^{-1}$) 2980s, 2920s, 2850s, 2660m, 1600w, 1565w, 1490w, 1450s, 1375s, 1300s, 1290m, 1270s, 1260s, 1230s, 1190s, 1140s, 1110s, 1020s, 945w, 890w, 860s, 845m, 810s, 800s, 885m, 875m, 870m, 725m, 690w, 640w, 630w, 600w, 585w, 510w, 490w, 460w, 440w, 370w, 350w, 320w.

X-Ray Crystallographic Studies

Crystals of **2**, **3**, and **4** suitable for X-ray crystallographic studies were obtained from saturated toluene solutions upon standing for 24 h. Crystals of **1** were collected from a saturated toluene solution after 48 h. at 5 ^{o}C. The crystals were removed from the Schlenk tubes and immediately covered with a layer of hydrocarbon oil. Suitable crystals were selected, mounted on a nylon cryoloop, and then placed in the cold nitrogen stream of the diffractometer. Data for **2**, **3**, and **4** were collected at 90(2) K with Mo $K\alpha_1$ radiation (λ = 0.71073 Å) using a Bruker D8 Venture dual source diffractometer in conjunction with a CCD detector while data for **1** was collected at 190(2) K with Mo $K\alpha_1$ radiation (λ = 0.71073 Å). The collected reflections were corrected for Lorentz and polarization effects and for absorption by using Blessing's method as incorporated into the program SADABS.[41,42] The structures were solved by direct methods and refined with the SHELXTL (2012, version 6.1) or SHELXTL (2013) software packages.[43] Refinement was by full-matrix least-squares procedures, with all carbon-bound hydrogen atoms

included in calculated positions and treated as riding atoms. The thermal ellipsoid plots were drawn using OLEX2 software.[44]

Spectroscopic Parameters

^{1}H NMR spectra were collected on a Bruker Avance III spectrometer operating at 399.77 MHz (9.4T). Using a 30^{o} tip angle (4.62 μs), 16 free induction decays (FIDs) were averaged for each experiment with a 4.1s acquisition time and a repetition time of 5.1s. Variable temperature (VT) NMR experiments were collected on a Bruker Avance Neo console operating at 300.37 MHz (7.0T). Using a 30^{o} tip angle (5.00 μs), 16 free induction decays (FIDs) were averaged for each experiment with a 2.8s acquisition time and a repetition time of 3.78s. The sample was allowed to equilibrate at the temperature for 10 minutes before data collection was begun. Temperatures were calibrated on a sample of neat methanol. All spectra were internally referenced to the residual ^{1}H in the deuterated solvent (toluene). ^{119}Sn{^{1}H} (149.07 MHz) NMR spectra were collected on a Bruker Avance III spectrometer operating at 400 MHz (9.4 T). The ^{119}Sn{^{1}H} spectra were referenced using the IUPAC referencing recommendation[45] using the frequency ratios of the solvent residual protons and the spectra were collected using a 30^{o} tip angle (4.152 ms) with inverse-gated decoupling (WALTZ16) applied to the ^{1}H spins. 24576 FIDs were averaged with an acquisition time of 260 ms and a repetition time of 760 ms. The ^{207}Pb (104.61 MHz) NMR spectra were collected on a Bruker Avance spectrometer operating at 500 MHz (11.7T). ^{207}Pb NMR spectra were collected using a 90^{o} pulse (7.5 ms) with 494-2048 FIDs averaged, depending on the temperature of the sample. Each FID used a 327 ms acquisition time with a 250 ms recycle delay between successive acquisitions. The ^{207}Pb chemical shift was referenced externally to a 1M solution of

$Pb(NO_3)_2$ in D_2O. For the variable temperature measurements, the sample was allowed to equilibrate at the temperature for 10 minutes before data collection began. Spectrometer temperatures were calibrated on a sample of neat methanol.

ASSOCIATED CONTENT

Supporting Information.

The following files are available free of charge.

^{1}H-NMR, IR, and UV-Vis spectra for **1-3** and **5-6**, crystallographic data for **1-6** (PDF).

Accession Codes

CCDC 2226833-2226835, 2227111, 2242704-2242705 contain the supplementary crystallographic data for this paper. These data can be obtained free of charge via www.ccdc.cam.ac.uk/data_request/cif, or by emailing data_request@ccdc.cam.ac.uk, or by contacting The Cambridge Crystallographic Data Centre, 12 Union Road, Cambridge CB2 1EZ, UK; fax: +44 1223 336033.

AUTHOR INFORMATION

Corresponding Author

***Philip P. Power** – *Department of Chemistry, University of California, Davis, California 95616, United States;*[a] orcid.org/0000-0002-6262-3209; Email: pppower@ucdavis.edu

Authors

Connor P. McLoughlin – *Department of Chemistry, University of California, Davis, California 95616, United States;*[a] orcid.org/0000-0002-4707-1135

Derrick C. Kaseman– *Nuclear Magnetic Resonance Facility, University of California, One Shields Avenue, Davis, California 95616, United States.*[b]

Biochemistry and Biotechnology Group, Los Alamos National Laboratory, Los Alamos, New Mexico 87545, United States;[c] *orcid.org/0000-0003-2076-1264*

James C. Fettinger – *Department of Chemistry, University of California, Davis, California 95616, United States*;[a] orcid.org/0000-0002-6428-4909

Notes

There are no conflicts of interest to declare.

ACKNOWLEDGMENT

We thank the U.S. National Science Foundation for funding (Grant No. CHE-2152760).

REFERENCES

[1] Harris, D.H.; Lappert, M.F. Monomeric, Volatile Bivalent Amides of Group IV_B Elements, $M(NR^1{}_2)_2$ and $M(NR^1R^2)_2$ (M = Ge, Sn, or Pb; R^1=Me_3Si, R^2 = Me_3C). *J.C.S. Chem. Comm*., **1974**, *21*, 895-896.

[2] Veinot, A.J.; Stack, D.L.; Clyburne, J.A.C.; Masuda, J.D.; Dickie, D.A.; Chadha, U.; Kemp, R.A. Calcium, Strontium, Germanium, Tin, and Lead Bis(trimethylsilyl)amido Derivatives and 2,2,6,6-tetramethylpiperidido and n-Isopropylphenylamido Derivatives of Potassium and Calcium. *Inorg. Synth.*, **2018**, *37*, 1st Ed., Chapter 2, 26-31.

[3] Seifner, M.S.; Biegger, F.; Lugstein, A.; Bernardi, J.; Barth, S. Microwave-Assisted $Ge_{1-x}Sn_x$ Nanowire Synthesis: Precursor Species and Growth Regimes. *Chem. Mater*., **2015**, *27*, 6125–6130.

[4] Hernandez-Sanchez, B.; Boyle, T.J.; Pratt, H.D.; Rodriguez, M.A.; Brewer, L.N.; Dunphy, D.R. Morphological and Phase Controlled Tungsten Based Nanoparticles: Synthesis and Characterization of Scheelite, Wolframite, and Oxide Nanomaterials. *Chem. Mater*., **2008**, *20*, 6643–6656.

[5] Buck, M.R.; Biacchi, A.J.; Popczun, E.J.; Schaak, R.E. Polymer-Assisted Synthesis of Colloidal Germanium Telluride Nano-Octahedra, Nanospheres, and Nanosheets. *Chem. Mater*., **2013**, *25*, 2163–2171.

[6] Boyle, T.J.; Tribby, L.J.; Ottley, L.A.M.; Han, S.M. Synthesis and Characterization of Germanium Coordination Compounds for Production of Germanium Nanomaterials. *Eur. J. Inorg. Chem.*, **2009**, 5550–5560.

[7] Gerung, H.; Boyle, T.J.; Tribby, L.J.; Bunge, S.D.; Brinker, C.J.; Han, S.M. Solution Synthesis of Germanium Nanowires Using a Ge^{2+} Alkoxide Precursor. *J. Am. Chem. Soc.*, **2006**, *128*, 5244–5250.

[8] Sze, S.M. *Physics of Semiconductor Devices*, 2nd ed., John Wiley & Sons, New York, **2002**.

[9] Kanoun, M.; Busseret, C.; Poncet, A.; Souifi, A.; Baron, T.; Gautier, E. Electronic Properties of Ge Nanocrystals for Nonvolatile Memory Applications. *Solid State Electronics*, **2006**, *50*, 1310–1314.

[10] Wang, L.; Kefalidis, C.E.; Roisnel, T.; Sinbandhit, S.; Maron, L.; Carpentier, J.; Sarazin, Y. Structure vs ^{119}Sn NMR Chemical Shift in Three-Coordinated Tin(II) Complexes: Experimental Data and Predictive DFT Computations. *Organometallics*, **2015**, *34*, 2139–2150.

[11] Cetinkaya, B.; Gumrukcu, I.; Lappert, M.F.; Atwood, J.L.; Rogers, R.D.; Zaworotko, M.J. Bivalent Germanium, Tin, and Lead 2,6-Di-*tert*-butylphenoxides and the Crystal and Molecular Structures of $M(OC_6H_2Me\text{-}4\text{-}Bu^t_2\text{-}2,6)_2$ (M = Ge or Sn). *J. Am. Chem. Soc.*, **1980**, *102*, 2088-2089.

[12] Kuriki, R.; Kuwabara, T.; Ishii, Y. Synthesis and Structures of Diaryloxystannylenes and -plumbylenes Embedded in 1,3-diethers of Thiacalix[4]arene. *Dalton Trans*., **2020**, *49*, 12234-12241.

[13] Stanciu, C.; Richards, A.F.; Stender, M.; Olmstead, M.M.; Power, P.P. New Terphenylphenoxides of Group 13 and 14 Elements. *Polyhedron*, **2006**, *25*, 477–483.

[14] Hascall, T.; Rheingold, A.L.; Guzei, I.; Parkin, G. Subvalent Germanium and Tin Complexes Supported by a Dianionic Calixarene Ligand: Structural Characterization of *Exo* and *Endo* isomers of $[Bu^tcalix^{(TMS)2}]Ge$. *Chem. Commun.*, **1998**, *1*, 101-102.

[15] Hascall, T.; Pang, K.; Parkin, G. *Exo* and *Endo* Isomerism of Subvalent Tin and Germanium Complexes Derived from 1,3-diethers of p-tert-butylcalix[4]arene. *Tetrahedron*, **2007**, *63*, 10826-10833.

[16] McBurnett, B.G.; Cowley, A.H. Binuclear Tin and Germanium Calix[4]arenes. *Chem. Commun*., **1999**, *1*, 17–18.

[17] Smith, G.D.; Fanwick, P.E.; Rothwell, I.P. Synthesis, Structure, and Spectroscopic Properties of Germanium and Tin Compounds Containing Aryloxide Ligation: Comparison of Aryloxide Bonding to Group 4 and Group 14 Metal Centers. *Inorg. Chem*., **1990**, *29*, 3221-3226.

[18] Boyle, T.J.; Doan, T.Q.; Steele, L.M.; Apblett, C.; Hoppe, S.M.; Hawthorne, K.; Kalinich, R.M.; Sigmund, W.M. Tin(II) Amide/Alkoxide Coordination Compounds

for Production of Sn-based Nanowires for Lithium Ion Battery Anode Materials. *Dalton Trans*., **2012**, *41*, 9349-9364.

[19] Yasuda, H.; Choi, J.; Lee, S.; Sakakura, T. Structure of Dialkyltin Diaryloxides and their Reactivity Toward Carbon Dioxide and Isocyanate. *J. Organomet. Chem.*, **2002**, *659*, 133-141.

[20] Van Zandt, W.; Huffman, J.C.; Stewart, J.L. Synthesis and X-Ray Crystal Structure of a Lead Oxide Dimer, $Pb_2(\mu\text{-}O\text{-}2,6\text{-}Ph_2C_6H_3)_2(O\text{-}2,6\text{-}Ph_2C_6H_3)_2$. *Main Group Met. Chem.* **1998**, *21*, 237-240.

[21] Weinert, C.S.; Guzei, I.A.; Rheingold, A.L.; Sita, L.R. Heterocumulene Metathesis of $Pb[N(SiMe_3)_2]_2$. High-Yield Syntheses of the Heteroleptic Dimer $\{Pb[N(SiMe_3)_2(\mu\text{-}OSiMe_3)\}_2$ and the Novel Lead(II) Oxo Cluster $Pb_7(\mu_3\text{-}O)(\mu_4\text{-}O)(\mu\text{-}OSiMe_3)_{10}$. *Organometallics*, **1998**, *17*, 498-500.

[22] Rekken, B.D.; Brown, T.M.; Olmstead, M.M.; Fettinger, J.C.; Power, P.P. Stable Plumbylene Dichalcogenolate Monomers with Large Differences in Their Interligand Angles and the Synthesis and Characterization of a Monothiolato Pb(II) Bromide and Lithium Trithiolato Plumbate. *Inorg. Chem.*, **2013**, *52*, 3054-3062.

[23] Weinert, C.S.; Fenwick, A.E.; Fanwick, P.E.; Rothwell, I.P. Synthesis, Structures and Reactivity of Novel Germanium(II) Aryloxide and Arylsulfide Complexes. *Dalton Trans.*, **2003**, *4*, 532-539.

[24] Wrackmeyer, B. *Annual Reports on NMR Spectroscopy*, **1999**, *38*, 203-264.

[25] Weinert, C.S. ^{73}Ge Nuclear Magnetic Resonance Spectroscopy of Germanium Compounds. *ISRN Spectroscopy*, **2012**, 1-18.

[26] Takeuchi, T.; Takayama, T. ^{73}Ge NMR Spectroscopy of Organogermanium Compounds. *Annu. Rep. NMR Spectrosc.*, **2005**, *54*, 155-200.

[27] Wrackmeyer, B.; Horchler, K. ^{207}Pb-NMR Parameters. *Annu. Rep. NMR Spectrosc.*, **1989**, *22*, 249-306.

[28] Claudio, E.S.; ter Horst, M.A.; Forde, C.E.; Stern, C.L.; Zart, M.K.; Godwin, H.A. ^{207}Pb–^{1}H Two-Dimensional NMR Spectroscopy: A Useful New Tool for Probing Lead(II) Coordination Chemistry. *Inorg. Chem.*, **2000**, *39*, 1391-1397.

[29] Ronconi, L.; Sadler, P.J. Applications of Heteronuclear NMR Spectroscopy in Biological and Medicinal Inorganic Chemistry. *Coord. Chem. Rev.*, **2008**, *252*, 2239-2277.

[30] Agustin, D.; Rima, G.; Gornitzka, H.; Barrau, J. Ligand Transfer Reactions between Schiff Base Divalent Group 14 Element Species and Titanium, Nickel, Boron, and Phosphorus Halides. *Organometallics*, **2000**, *19*, 4276-4282.

[31] Wang, L.; Roşca, S.C.; Poirier, V.; Sinbandhit, S.; Dorcet, V.; Roisnel, T.; Carpentier, J.F.; Sarazin, Y. Stable Divalent Germanium, Tin and Lead Amino(ether)-phenolate Monomeric Complexes: Structural Features, Inclusion Heterobimetallic Complexes, and ROP catalysis. *Dalton Trans.*, **2014**, *43*, 4268–4286.

[32] Green, R.A.; Moore, C.; Rheingold, A.L.; Weinert, C.S. Formation and Structures of Germanium(II) Aryloxo/Oxo Clusters. *Inorg. Chem.*, **2009**, *48*, 7510–7512.

[33] Green, R.A.; Rheingold, A.L.; Weinert, C.S. *CSD Communication*, **2019**.

[34] Charton, M. Steric Effects. I. Esterification and Acid-Catalyzed Hydrolysis of Esters. *J. Am. Chem. Soc.*, **1975**, *97*, 1552-1556.

[35] Pinter, B.; Fievez, T.; Bickelhaupt, F.M.; Geerlings, P.; De Proft, F. On the Origin of the Steric Effect. *Phys. Chem. Chem. Phys.,* **2012**, *14*, 9846-9854.

[36] Grimme, S. Accurate Description of van der Waals Complexes by Density Functional Theory Including Empirical Corrections. *J. Comput. Chem.,* **2004**, *25*, 1463–1473.

[37] Grimme, S.; Huenerbein, R.; Ehrlich, S. On the Importance of the Dispersion Energy for the Thermodynamic Stability of Molecules. *ChemPhysChem*, **2011**, *12*, 1258−1261.

[38] Dickie, D.A.; MacIntosh, I.S.; Ino, D.D.; He, Q.; Labeodan, O.A.; Jennings, M.C.; Schatte, G.; Walsby, C.J.; Clyburne, J.A.C. Synthesis of the Bulky *m*-terphenyl Phenol Ar*OH (Ar* = C_6H_3-2,6-Mes_2, Mes = 2,4,6-trimethylphenyl) and the Preparation and Structural Characterization of Several of its Metal Complexes. *Can. J. Chem.*, **2008**, *86*, 20-31.

[39] Pyykkö, P.; Atsumi, M. Molecular Single-Bond Covalent Radii for Elements 1–118. *Chem. Eur. J.,* **2009**, *15*, 186-197.

[40] Pangborn, A.B.; Giardello, M.A.; Grubbs, R.H.; Rosen, R.K.; Timmers, F.J. Safe and Convenient Procedure for Solvent Purification. *Organometallics,* **1996,** *15*, 1518−1520.

[41] Sheldrick, G.M. *SADABS, Siemens Area Detector Absorption Correction*; Göttingen Universitat: Göttingen, Germany, **2008**; p 33.

[42] Blessing, R.H. An Empirical Correction for Absorption Anisotropy. *Acta Cryst. Sect. A: Found. Cryst*. **1995**, *51*, 33−38.

[43] Sheldrick, G.M.; *SHELXTL*, Ver. 6.1; Bruker AXS: Madison, WI, **2002**.

[44] Dolomanov, O.V.; Bourhis, L.J.; Gildea, R.J.; Howard, J.A.K.; Puschmann, H. OLEX2: A Complete Structure Solution, Refinement and Analysis Program. *J. Appl. Crystallogr.*, **2009**, *42*, 339−341.

[45] Harris, R.K.; Becker, E.D.; Cabral de Menezes, S.M.; Granger, P.; Hoffman, R.E.; Zilm, K.W. Further Conventions for NMR Shielding and Chemical Shifts (IUPAC Recommendations 2008). *Pure Appl. Chem.*, **2008**, *80*, 59-84.

Dispersion Energy Donor Ligand Supports the Isolation of Ge(II), Sn(II), and Lewis-Base Free Pb(II) Arylthiolate Dimers {M(SC_6H_2-2,4,6-Cy_3)$_2$}$_2$ (M = Ge, Sn, Pb; Cy = cyclohexyl)

Citation: C.P. McLoughlin, A.J. Witt, J.P.D. Nelson, H.M. Tuononen, P.P. Power. *Polyhedron*, **2024**, *252*, 116877, 1-9

4.1. ABSTRACT

We report the isolation of a series of cyclohexyl-substituted, homoleptic main group arylthiolates, {Ge(SC_6H_2-2,4,6-Cy_3)$_2$}$_2$ (**1**), {Sn(SC_6H_2-2,4,6-Cy_3)$_2$}$_2$ (**2**), and {Pb(SC_6H_2-2,4,6-Cy_3)$_2$}$_2$ (**3**), as well as an improved one-pot synthesis of the thiol HSC_6H_2-2,4,6-Cy (**4**) with increased purity and yield. The solid-state structures of compounds **1**–**3** show that the group 14 atoms are bridged by two thiolato ligands whose hydrocarbon substituents are in either *cis* (**1** and **2**) or *trans* (**3**) conformations. In solution, the Ge(II) derivative **1** exists as a mixture of dimeric *cis* and *trans* isomers or as the monomer Ge(SC_6H_2-2,4,6-Cy_3)$_2$, as inferred from ^{1}H NMR data. Contrary to a previous report of derivatives of the isopropyl-substituted thiol HSC_6H_2-2,4,6-Pr^i_3, which led to the formation of a Ge(IV) hydride, no such hydride was observed during the synthesis of **1**. Computational studies showed that the dimeric structure of **1** is stabilized by intramolecular dispersion interactions that are higher than those in similar systems employing the isopropyl-

substituted ligand, in agreement with the preferred formation of $HGe(SC_6H_2\text{-}2,4,6\text{-}Pr^i_3)_3$ over the putative dimer $\{Ge(SC_6H_2\text{-}2,4,6\text{-}Pr^i_3)_2\}_2$, although the exact mechanism leading to the hydride remains unclear. The corresponding Sn(II) derivative **2** is the first structurally characterized dimeric tin(II) thiolate. The Pb(II) species **3** is a rare example of a lead(II) arylthiolate that crystallizes in the absence of additional donor molecules.

4.2. INTRODUCTION

Despite well-established exchange reactions of the heavier group 14 silylamides[1,2] $M(N(SiMe_3)_2)_2$ (M = Ge, Sn, and Pb) with protic species to form a range of main group aryloxo compounds,[3–18] there are relatively few studies on low-coordinate (coordination number ≤ 3) Ge(II), Sn(II), and Pb(II) thiolates. The work of Lappert showed that the reactions of $M(N(SiMe_3)_2)_2$ with $HSC_6H_3\text{-}2,6\text{-}Pr^i_2$ (Pr^i = isopropyl) and $HSC_6H_2\text{-}2,4,6\text{-}Bu^t_3$ (Bu^t = *tert*-butyl) gave trimeric complexes $\{M(SC_6H_3\text{-}2,6\text{-}Pr^i_2)_2\}_3$ (M = Sn and Pb) as well as monomers $M(SC_6H_3\text{-}2,4,6\text{-}Bu^t_3)_2$ (M = Ge, Sn), and Pb.[19] Later studies also provided crystallographic data for Ge(II) arylthiolates, but the variety of characterized systems is limited to only a few anionic[20] and monomeric[21] species of the formula $[Ge(SC_6H_5)_3]^-$ and $Ge(SAr)_2$ (Ar = terphenyl-based ligand). In a similar fashion, X-ray crystallographic data on low-coordinate Sn(II) arylthiolates concern only some Sn(II) terphenyl complexes with the formula $Sn(SAr)_2$ (Ar = terphenyl-based ligand),[21] the structures reported by Lappert,[19] and two independent reports on the structure of the anion $[Sn(SC_6H_5)_3]^-$ with two different counter-cations.[22,23] In contrast, Pb(II) thiolates are notoriously difficult to crystallize in the absence of additional donors due to their tendency to polymerize, resulting in an inherent insolubility in hydrocarbon solvents.[24] Accordingly, only a few molecular Pb(II) arylthiolates free from Lewis-base stabilization have been structurally characterized in the

solid state. Besides the work of Lappert,[19] these include species analogous to those of the lighter congeners, that is to say, the anion $[Pb(SC_6H_5)_3]^-$[22,25,26] and the monomers $Pb(SAr)_2$ (Ar = terphenyl-based ligand),[17,21] as well as the dication $[Pb(SC_6H_4\text{-}4\text{-}NMe_3)_3]^{2+}$ and its trimeric analogue $[\{Pb(SC_6H_4\text{-}4\text{-}NMe_3)_2\}_3]^{6+}$.[27,28]

In light of the existing structural data on low-coordinate Ge(II), Sn(II), and Pb(II) arylthiolates, we chose to try to isolate the first dimeric arylthiolate complexes of group 14 elements. To do this, a phenylthiol with cyclohexyl (Cy) substituents was chosen as they provide steric shielding[29,30] to an extent that lies roughly between that of isopropyl and *tert*-butyl groups that allowed the synthesis of the trimers $\{M(SC_6H_3\text{-}2,6\text{-}Pr^i_2)_2\}_3$ (M = Sn and Pb) and the monomers $M(SC_6H_3\text{-}2,4,6\text{-}Bu^t_3)_2$ (M = Ge, Sn, and Pb), respectively.[19] In addition, the three substituents Pr^i, Bu^t, and Cy have different dispersion energy donor properties,[31] with the bulky and spherical Bu^t substituents providing slightly stronger interactions than the smaller Pr^i and Cy groups.[32] We found that the use of cyclohexyl-substituted thiol led to the desired dimers $\{M(SC_6H_2\text{-}2,4,6\text{-}Cy_3)_2\}_2$ (M = Ge (**1**), Sn (**2**), and Pb (**3**)). These crystallize from their benzene or toluene solutions in good yield, thereby establishing the first structurally characterized series of homoleptic and dimeric M(II) arylthiolates. The detailed structural study of compounds **1**–**3** is augmented with a spectroscopic analysis of the behavior of the Ge(II) derivative **1** in solution, corroborated with computational investigations and a reactivity study of the new dimeric Sn(II) arylthiolate **2** with phenylacetylene and pinacolborane. Finally, the thiol used in the synthesis of **1**–**3**, $HSC_6H_3\text{-}2,4,6\text{-}Cy_3$ (**4**), has previously been employed as a hydrogen atom transfer catalyst,[33] but it has not been used as a ligand. An alternative synthetic method to **4** is reported herein that gives the thiol in excellent (80 %) yield and with high synthetic purity.

4.3. RESULTS AND DISCUSSION

Synthesis and Structure of Ge(II) Dimer

The reaction between two equivalents of the thiol HSC_6H_2-2,4,6-Cy_3 with one equivalent of $Ge(N(SiMe_3)_2)_2$ gave the Ge(II) derivative $\{Ge(SC_6H_2\text{-}2,4,6\text{-}Cy_3)_2\}_2$ (**1**) as a monosolvate from benzene solution at room temperature. Its structure features C_2 symmetry and a *cis* arrangement of the arylthiolato ligands, with the cyclohexyl residues of the bridging ligands facing each other above and below the Ge_2S_2 core (Figure 1). At 2.2753(8) Å, the Ge1–S1 bond distance is significantly shorter than the bridging Ge1–S2 and Ge1–S2A distances, 2.4105(8) and 2.5049(8) Å, respectively. However, at 1.802(3) and 1.798(3) Å, the S1–C1 and the S2– C25 distances involving the terminal and bridging ligands, respectively, are statistically identical. The Ge atom displays a distorted trigonal pyramidal geometry, with the sum of bond angles equaling 268.63(5)°. The C1–S1–Ge1 angle is 89.89(9)°, while the C25–S2–Ge1 angle involving the bridging ligand is significantly wider, 106.67(10)°.

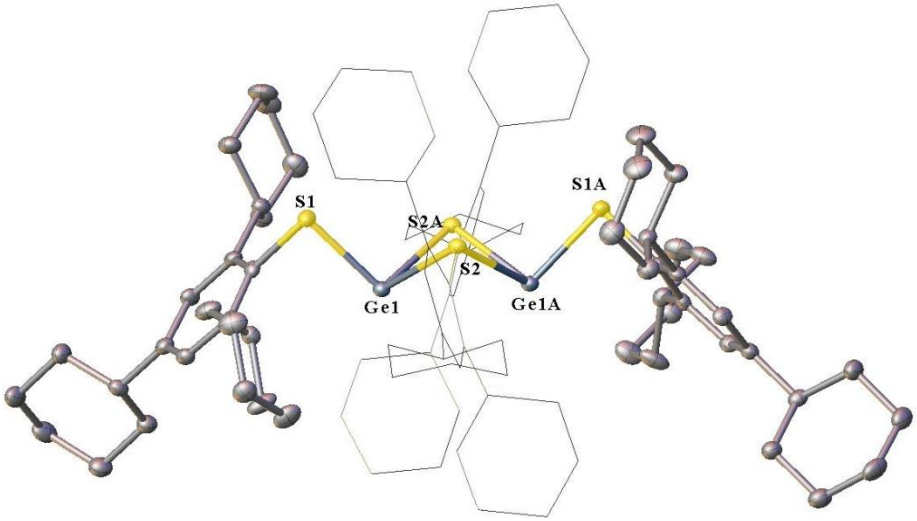

Figure 1. Thermal ellipsoid (50 %) plot of $\{Ge(SC_6H_2\text{-}2,4,6\text{-}Cy_3)_2\}_2$ (**1**). Two ligands are shown wireframe format and all hydrogen atoms and the molecule of crystallization solvent (benzene) are

omitted for clarity. Selected distances (Å) and angles (°): Ge1–S1 2.2753(8), Ge1–S2 2.4105(8), Ge1–S2A 2.5049(8), Ge1···Ge1A 3.26343(10), S1–C1 1.802(3), S2–C25 1.798(3), S1–Ge1–S2 98.27(3), S1–Ge1–S2A 97.98(3), S2–Ge1–S2A 72.38(3), C1–S1–Ge1 89.89(9), C25–S2–Ge1 106.67(10), C25–S2–Ge1A 121.65(10), Ge1–S2–Ge1A 83.17(3), $\Sigma_{\angle}$ Ge1 268.63(5).

Because no structures of dimeric Ge(II) arylthiolates have been reported to date, metrical comparisons of distances and angles were made with data for Ge(II) arylthiolate monomers[21,34] as well as for dimers with alkyl-[35] and silylthiolato[3] ligands (Table 1). The terminal Ge1–S1 distance in **1** is shorter than that in $\{Ge(SSi(Ph_3))_2\}_2$[3] but statistically identical with the average terminal Ge–S distance in $\{Ge(SBu^t)_2\}_2$ that carries a large standard uncertainty.[35] Interestingly, the terminal Ge1–S1 distance in **1** differs less than 0.2 Å from Ge–S distances in many monomeric Ge(II) arylthiolates with sterically encumbering terphenyl ligands,[21] with the short Ge–S bonds in the structure of $Ge(SC_6H_3\text{-}2,6\text{-}(C_6H_2\text{-}2,4,6\text{-}Pr^i_3)_2)_2$ making a noticeable exception. The bridging Ge1–S2 and Ge1–S2A distances in **1** differ by nearly 0.1 Å but their average value is similar to that in $\{Ge(SSi(Ph_3))_2\}_2$,[3] while longer than that in $\{Ge(SBu^t)_2\}_2$.[35] The S–C distances in **1** are shorter than those in alkyl-substituted dimers,[3,35] and much closer to those in monomeric Ge(II) arylthiolates with similar type of S–C bonds.[21] Compound **1** features the narrowest C–S–Ge angle of all related structurally characterized Ge(II) thiolates and contains the most puckered Ge_2S_2 core of all dimeric structures,[3,21,34,35] presumably owing to the spatial requirements of its sterically encumbering ligands in a *cis* arrangement.

Table 1. Selected Distances (Å) and Angles (°) for $\{Ge(SC_6H_2\text{-}2,4,6\text{-}Cy_3)_2\}_2$ (1) and in Related Ge(II) Thiolates

Compound	Ge–S[b]	Ge–μS	C–S[b]–Ge	S[b]–Ge–S[c]	μS-Ge–μS	Ge–μS–Ge	S–C
$\{Ge(SC_6H_2\text{-}2,4,6\text{-}Cy_3)_2\}_2$ (**1**)	2.2753(8)	2.4105(8) 2.5049(8)	89.89(9)	97.98(3) 98.27(3)	72.38(3)	83.17(3)	1.798(3) 1.802(3)
$\{Ge(SBu^t)_2\}_2$[35]	2.260(4) 2.267(4)	2.388(4)[a] 2.465(4)[a]	102.8(3) 104.1(3)	88.01(9)[a] 96.31(9)[a]	85.37(5) 85.60(9)	91.19(9) 91.46(9)	1.855(4)[a]
$\{Ge(SSi(Ph_3))_2\}_2$[3]	2.321(1)	2.472(1) 2.4571(9)	99.95(5)*	92.68(4) 94.12(4)	78.43(4)	88.43(3)	-
$Ge(SC(SiMe_3)_3)_2$[34]	2.2272(6) 2.2274(6)	-	108.44(6) 109.46(7)	90.25(2)	-	-	1.865(2) 1.869(2)
$Ge(SC_6H_3\text{-}2,6\text{-}(C_6H_2\text{-}2,6\text{-}Pr^i_2)_2)_2$[21]	2.284(4)	-	113.58(5)	81.26(2)	-	-	1.778(1)
$Ge(SC_6H_3\text{-}2,6\text{-}(C_6H_2\text{-}2,4,6\text{-}Me_3)_2)_2$[21]	2.2636(5) 2.2657(6)	-	99.74(5) 106.04(6)	88.68(2)	-	-	1.784(2) 1.785(2)
$Ge(SC_6H_3\text{-}2,6\text{-}(C_6H_2\text{-}2,4,6\text{-}Pr^i_3)_2)_2$[21]	2.211(2) 2.218(3)	-	114.8(3) 116.9(3)	81.8(1)	-	-	1.756(8) 1.778(8)
$Ge(SC_6H_1\text{-}2,6\text{-}(C_6H_2\text{-}2,4,6\text{-}Pr^i_3)_2\text{-}3,5\text{-}Pr^i_2)_2$[21]	2.2940(6)	-	119.42(6)	77.01(2)	-	-	1.782(2)

[a]Average value. [b]Terminal S atom if dimeric structure. [c] Bridging S atom if dimeric structure. *Silicon atom in place of carbon.

Since we have previously investigated the importance of interligand H···H close (less than the sum of van der Waals radii of two hydrogen atoms, *ca.* 2.5 Å)[36] contacts to the stability of main group[37] and transition metal aryloxides,[38] a similar analysis was conducted for **1**. Interestingly, despite the favorable face-on orientation of the ligands, there are just five interligand H···H close contacts (≤ 2.5 Å) and this value remains unchanged if the threshold is increased to 2.6 Å (Figure 2).

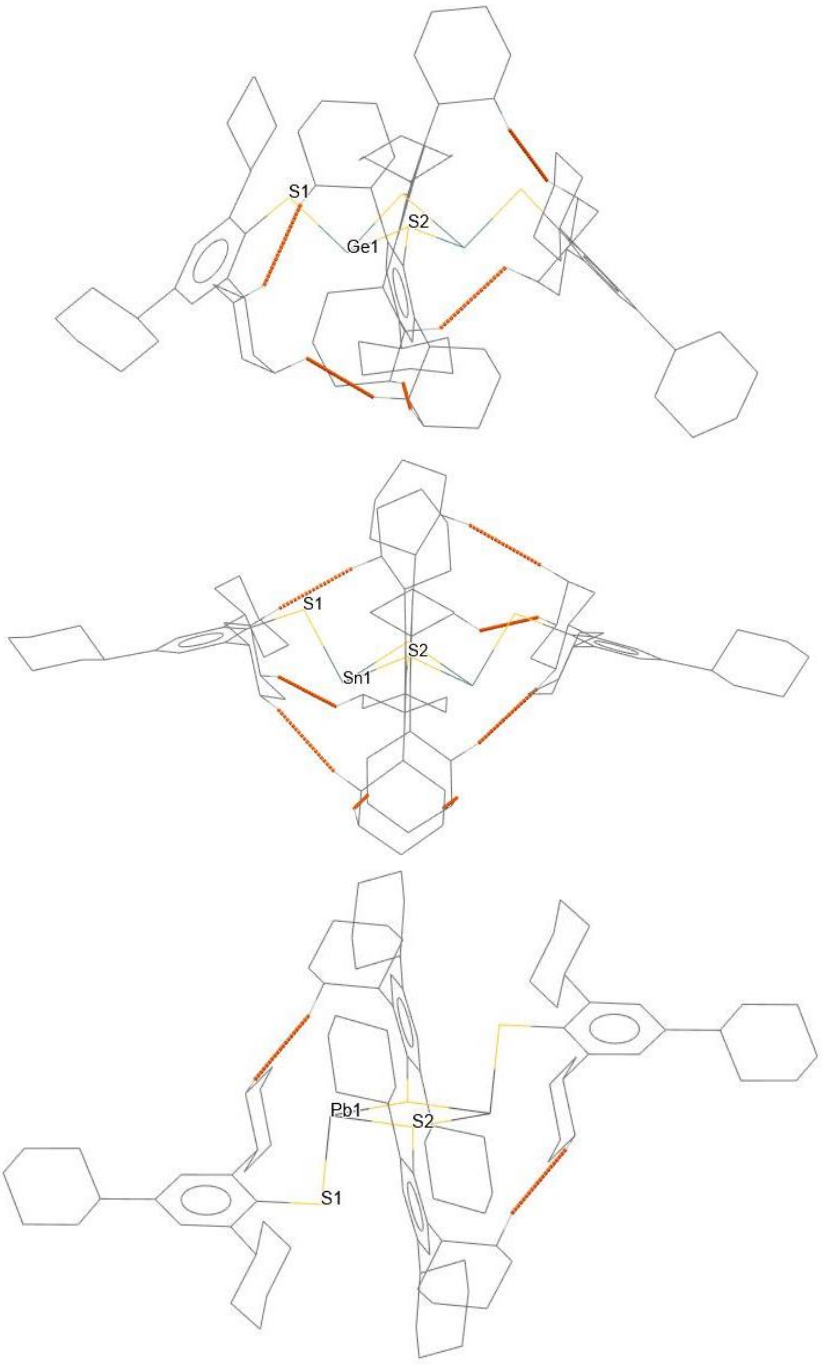

Figure 2. Wireframe structures of **1** (top), **2** (middle), and **3** (bottom) illustrating the location of close (≤ 2.5 Å) interligand H···H contacts (orange dashed lines) from two orientations. Crystallization solvents (benzene and toluene) and hydrogen atoms not involved in the visualized H···H contacts are omitted for clarity.

NMR Spectroscopy and DFT Calculations

The *in situ* room temperature ^{1}H NMR spectrum of **1** in C_6D_6 indicates that its solid-state structure is not retained in solution. Instead, a mixture of species is observed, which presumably contains *cis* and *trans* isomers of **1** and the monomer $Ge(SC_6H_2\text{-}2,4,6\text{-}Cy_3)_2$ (Equation 1), with the *cis* isomer being the preferred species.

$$2\ Ge(N(SiMe_3)_2)_2 + 4\ HSC_6H_2\text{-}2,4,6\text{-}Cy_3 \rightarrow x\ cis\text{-}\{Ge(SC_6H_2\text{-}2,4,6\text{-}Cy_3)_2\}_2 + y\ trans\text{-}\{Ge(SC_6H_2\text{-}2,4,6\text{-}Cy_3)_2\}_2 + z\ Ge(SC_6H_2\text{-}2,4,6\text{-}Cy_3)_2 + 4\ HN(SiMe_3)_2$$

Scheme 1. Proposed equilibrium between the monomeric germylene and the isomers of **1** in saturated solution.

For comparison, a singlet signal in the ^{29}Si spectrum of the dimer $\{Ge(SSi(Ph_3))_2\}_2$ indicated that it dissociates to $Ge(SSi(Y5Ph_3))_2$ monomers in $CDCl_3$ with no evidence of dynamic behavior at room temperature,[3] while the presence of both *cis* and *trans* isomers was reported for the related Ge(IV) species $(PhH_2C)(NR_2)Ge(\mu\text{-}S)_2Ge(NR_2)(CH_2Ph)$ (R = $SiMe_3$) in toluene.[39]

Initially, the presence of three separate signals in the aryl region of the ^{1}H NMR spectrum of a freshly prepared sample of **1** suggested that a Ge(IV) hydride $HGe(SC_6H_2\text{-}2,4,6\text{-}Cy_3)_3$, similar to that reported with the ligand $HSC_6H_2\text{-}2,4,6\text{-}Pr^i_3$,[18] may have formed. For $HGe(SC_6H_2\text{-}2,4,6\text{-}Pr^i_3)_3$, the hydride signal appears at 5.73 ppm and integrates to exactly 1 H, with the remaining signals observed in the ^{1}H NMR spectrum being fully consistent with the structural characterization confirmed by X-ray crystallography.[18] In contrast, no signals were observed in the ^{1}H NMR spectrum of **1** around 5.7 ppm and the signals observed in the aryl region could not be rationalized by assuming a single species, namely the hydride $HGe(SC_6H_2\text{-}2,4,6\text{-}Cy_3)_3$. Consequently, a second sample of **1** was synthesized, crystallized, and structurally characterized by X-ray diffraction. The ^{1}H NMR spectrum of the new sample matched that of the original, with three separate signals in

the aryl region. To assign these signals, the reaction between $Ge(N(SiMe_3)_2)_2$ and HSC_6H_2-2,4,6-Cy_3 was monitored *via* ^{1}H NMR spectroscopy to reference the observed signals to the $HN(SiMe_3)_2$ formed in the reaction, thereby allowing the determination of which of the aryl signals observed was the residual solvent signal of C_6D_6. Setting the methine signal at 3.67 ppm to exactly 4 H, followed by integration of the remaining signals, gave a good match with the dimeric structure of *cis* **1** for all but three key signals in the spectrum. Two of these reside in the aryl region, at 6.97 and 6.12 ppm, integrating to *ca.* 1.50 and 1.30 H, respectively, while the third one involves the entire cyclohexyl methylene region spanning from 1.20 to 2.03 ppm and integrating to 162 H. Provided the reaction yields no side products, such as the hydride $HGe(SC_6H_2$-2,4,6-$Cy_3)_3$, the integration of the methyl signal for $HN(SiMe_3)_2$ at 0.09 ppm should afford 72 hydrogens, following the employed stoichiometry (Eq 1). Setting the key methyl signal to exactly 72 H led to the same integration ratios observed earlier, which could be explained by assuming the presence of both *cis* and *trans* isomers of **1**. The original assumption was that the signal at 6.12 ppm corresponds to the monomeric germylene. However, a VT-study of a dilute, crystalline sample of **1** revealed that the signal at 6.12 ppm was no longer present, and that this peak in the *in situ* spectrum indicates the formation of an unidentifiable intermediate that is in equilibrium with the desired dimeric species **1**. Instead, the spectrum of the dilute sample of **1** showed a single aryl resonance at 7.20 ppm that did not change in intensity as a function of temperature and is thereby assigned to the monomeric germylene. These data suggest that at low concentrations, the structure of **1** is monomeric, while a dimeric structure is favored in saturated solutions.

To further investigate the different isomers of **1** and the monomeric germylene (Scheme 1), all three species in question were examined computationally with density functional theory (DFT) using a universal solution model (SMD). The results (Figure 3) show that the dimerization of the

germylene monomer $Ge(SC_6H_2\text{-}2,4,6\text{-}Cy_3)_2$ is favored by 43 kJ mol^{-1}, while the *cis* isomer of **1** is energetically comparable with the *trans* isomer. Thus, provided that the *cis*-*trans* isomerization has a sizable kinetic barrier owing to the bulky substituents, while that associated with the exchange of bridging and terminal ligands is smaller, the calculations provide support for the coexistence of the *cis* and *trans* isomers of **1** in solution. Furthermore, as implied by the calculated energies excluding empirical dispersion correction (Figure 3), the dimerization is greatly driven by dispersion energy stabilization, whose effect is most likely overestimated as the calculations do not consider ligand dynamics (rotation of substituents) in solution. Even though the *cis* isomer of **1** is certainly the preferred species in the solid state, the monomer-dimer balance is less clear in solution. Complex **1** can dissociate to monomers at low concentrations provided that the associated energy barrier is of appropriate height.

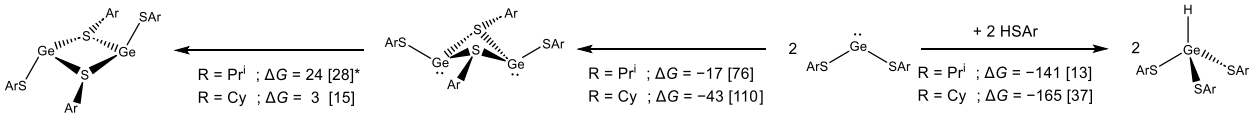

Figure 3. Calculated Gibbs energies (benzene, 298.15 K, kJ mol^{-1}) of reactions involving dimerization of monomeric Ge(II) arylthiolates $Ge(SAr)_2$ (Ar = $-C_6H_2\text{-}2,4,6\text{-}R_3$) and their oxidative addition with the arythiol HSAr. Values in square brackets exclude empirical dispersion correction. * The C_i-symmetric *trans* isomer of $\{Ge(SC_6H_2\text{-}2,4,6\text{-}Pr^i_3)_2\}_2$ has one imaginary frequency leading to puckering of the Ge_2S_2 ring.

As discussed above, a reaction between $Ge(N(SiMe_3)_2)_2$ and $HSC_6H_2\text{-}2,4,6\text{-}Pr^i_3$ has been reported to yield the Ge(IV) hydride $HGe(C_6H_2\text{-}2,4,6\text{-}Pr^i_3)_3$ irrespective of stoichiometry (1:2 or 1:3), with no indication of the formation of the dimer $\{Ge(SC_6H_2\text{-}2,4,6\text{-}Pr^i_3)_2\}_2$ or the monomer $Ge(SC_6H_2\text{-}2,4,6\text{-}Pr^i_3)_2$.[18] In contrast, a reaction between $Ge(N(SiMe_3)_2)_2$ and the selenol $HSeC_6H_2\text{-}2,4,6\text{-}Me_3$ is known to form the tetra-substituted Ge(IV) species $Ge(SeC_6H_2\text{-}2,4,6\text{-}Me_3)_4$.[40] The

formation $Ge(SeC_6H_2\text{-}2,4,6\text{-}Me_3)_4$ was monitored *via* ^1H NMR and ^{77}Se NMR spectroscopy and two intermediates were detected along with the formation of H_2 gas. The first intermediate was identified as the germylene $Ge(SeMes)_2$, which reacts with another equivalent of the selenol to form a Ge(IV) hydride $HGe(SeC_6H_2\text{-}2,4,6\text{-}Me_3)_3$ and, ultimately, $Ge(SeC_6H_2\text{-}2,4,6\text{-}Me_3)_4$.[40] We therefore calculated the energies associated with the formation of the Ge(IV) hydride and compared the results obtained for the two related ligands $–SC_6H_2\text{-}2,4,6\text{-}Cy_3$ and $–SC_6H_2\text{-}2,4,6\text{-}Pr^i_3$. As shown in Figure 3, the dimerization of $Ge(SC_6H_2\text{-}2,4,6\text{-}Pr^i_3)_2$ is favored only by 17 kJ mol^{-1} in solution (*cf.* 43 kJ mol^{-1} for $Ge(SC_6H_2\text{-}2,4,6\text{-}Cy_3)_2$), with a significantly smaller dispersion component compared to its cyclohexyl analogue. As ligand dynamics are not accounted for, the stability of the Ge(IV) hydrides in solution is likely slightly overestimated. Irrespective of this, the hydrides are clearly the thermodynamically most favored products regardless of the identity of the substituent on the aryl ligand (Pr^i or Cy). In the publication reporting the synthesis of $HGe(SC_6H_2\text{-}2,4,6\text{-}Pr^i_3)_3$, the formation of a Ge(IV) hydride over other possible products was rationalized by assuming that the rate of insertion of the Ge(II) atom to the H–S bond in the thiol is faster than the rate of proton transfer from the thiol to the amide.[18] Our calculations show that the transition state for the insertion of $Ge(SC_6H_2\text{-}2,4,6\text{-}Pr^i_3)_2$ or $Ge(SC_6H_2\text{-}2,4,6\text{-}Cy_3)_2$ to the H–S bond in $HSC_6H_2\text{-}2,4,6\text{-}Pr^i_3$ or $HSC_6H_2\text{-}2,4,6\text{-}Cy_3$, respectively, has a Gibbs energy of activation of *ca.* 120 kJ mol^{-1} irrespective of the substituent, which disagrees with the experimental reaction rate indicating completion within minutes. Hence, taking all the above into account, the results from DFT calculations support the notion that dispersion interactions play a greater role in cyclohexyl-substituted Ge(II) arylthiolates over the corresponding isopropyl-substituted derivatives, rendering the formation of the dimer $\{Ge(SC_6H_2\text{-}2,4,6\text{-}Pr^i_3)_2\}_2$ less probable than that of **1**, both in solution and in the solid state, as observed experimentally. Furthermore, even though

the Ge(IV) hydrides $HGe(SC_6H_2\text{-}2,4,6\text{-}Pr^i_3)_3$ and $HGe(SC_6H_2\text{-}2,4,6\text{-}Cy_3)_3$ are calculated to be thermodynamically the most favored products in solution, they are unlikely to form through the addition of a Ge(II) monomer to the H–S bond in the corresponding arylthiol, as suggested earlier.[18] At this point, the mechanism for the formation of $HGe(SC_6H_2\text{-}2,4,6\text{-}Pr^i_3)_3$ is unclear but it must involve a process that is unattainable for the heavier cyclohexyl ligand $HSC_6H_2\text{-}2,4,6\text{-}Cy_3$ because $HGe(SC_6H_2\text{-}2,4,6\text{-}Cy_3)_3$ was not observed in our experiments.

Synthesis and Structures of Sn(II) and Pb(II) Dimers

The Sn(II) derivative $\{Sn(SC_6H_2\text{-}2,4,6\text{-}Cy_3)_2\}_2$ (**2**) is the first dimeric Sn(II) arylthiolate. It was synthesized in an analogous manner to **1** and crystallizes readily as large, colorless blocks from benzene solution. Unlike **1**, the *in situ* room temperature ^{1}H NMR spectrum of **2** in C_6D_6 shows a single signal in the aryl region, suggesting the presence of only one species. However, all signals in the ^{1}H NMR spectrum are broadened, indicating a dynamic process that equalizes the signals of the bridging and terminal ligands. Unfortunately, no ^{119}Sn NMR signal was detected at room temperature and variable temperature NMR studies were not performed.

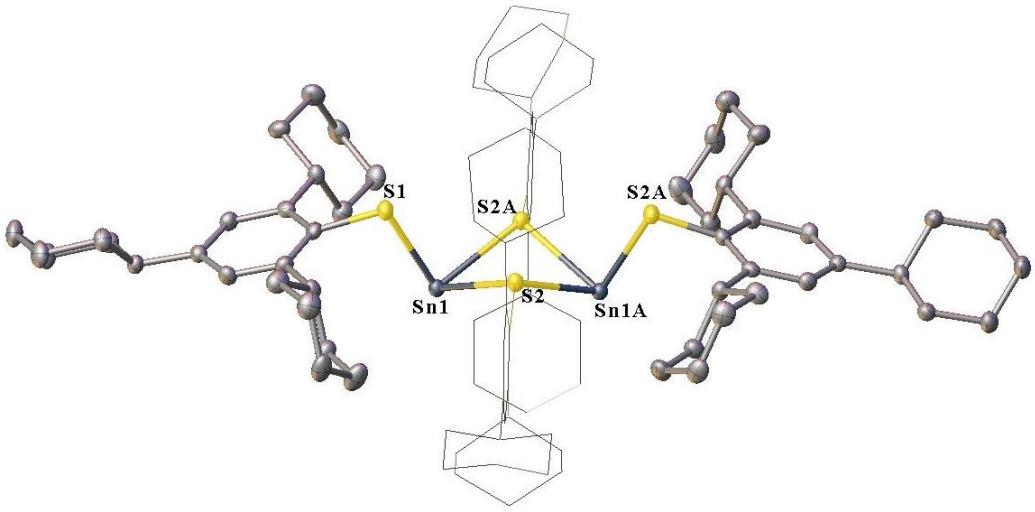

Figure 4. Thermal ellipsoid (50 %) plot of $\{Sn(SC_6H_2\text{-}2,4,6\text{-}Cy_3)_2\}_2$ (**2**). Two ligands are shown in wireframe format and all hydrogen atoms and co-crystallized solvent molecules (benzene) are omitted for clarity. Atoms C43–C48 and Sn1 are disordered over two positions, with only the higher occupancy (92 % and 98 %, respectively) atoms shown. Selected distances (Å) and angles (°): Sn1–S1 2.4567(7), Sn1–S2 2.6235(6), Sn1–S2A 2.6390(6), Sn1···Sn1A 3.8710(11), S1–C1 1.799(2), S2–C25 1.783(2), S1–Sn1–S2 90.58(2), S1–Sn1–S2A 91.66(2), S2–Sn1–S2A 66.46(2), C1–S1–Sn1 100.35(8), C25–S2–Sn1 116.36(8), C25–S2–Sn1A 120.08(8), Sn1–S2–Sn1A 94.70(2), $\Sigma_{\angle}$ Sn1 248.70(3).

Compound **2** crystallizes from benzene as a disolvate (Figure 4). Like its germanium analogue **1**, the solid-state structure of **2** features C_2 symmetry and a *cis* arrangement of the arylthiolato ligands. Even though the synthesis of a dimeric Sn(II) silylthiolate $\{Sn(SSi(SiMe_3)_3)_2\}_2$ has been reported,[41] no crystallographic data are available for it, precluding structural comparisons. Consequently, compounds that are most closely related to **2** include the trimer $\{Sn(SC_6H_3\text{-}2,6\text{-}Pr^i)_2\}_3$[19] and a series of Sn(II) arylthiolate monomers (Table 2).[19,21] At 2.4567(7) Å, the Sn1–S1 distance in **2** is comparable to the terminal Sn–S distance in the trimer $\{Sn(SC_6H_3\text{-}2,6\text{-}Pr^i)_2\}_3$,

2.471(5) Å. The same also holds between **2** and many Sn(II) arylthiolate monomers, though the Sn–S distance in the derivative $Sn(SC_6H_2\text{-}2,4,6\text{-}Bu^t_3)_2$ is particularly short, 2.4356(3),[19] while that in $Sn(SC_6H_1\text{-}2,6\text{-}(C_6H_2\text{-}2,4,6\text{-}Pr^i_3)_2\text{-}3,5\text{-}Pr^i_2)_2$ with eight isopropyl substituents on each ligand is noticeably long, 2.5009(6) Å.[21] The Sn1–S2 and Sn1–S2A bonds in **2** differ by less than 0.02 Å and are, rather expectedly, longer than the terminal Sn1–S1 bond in **2** and the related Sn–S distances in the trimer $\{Sn(SC_6H_3\text{-}2,6\text{-}Pr^i)_2\}_3$.[19] The C1–S1–Sn1 angle in **2** is narrower than the corresponding angle in most structurally characterized Sn(II) arylthiolates, though wider than that in the trimer $\{Sn(SC_6H_3\text{-}2,6\text{-}Pr^i)_2\}_3$;[19] the C1–S1–Sn1 angle is also significantly less acute than the C1–S1–Ge1 angle in **1**. The S2–Sn1–S2A angle in **2** is very acute, 66.46(2)°, but the only available reference value, 74.4(1)°, is from a trimeric structure and, therefore, not strictly comparable.[19] A comparison of the sum of bond angles for the group 14 element in **1** and **2** shows a *ca.* 20° decrease on moving from Ge(II) to Sn(II), illustrating that the M_2S_2 core (M = Ge, Sn) is more puckered in **2** than in **1**. Compound **2** features eight interligand H···H close contacts (≤ 2.5 Å) (Figure 2), suggesting that the role of dispersion interactions in stabilizing its solid-state structure might be even greater than that for **1**.

Table 2. Selected Distances (Å) and Angles (°) for $\{Sn(SC_6H_2\text{-}2,4,6\text{-}Cy_3)_2\}_2$ (2) and Related Sn(II) Thiolates

Compound	**Sn–S^b**	**Sn–μS**	**C–S^b–Sn**	**S^b–Sn–S^c**	**μS–Sn–μS**	**Sn–μS–Sn**	**S–C**
$\{Sn(SC_6H_2\text{-}2,4,6\text{-}Cy_3)_2\}_2$ (**2**)	2.4567(7)	2.6235(6) 2.6391(6)	100.35(8)	90.58(2) 91.66(2)	66.46(2)	94.70(2)	1.783(2) 1.799(2)
$\{Sn(SC_6H_3\text{-}2,6\text{-}Pr^i)_2\}_3$[19]	2.471(5)	2.583(3) 2.6428(4)	96.829(8)	89.8(2) 95.0(1)	74.4(1)	96.758(13) 101.662(12)	1.8146(3)[a]
$Sn(SC_6H_2\text{-}2,4,6\text{-}Bu^t_3)_2$[19]	2.4356(3)	-	101.64(12)	85.4(1)	-	-	1.8087(2)
$Sn(SC_6H_3\text{-}2,6\text{-}(C_6H_2\text{-}2,6\text{-}Pr^i_2)_2)_2$[21]	2.470(1)	-	113.8(1)	78.63(3)	-	-	1.778(4)
$Sn(SC_6H_3\text{-}2,6\text{-}(C_6H_2\text{-}2,4,6\text{-}Me_3)_2)_2$[21]	2.4744(4) 2.4844(4)	-	98.88(4) 108.61(4)	85.55(1)	-	-	1.781(1) 1.782(1)

$Sn(SC_6H_3$-2,6-$(C_6H_2$-2,4,6-$Pr^i_3)_2)_2$[21]	2.4723(5)[§] 2.4813(4)[§]	-	111.55(5)[§] 113.69(6)[§]	78.27(2)[§]	-	-	1.776(2)[§] 1.777(2)[§]
$Sn(SC_6H_1$-2,6-$(C_6H_2$-2,4,6-$Pr^i_3)_2$-3,5-$Pr^i_2)_2$[21]	2.5009(6)	-	119.15(8)	73.09(2)	-	-	1.776(2)

[a]Average value. [b]Terminal S atom if dimeric/trimeric [c]Bridging S atom if dimeric or trimeric structure. [§]Data is reported for only one crystallographically identical molecule.

The hydrophobic character of the cyclohexane substituents gave the Pb(II) derivative $\{Pb(SC_6H_2$-2,4,6-$Cy_3)_2\}_2$ (**3**) sufficient solubility in hexane, benzene, and toluene to allow its isolation and crystallization in the absence of additional Lewis bases. Like its aryloxo analogue $\{Pb(OC_6H_2$-2,4,6-$Cy_3)_2\}_2$ and other related Pb(II) chalcogenolates,[37] **3** is thermochromic and turns red above *ca.* 80 ^oC in toluene and returns to orange at room temperature. Moreover, compound **3** is stable in the presence of light both in solution and in the solid state. The *in situ* room temperature ^1H NMR spectrum of **3** in C_6D_6 shows two resonances in the aryl region with broadening of signals, indicating of a mixture of species and/or a dynamic process in solution. Unfortunately, no ^{207}Pb NMR signal was detected at room temperature and variable temperature NMR studies were not performed.

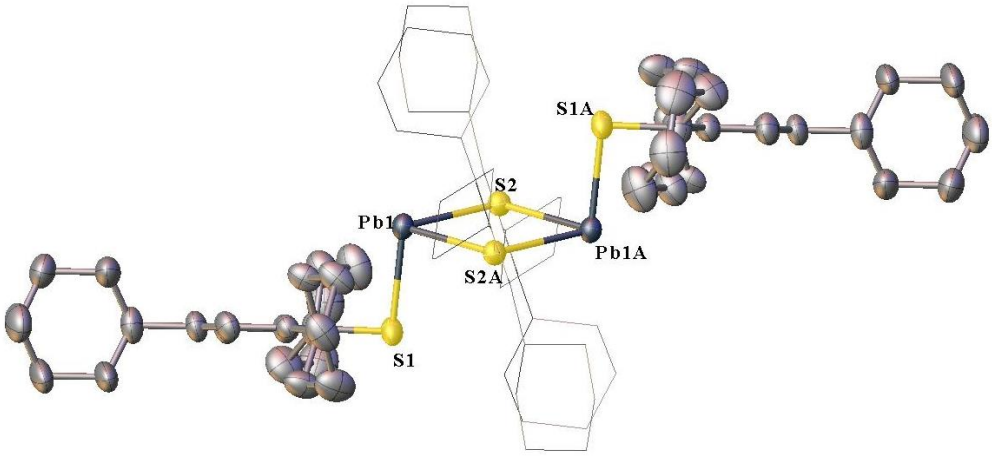

Figure 5. Thermal ellipsoid (50 %) plot of $\{Pb(SC_6H_2\text{-}2,4,6\text{-}Cy_3)_2\}_2$ (**3**). Ligands are shown in wireframe format and all hydrogen atoms and co-crystallized solvent molecules (toluene) are omitted for clarity. Atoms C43–C48 and C19–C24 are disordered over two positions, with only the higher occupancy (65 %) atoms shown. Selected distances (Å) and angles (°): Pb1–S1 2.5522(5), Pb1–S2 2.7138(5), Pb1–S2A 2.7294(5), Pb···Pb 4.4276(9), S1–C1 1.7890(19), S2–C25 1.7828(18), S1–Pb1–S2 99.244(15), S1–Pb1–S2A 89.542(16), S2–Pb1–S2A 71.138(15), C1–S1–Pb1 93.29(6), C25–S2–Pb1 117.65(6), C25–S2–Pb1A 121.89(6), Pb1–S2–Pb1A 108.863(15), $\Sigma\angle$ Pb1 259.924(27).

In contrast to the solid-state structures of **1** and **2**, **3** displays C_i symmetry and a *trans* arrangement of ligands similar to that observed in $\{Pb(OC_6H_2\text{-}2,4,6\text{-}Cy_3)_2\}_2$ (Figure 5).[37] The Pb1–S1 bond in **3** is shorter than the related Pb–S bond in the other reported dimeric Pb(II) thiolate,[42] but comparable to that in the trimer $\{Pb(SC_6H_3\text{-}2,6\text{-}Pr^i)_2\}_3$.[19] The C1–S1–Pb1 angle in **3** is significantly more acute than the related angles in other Pb(II) alkyl- or arylthiolates, presumably owing to the *trans* orientation of the terminal ligands in **3**, which also rationalizes the *ca.* 10 ° difference between the S1–Pb1–S2 and S1–Pb1–S2A angles. Consequently, the metrical parameters of the Pb_2S_2 core in **3** are not strictly comparable to those in the other dimeric Pb(II)

thiolate since the Pb_2S_2 ring is planar in **3** but it is puckered in $\{Pb(SSi(OBu^t)_3)_2\}_2$.[42] The *trans* arrangement of substituents in **3** also affects the S2–Pb1–S2A and Pb1–S2–Pb1A angles, making the former narrower and the latter wider compared to the corresponding angles in the dimer $Pb(SSi(OBu^t)_3)_2\}_2$.[42] Compound **3** has only two interligand H···H close contacts (≤ 2.5 Å) (Figure 2) compared to the eight interactions present in its aryloxo analogue $\{Pb(OC_6H_2\text{-}2,4,6\text{-}Cy_3)_2\}_2$ with significantly shorter Pb–O bonds compared to the Pb–S distances in **3**.[37] The value of interligand H···H close contacts increases to four if the threshold is increased to 2.6 Å. This suggests that the role of dispersion interactions in stabilizing the dimeric solid-state structure of **3** should be the smallest of the three compounds considered.

Table 3. Selected Distances (Å) and Angles (°) for $\{Pb(SC_6H_2\text{-}2,4,6\text{-}Cy_3)_2\}_2$ (**3**) and Related Pb(II) Thiolates

Compound	Pb–S[b]	Pb–μS	C–S[b]–Pb	S[b]–Pb–S[c]	μS–Pb–μS	Pb–μS–Pb	S–C
$\{Pb(SC_6H_2\text{-}2,4,6\text{-}Cy_3)_2\}_2$ (**3**)	2.5522(5)	2.722(11)[a]	93.29(6)	89.542(16) 99.244(15)	71.138(15)	108.863(15)	1.7828(18) 1.7890(19)
$\{Pb(SSi(OBu^t)_3)_2\}_2$[42]	2.585(5)[a]	2.768(3)[a] 2.808(4)[a]	98.7(7)[a]*	88.7(9)[a] 93.1(8)[a]	79.2(6)[a]	90.0(2)[a]	-
$\{Pb(SC_6H_3\text{-}2,6\text{-}Pr^i)_2\}_3$[19]	2.5534(9)	2.6738(8) 2.7806(3)	98.035(12)	92.64(9) 92.77(9)	73.493(19)	-	1.7586(4)[a]
$Pb(SC_6H_3\text{-}2,6\text{-}(C_6H_3\text{-}2,6\text{-}Pr^i{}_2)_2)_2$[17]	2.56(9)	-	113.42(11)	77.21(4)	-	-	1.771(3)
$Pb(SC_6H_3\text{-}2,6\text{-}(C_6H_3\text{-}2,4,6\text{-}Pr^i{}_3)_2)_2$[21]	2.5746(6) 2.5838(6)	-	114.16(6) 115.63(5)	77.27(2)	-	-	1.770(2) 1.773(2)
$Pb(SC_6H_1\text{-}2,6\text{-}(C_6H_2\text{-}2,4,6\text{-}Pr^i{}_3)_2\text{-}3,5\text{-}Pr^i{}_2)_2$[21]	2.5797(7) 2.5940(5)	-	116.49(5) 118.35(5)	80.07(2)	-	-	1.781(2) 1.783(1)

[a]Average value. [b]Terminal S atom if dimeric/trimeric. [c]Bridging S atom if dimeric or trimeric structure. *Silicon atom in place of carbon.

Reactivity Studies

Considering that **2** crystallizes readily in high yield and its synthesis involves relatively inexpensive starting materials, reactivity studies with selected molecular substrates were conducted in an attempt to isolate new, monomeric Sn(II) species. Addition of two equivalents of pinacolborane to one equivalent of **2** at *ca.* −18 °C in hexane led to immediate color change and precipitation of a tan powder that could not be identified by ^{1}H NMR spectroscopy. This insoluble tan powder likely originates from the dismutation of pinacolborane.[43,44] Filtration of the dark orange solution, followed by its concentration and storage at ca. −18 °C led to the precipitation of colorless crystals after 48 h. X-ray crystallography and ^{1}H NMR spectroscopy confirmed that the crystals are unambiguously **2**. Filtration of the supernatant liquid from the crystalline material followed by further concentration produced a second crop of colorless crystals of **2** and repeated fractional crystallizations provided no other identifiable products. In a similar fashion, addition of two equivalents of phenylacetylene to one equivalent of **2** in benzene and refluxing the solution for 4 days in a J. Young ampoule produced a large cluster of colorless crystals when the solution was cooled to room temperature. Analysis by X-ray crystallography and ^{1}H NMR spectroscopy confirmed the crystalline material to be pure **2** that could be recovered in 99 % yield by mass analysis.

Ligand Synthesis

While a synthesis of HSC_6H_2-2,4,6-Cy_3 (**4**) has been published,[33,45] contaminants were clearly present in the published spectroscopic data despite purification by column chromatography (SiO_2, pentane).[33] An improved one-pot synthesis of the thiol **4** was undertaken using *in situ* lithiation of BrC_6H_2-2,4,6-Cy_3[45] with *t*-butyl lithium. This afforded the thiol in good yield and excellent purity,

with no extraneous signals present in the NMR spectra. Furthermore, purification *via* column chromatography was not required after the organic work-up since **4** can be crystallized in large quantity from a concentrated, boiling ethyl acetate solution. After isolation of the first crop of crystals, a second crop could be collected from the mother liquor after *ca.* 2 days *via* slow evaporation of the solvent to give an overall yield of ca. 80 %. While all spectroscopic data obtained for **4** matches those reported previously,[33] an X-ray crystallographic determination of its structure (Figure S12) was not presented.

4.4. CONCLUSIONS

We have synthesized and characterized three new arylthiolato complexes of group 14 elements M(II) (M = Ge, Sn, and Pb). The compounds $\{Ge(SC_6H_2\text{-}2,4,6\text{-}Cy_3)_2\}_2$ (**1**), $\{Sn(SC_6H_2\text{-}2,4,6\text{-}Cy_3)_2\}_2$ (**2**), and $\{Pb(SC_6H_2\text{-}2,4,6\text{-}Cy_3)_2\}_2$ (**3**) all have dimeric structures in the solid state, with **1** and **2** showing a *cis* arrangement of ligands while **3** displays a *trans* orientation. Collectively, **1**–**3** establish a unique crystallographically characterized series of dimeric group 14 arylthiolates. Specifically, **2** is the first dimeric Sn(II) thiolate with structural data available, while **3** is a rare example of a Pb(II) thiolate that crystallizes in the absence of additional donor ligands. The sterically encumbering ligand $–SC_6H_2\text{-}2,4,6\text{-}Cy_3$, used for the first time for the synthesis of metal complexes, gives compounds **1**–**3** structural features that differentiate them from related systems reported in the literature. In contrast to the dimeric structures observed in the solid state, NMR studies of **1**–**3** indicated the presence of a dynamic process in solution at room temperature, which in the case of the Ge(II) derivative leads to a mixture of species, presumably containing the *cis* and *trans* isomers of **1** and the monomeric germylene $Ge(SC_6H_2\text{-}2,4,6\text{-}Cy_3)_2$. Results from computational studies indicated that the *cis* isomer of **1** is the energetically preferred species in solution, largely owing to the significant stabilization provided by intramolecular dispersion,

though the *trans* isomer is energetically comparable and the dissociation of **1** to the corresponding monomers is a plausible explanation for the species observed in the ^{1}H NMR spectra recorded from a dilute solution of **1**. The calculations also demonstrated that the addition of Ge(SC_6H_2-2,4,6-Pr^i_3)$_2$ to the H–S bond in HSC_6H_2-2,4,6-Pr^i_3 is associated with a high energy barrier and is therefore a less-likely route to the Ge(IV) hydride HGe(SC_6H_2-2,4,6-Pr^i_3)$_3$ reported earlier. This result agrees with the fact that its cyclohexyl analogue HGe(SC_6H_2-2,4,6-Cy)$_3$ was not observed in any of the performed experiments, even though the Ge(IV) hydride was calculated to be the thermodynamic sink on the potential energy surface. Reactions of Sn(II) arylthiolate **2** with pinacolborane and phenylacetylene yielded only crystalline starting material despite the use of forceful conditions, which implies of the thermodynamic stability of the dimeric structure of **2** in the solid state. Finally, a one-pot synthetic procedure was devised for the thiol HSC_6H_2-2,4,6-Cy_3 (**4**), giving it in high (ca. 80 %) yield and with excellent synthetic purity.

4.5. EXPERIMENTAL SECTION

General Considerations

All manipulations were carried out under anaerobic and anhydrous conditions by using standard Schlenk techniques or in a Vacuum Atmospheres OMNI-Lab drybox under an atmosphere of dry argon or nitrogen. Solvents were dried by the method of Grubbs and co-workers,[46] stored over potassium or sodium, and then degassed by the freeze−pump−thaw method. All physical measurements were made under strictly anaerobic and anhydrous conditions. Melting points of samples were determined in flame-sealed capillaries using a Meltemp II apparatus equipped with a partial immersion thermometer with a device limit of 250 ^{o}C. IR spectra were recorded as Nujol mulls between CsI plates on a PerkinElmer 1430 spectrometer. UV−Vis spectra were recorded as dilute toluene solutions in 3.5 mL quartz cuvettes using a modernized Olis 17 Cary 14

UV−Vis−Near-IR spectrophotometer. NMR spectra were recorded on a Varian Inova 600 MHz spectrometer or a Bruker 400 MHz AVANCE III HD Nanobay spectrometer, and the ^{1}H NMR spectra were referenced to the residual solvent signals in deuterated benzene (**1**-**3**) or deuterated chloroform (**4**). Unless otherwise stated, all materials were obtained from commercial sources and used as received. The ligand 2,4,6-tricyclohexylphenylthiol was synthesized based on a modified literature procedure.[33] Group 14 silylamides $M(N(SiMe_3)_2)_2$ (M = Ge, Sn, and Pb) were synthesized by published procedures.[1,2] Compounds **1**–**3** were synthesized *via* protonolysis between one equivalent of $M(N(SiMe_3)_2)_2$ (M = Ge, Sn, and Pb) and two equivalents of HSC_6H_2-2,4,6-Cy_3 (Cy = cyclohexyl) in *ca.* 80 mL of hexanes at room temperature. The solutions were stirred for 2 h after which the solvent was exchanged for benzene or toluene (*vide infra*).

X-Ray Crystallographic Studies

Crystals of **1**–**3** suitable for X-ray crystallographic studies were obtained from saturated benzene (**1** and **2**) and toluene (**3**) solutions upon standing for 24 h at room temperature. The crystals were removed from the Schlenk tubes and immediately covered with a layer of hydrocarbon oil. Suitable crystals were selected, mounted on a nylon cryoloop, and then placed in the cold nitrogen stream of the diffractometer. Data for **1**, **2**, and **3** were collected at 90(2) K with Mo $K\alpha_1$ radiation (λ = 0.71073 Å) using a Bruker D8 Venture dual source diffractometer in conjunction with a CCD detector. The collected reflections were corrected for Lorentz and polarization effects and for absorption by using Blessing's method as incorporated into the program SADABS.[47,48] The structures were solved by direct methods and refined with the SHELXTL (2012, version 6.1) or SHELXTL (2013) software packages.[49] Refinement was by full-matrix least-squares procedures, with all carbon-bound hydrogen atoms included in calculated positions and treated as riding atoms. The thermal ellipsoid plots were drawn using OLEX2 software.[50]

Synthesis

{Ge(SC$_6$H$_2$-2,4,6-Cy$_3$)$_2$}$_2$ (**1**). 0.657 g (1.843 mmol) of HSC$_6$H$_2$-2,4,6-Cy$_3$ and 0.362 g (0.921 mmol) of Ge(N(SiMe$_3$)$_2$)$_2$ were combined in a 100 mL Schlenk flask and dissolved in hexane to give a yellow solution. The flask was dried at *ca.* 40 ^{o}C under reduced pressure (*ca.* 0.01 torr) and the solvent was exchanged for benzene. Room temperature crystallization from *ca.* 20 mL benzene solution gave 0.383 g (53.1 %) of **1** as colorless crystalline material. X-ray quality single crystals were obtained from hot (*ca.* 80 ^{o}C) benzene-d_6 solution in a J. Young NMR tube. ^{1}H NMR (400 MHz, C$_6$D$_6$, 25 ^{o}C, δ/ppm, *in situ*, saturated sample): 7.14 (8H, *cis*), 6.97 (1.17H, *trans*), 6.12 (1.25H, *intermediate*), 3.67 (4H), 2.48 (8H), 2.03–1.20 (162 H), 0.09 (72H, *H*N(SiMe$_3$)$_2$). IR (Nujol, $\tilde{\nu}$/cm^{-1}): 2960 (s), 2925 (s), 2860 (s), 2600 (w), 1600 (w), 1560 (w), 1450 (m, broad), 1350 (w, broad), 1260 (s), 1100 (s), 1020 (s), 930 (w), 800 (s), 680 (m), 620 (w), 560 (w), 530 (w), 500 (w), 430 (w), 395 (w), 370 (w), 290 (w). UV-vis (λ/nm; ε/M^{-1} cm^{-1}): 283 (3,300). ^{1}H NMR (400 MHz, C$_6$D$_6$, 25 ^{o}C, δ/ppm, dilute, crystalline sample): 7.20 (4H), 3.62 (4H), 2.50 (2H), 1.94-1.30 (*cyclohexyl*) Melting point: > 250 ^{o}C.

{Sn(SC$_6$H$_2$-2,4,6-Cy$_3$)$_2$}$_2$ (**2**). 0.961 g (2.695 mmol) of HSC$_6$H$_2$-2,4,6-Cy$_3$ and 0.592 g (1.347 mmol) of Sn(N(SiMe$_3$)$_2$)$_2$ were combined in a 100 mL Schlenk flask and dissolved in hexane to give a light-yellow solution. The flask was dried at *ca.* 40 ^{o}C under reduced pressure (*ca.* 0.01 torr) and the solvent was exchanged for benzene. Crystallization from slowly cooling a *ca.* 30 mL hot (*ca.* 80 ^{o}C) benzene solution gave 0.686 g (61.4 %) of **2** as colorless X-ray quality single crystals. ^{1}H NMR (400 MHz, C$_6$D$_6$, 25 ^{o}C, δ/ppm): 7.14–7.11 (8H), 3.89 (6H), 2.44 (6H), 1.94–1.12 (120 H). IR (Nujol, $\tilde{\nu}$/cm^{-1}): 2925 (s), 2860 (s), 2670 (w), 1600 (m), 1560 (m), 1450 (m), 1380 (m), 1350 (m), 1270 (m), 1240 (w), 1170 (w), 1100 (m), 1060 (m), 1025 (m), 1000 (w), 950 (w), 890

(w), 870 (m), 850 (w), 810 (m), 755 (w), 730 (w), 680 (w), 630 (w), 535 (w), 435 (w), 320 (w), 270 (w). UV-vis (λ/nm; ε/$M^{-1}cm^{-1}$): 284 nm (7,300). Melting point: > 250 °C.

{Pb(SC$_6$H$_2$-2,4,6-Cy$_3$)$_2$}$_2$ (**3**). 0.995 g (2.790 mmol) of HSC$_6$H$_2$-2,4,6-Cy$_3$ and 0.737 g (1.396 mmol) of Pb(N(SiMe$_3$)$_2$)$_2$ were combined in a 100 mL Schlenk flask and dissolved in hexane to give an orange solution. The flask was dried at *ca.* 40 °C under reduced pressure (*ca.* 0.01 torr) and the solvent was exchanged for toluene. Crystallization from slowly cooling a *ca.* 40 mL hot (*ca.* 100 °C) toluene solution gave 1.106 g (86.3 %) of **3** as orange X-ray quality single crystals. ^{1}H NMR (400 MHz, C$_6$D$_6$, 25 °C, δ/ppm): 7.15–6.99 (8H), 3.95 (8H), 2.51 (6H), 2.04–1.19 (120H). IR (Nujol, $\tilde{\nu}$/cm^{-1}): 2920 (s), 2840 (s), 1595 (w). 1550 (w), 1460 (s), 1450 (s), 1370 (m), 1345 (w), 1250 (s), 1085 (s), 1015 (s), 855 (m), 840 (w), 795 (s), 720 (w), 680 (w), 550 (w), 520 (w), 390 (w), 280 (w). UV-vis (λ/nm; ε/$M^{-1}cm^{-1}$): 284 (18,970), 413 (2,900). Melting point: > 250 °C.

HSC$_6$H$_2$-2,4,6-Cy$_3$. 6.00 g (14.872 mmol) of BrC$_6$H$_2$-2,4,6-Cy$_3$[45] was added through a funnel to a 250 mL round-bottom Schlenk flask and *ca.* 150 mL of diethyl ether was added to create a colorless suspension of the bromide. The reaction flask was cooled to −25 °C and 18.8 mL of 1.7 M *t*-BuLi (2.15 equiv.) was added dropwise *via* cannula. After stirring at −25 °C for 2 h, the cold bath was removed, and the solution was warmed to room temperature. After 7 h of stirring at room temperature, the solvent was exchanged for *ca.* 150 mL of THF and 1.431 g (44.635 mmol) of crystalline sulfur were added *via* funnel in 3 portions to give a dark red solution. After stirring for 48 h at room temperature, the reaction mixture was cooled to −78 °C and 5.202 g (37.180 mmol) of Li[AlH$_4$] dissolved in Et$_2$O were added dropwise *via* cannula. The resultant yellow solution was stirred for 24 h and then quenched dropwise with deionized H$_2$O at 0 °C. Concentrated HCl was added dropwise until the pH of the solution became acidic. The organic and aqueous layers were

separated with a separatory funnel and the aqueous layer was washed three times with *ca.* 100 mL portions of Et_2O. The organic layers were combined, dried with *ca.* 20 g of $MgSO_4$, and the solvent was removed using a rotary evaporator. The resultant yellow solid was redissolved in *ca.* 100 mL of boiling ethyl acetate and crystallized at room temperature to give 4.241 g (80.0 %) of colorless, air and moisture stable crystals of 2,4,6-tricyclohexylphenylthiol. ^{1}H NMR (600 MHz, $CDCl_3$, 25 ^{o}C, δ/ppm) 6.95 (2H), 3.08–3.06 (2H), 3.05 (1H, *H*SAr) 2.44 (1H), 1.89–1.25 (*ca.* 30H).

Computational Details

Geometries of all studied systems were optimized in a solvent (SMD, benzene)[51] with dispersion corrected density functional theory, namely the PBE1PBE functional,[52-55] def2-TZVP basis sets,[56] and Grimme's D3 correction with Becke-Johnson damping,[57,58] using the Gaussian 16-C.01 program suite.[59] The structures were confirmed to be minima or transition states on the singlet potential energy hypersurface *via* calculation of the associated vibrational frequencies (all positive or one imaginary frequency, respectively).

ASSOCIATED CONTENT

Appendix A. Supplementary data

CCDC contains the supplementary crystallographic data for **1**–**4**, CCDC Accession numbers: 2294334-2294337. These data can be obtained free of charge *via* http://www.ccdc.cam.ac.uk/conts/retrieving.html, or from the Cambridge Crystallographic Data Centre, 12 Union Road, Cambridge CB2 1EZ, UK; fax: (+44) 1223-336-033; or e-mail: deposit@ccdc.cam.ac.uk. Spectroscopic (^{1}H NMR, IR, and UV-Vis) data of **1**–**3**, ^{1}H-NMR data for **4**, crystallographic tables for **1**–**4**, and optimized structures (*xyz*-coordinates) (PDF).

AUTHOR CONTRIBUTION

Connor P. McLoughlin: Investigation, methodology, writing, supervision

Anthony J. Witt: Investigation, writing

Jonah Nelson: Computational analysis, writing

AUTHOR INFORMATION

Corresponding Authors

*Philip P. Power, Department of Chemistry, University of California, Davis, California 95616, USA. orcid.org/0000-0002-6262-3209

E-mail: pppower@ucdavis.edu

*Heikki M. Tuononen, Department of Chemistry, NanoScience Centre, University of Jyväskylä, P.O. Box 35, FI-40014, Jyväskylä, Finland. orcid.org/0000-0002-4820-979X

E-mail: heikki.m.tuononen@jyu.fi

Authors

Connor P. McLoughlin, Department of Chemistry, University of California, Davis, California 95616, USA. orcid.org/0000-0002-4707-1135

Anthony J. Witt, Department of Chemistry, University of California, Davis, California 95616, USA

Jonah P. D. Nelson, Department of Chemistry, NanoScience Centre, University of Jyväskylä, P.O. Box 35, FI-40014, Jyväskylä, Finland and Department of Chemistry, 2500 University Drive N.W., University of Calgary, Calgary, Alberta, Canada, T2N 1N4.

ACKNOWLEDGMENT

C.P.M. would like to thank James C. Fettinger for his assistance with modeling the disorder present in complexes **1**–**3**. C.P.M. would also like to thank Dr. Ping Yu from the U.C. Davis NMR facility. We acknowledge the U.S. National Science Foundation (Grant No. CHE-2152760 to P.P.P.) and the University of Jyväskylä (H.M.T.) for funding.

DECLARATION OF INTEREST

There are no competing interests to declare.

REFERENCES

[1] Harris, D. H.; Lappert, M. F. Monomeric, Volatile Bivalent Amides of Group IV_B Elements, $M(NR^1{}_2)_2$ and $M(NR^1R^2)_2$ (M = Ge, Sn, or Pb; R^1=Me_3Si, R^2 = Me_3C). *J.C.S. Chem. Comm.*, **1974**, *21*, 895-896.

[2] Veinot, A.J.; Stack, D.L.; Clyburne, J.A.C.; Masuda, J.D.; Dickie, D.A.; Chadha, U.; Kemp, R.A. Calcium, Strontium, Germanium, Tin, and Lead Bis(trimethylsilyl)amido Derivatives and 2,2,6,6-tetramethylpiperidido and n-Isopropylphenylamido Derivatives of Potassium and Calcium. *Inorg. Synth.*, **2018**, *37*, 1st Ed., Chapter 2, 26-31.

[3] Boyle, T.J.; Tribby, L.J.; Ottley, L.A.M.; Han, S.M. Synthesis and Characterization of Germanium Coordination Compounds for Production of Germanium Nanomaterials. *Eur. J. Inorg. Chem.*, **2009**, 5550–5560.

[4] Gerung, H.; Boyle, T.J.; Tribby, L.J.; Bunge, S.D.; Brinker, C.J.; Han, S.M. Solution Synthesis of Germanium Nanowires Using a Ge^{2+} Alkoxide Precursor. *J. Am. Chem. Soc.*, **2006**, *128*, 5244–5250.

[5] Wang, L.; Kefalidis, C.E.; Roisnel, T.; Sinbandhit, S.; Maron, L.; Carpentier, J.; Sarazin, Y. Structure vs ^{119}Sn NMR Chemical Shift in Three-Coordinated Tin(II) Complexes: Experimental Data and Predictive DFT Computations. *Organometallics,* **2015**, *34*, 2139–2150.

[6] Cetinkaya, B.; Gumrukcu, I.; Lappert, M.F.; Atwood, J.L.; Rogers, R.D.; Zaworotko, M.J. Bivalent Germanium, Tin, and Lead 2,6-Di-*tert*-butylphenoxides and the Crystal and Molecular Structures of $M(OC_6H_2Me\text{-}4\text{-}Bu^t_2\text{-}2,6)_2$ (M = Ge or Sn). *J. Am. Chem. Soc.*, **1980**, *102*, 2088-2089.

[7] Kuriki, R.; Kuwabara, T.; Ishii, Y. Synthesis and Structures of Diaryloxystannylenes and -plumbylenes Embedded in 1,3-diethers of Thiacalix[4]arene. *Dalton Trans*., **2020**, *49*, 12234-12241.

[8] Stanciu, C.; Richards, A.F.; Stender, M.; Olmstead, M.M.; Power, P.P. New Terphenylphenoxides of Group 13 and 14 Elements. *Polyhedron*, **2006**, *25*, 477–483.

[9] Hascall, T.; Rheingold, A.L.; Guzei, I.; Parkin, G. Subvalent Germanium and Tin Complexes Supported by a Dianionic Calixarene Ligand: Structural Characterization of *Exo* and *Endo* isomers of [Bu^{t}calix$^{(TMS)2}$]Ge. *Chem. Commun.*, **1998**, *1*, 101-102.

[10] Hascall, T.; Pang, K.; Parkin, G. *Exo* and *Endo* Isomerism of Subvalent Tin and Germanium Complexes Derived from 1,3-diethers of p-tert-butylcalix[4]arene. *Tetrahedron*, **2007**, *63*, 10826-10833.

[11] McBurnett, B.G.; Cowley, A.H. Binuclear Tin and Germanium Calix[4]arenes. *Chem. Commun*., **1999**, *1*, 17–18.

[12] Smith, G.D.; Fanwick, P.E.; Rothwell, I.P. Synthesis, Structure, and Spectroscopic Properties of Germanium and Tin Compounds Containing Aryloxide Ligation: Comparison of Aryloxide Bonding to Group 4 and Group 14 Metal Centers. *Inorg. Chem.*, **1990**, *29*, 3221-3226.

[13] Boyle, T.J.; Doan, T.Q.; Steele, L.M.; Apblett, C.; Hoppe, S.M.; Hawthorne, K.; Kalinich, R.M.; Sigmund, W.M. Tin(II) Amide/Alkoxide Coordination Compounds for Production of Sn-based Nanowires for Lithium Ion Battery Anode Materials. *Dalton Trans.*, **2012**, *41*, 9349-9364.

[14] Yasuda, H.; Choi, J.; Lee, S.; Sakakura, T. Structure of Dialkyltin Diaryloxides and their Reactivity Toward Carbon Dioxide and Isocyanate. *J. Organomet. Chem.*, **2002**, *659*, 133-141.

[15] Van Zandt, W.; Huffman, J.C.; Stewart, J.L. Synthesis and X-Ray Crystal Structure of a Lead Oxide Dimer, $Pb_2(\mu\text{-}O\text{-}2,6\text{-}Ph_2C_6H_3)_2(O\text{-}2,6\text{-}Ph_2C_6H_3)_2$. *Main Group Met. Chem.* **1998**, *21*, 237-240.

[16] Weinert, C.S.; Guzei, I.A.; Rheingold, A.L.; Sita, L.R. Heterocumulene Metathesis of $Pb[N(SiMe_3)_2]_2$. High-Yield Syntheses of the Heteroleptic Dimer $\{Pb[N(SiMe_3)_2(\mu\text{-}OSiMe_3)\}_2$ and the Novel Lead(II) Oxo Cluster $Pb_7(\mu_3\text{-}O)(\mu_4\text{-}O)(\mu\text{-}OSiMe_3)_{10}$. *Organometallics*, **1998**, *17*, 498-500.

[17] Rekken, B.D.; Brown, T.M.; Olmstead, M.M.; Fettinger, J.C.; Power, P.P. Stable Plumbylene Dichalcogenolate Monomers with Large Differences in Their Interligand Angles and the Synthesis and Characterization of a Monothiolato Pb(II) Bromide and Lithium Trithiolato Plumbate. *Inorg. Chem.*, **2013**, *52*, 3054-3062.

[18] Weinert, C.S.; Fenwick, A.E.; Fanwick, P.E.; Rothwell, I.P. Synthesis, Structures and Reactivity of Novel Germanium(II) Aryloxide and Arylsulfide Complexes. *Dalton Trans.*, **2003**, *4*, 532-539.

[19] Hitchcock, P. B.; Lappert, M. F.; Samways, B. J.; Weinberg, E. L. Metal (Li, Ge^{II}, Ge^{III}, Sn^{II}, and Pb^{II}) 2,6-dialkylbenzenethiolates; *X*-ray crystal structures of $Sn(SAr)_2$ (Ar = $C_6H_2Bu^t_3$-2,4,6) and $[M(SAr')_2]^3$(M = Sn or Pb, Ar′= $C_6H_3Pr^i_2$-2,6). *J. Chem. Soc., Chem. Commun*., **1983**, *24*, 1492–1494.

[20] Kersting, B.; Krebs, B. Syntheses and Structures of Germanium(II) and Germanium(IV) Thiolate and Selenolate Complexes: $[Et_4N][Ge(SPh)_3]$, $[Ph_4P][Ge(SePh)_3]$, $[Ph_4P]_2[Ge_2(SCH_2CH_2S)_3]$, $Ge(S\text{-}4\text{-}MeC_6H_4)_4$, and $Ge(Se\text{-}2,4,6\text{-}Me_3C_6H_2)_4$. Examples of the First Anionic Germanium(II) Complexes Containing the Trigonal Pyramidal $Ge^{II}S_3$ and $Ge^{II}Se_3$ Cores. *Inorg. Chem*., **1994**, *33*, 3886–3892.

[21] Rekken, B. D.; Brown, T. M.; Fettinger, J. C.; Lips, F.; Tuononen, H. M.; Herber, R. H.; Power, P. P. Dispersion Forces and Counterintuitive Steric Effects in Main Group Molecules: Heavier Group 14 (Si–Pb) Dichalcogenolate Carbene Analogues with Sub-90° Interligand Bond Angles. *J. Am. Chem. Soc*., **2013**, *135*, 10134−10148.

[22] Dean, P. A. W.; Vittal, J. J.; Payne, N. C. Syntheses and X-ray structural analyses of $[(C_6H_5)_4As][Sn(EC_6H_5)_3]$, E = S and Se. *Can. J. Chem*., **1985**, *63*, 394-400.

[23] Barone, G.; Hibbert, T. G.; Mahon, M. F.; Molloy, K. C.; Parkin, I. P.; Price, L. S.; Silaghi-Dumitrescu, I. Structural Distortions in Homoleptic $(RE)_4A$ (E = O, S, Se; A = C, Si, Ge, Sn): Implications for the CVD of Tin Sulfides. *J. Chem. Soc., Dalton Trans*., **2001**, *23*, 3435-3445.

[24] Shaw, R. A.; Woods, M. Preparation and Some Properties of Lead Thiolates. *J. Chem. Soc*., **1971**, *A*, 1569–1571.

[25] Glegg, W. CCDC 1500411, *CSD Communication,* **2016**.

[26] Christou, G.; Folting, K.; Huffman, J. C. Mononuclear, Three-Coordinate Metal Thiolates: Preparation and Crystal Structures of $[NBu^n_4][Hg(SPh)_3]$ and $[NPr^n_4]$ $[Pb(SPh)_3]$. *Polyhedron*, **1984**, *3*, 1247–1253.

[27] Briand, G. G.; Decken, A.; Finniss, M. C.; Gordon, A. D.; Hughes, N. E.; Scott, L. M. Structure and Reactivity of the Cationic Lead(II) Thiolate $[(4\text{-}Me_3NC_6H_4S)_6Pb_3][PF_6]_6$. *Polyhedron*, **2012**, *33*, 171–178.

[28] Ren, Z.-G.; Tang, X.-Y.; Li, L.; Liu, G.-F.; Li, H.-X.; Chen, Y.; Zhang, Y.; Lang, J.-P. Electrochemical Syntheses and Structures of Lead(II) and Bismuth(III) Complexes of 4-(trimethylammonio)benzenethiolate. *Inorg. Chem. Comm*., **2007**, *10*, 1253–1256.

[29] Charton, M. Steric Effects. I. Esterification and Acid-Catalyzed Hydrolysis of Esters. *J. Am. Chem. Soc*., **1975**, *97*, 1552–1556.

[30] Pinter, B.; Fievez, T.; Bickelhaupt, F. M.; Geerlings, P.; De Proft, F. On the origin of the steric effect. *Phys. Chem. Chem. Phys*., **2012**, *14*, 9846–9854.

[31] Grimme, S.; Huenerbein, R.; Ehrlich, S. On the importance of the dispersion energy for the thermodynamic stability of molecules. *ChemPhysChem*., **2011** *12*, 1258–1261.

[32] Rosel, S.; Becker, J.; Allen, W. D.; Schreiner, P. R. Probing the Delicate Balance between Pauli Repulsion and London Dispersion with Triphenylmethyl Derivatives. *J. Am. Chem. Soc*., **2018**, *140*, 14421−14432.

[33] Wong, M. L. J.; Sterling, A. J.; Mousseau, J. J.; Duarte, F.; Anderson, E. A. Direct Catalytic Asymmetric Synthesis of α-chiral Bicyclo[1.1.1]pentanes. *Nat. Commun*., **2021**, *12*, 1644/1–9.

[34] Kunz, T.; Schrenk, C.; Schnepf, A. Reactions of $GeCl_2$ with the Thiolate $LiSC(SiMe_3)_3$: From THF Activation to Insertion of $GeCl_2$ Molecules into C−S Bonds. *Chem. Eur. J*., **2019**, *25*, 7210−7217.

[35] Veith, M.; Hobein, P.; Rösler, R. Cyclische Diazastannylene, XXX [1] Symmetrisch und asymmetrisch substituierte German- und Stannandiyle mit Amid-, Alkoholat- und Thiolat-Liganden, Teil I [2]. *Z. Naturforsch*. **1989**, *44b*, 1067−1081.

[36] Bondi, A. Van der Waals Volumes and Radii. *J. Phys. Chem*., **1964**, *68*, 441−451.

[37] McLoughlin, C. P.; Kaseman, D. C.; Fettinger, J. C.; Power, P. P. Rearrangement of a Ge(II) Aryloxide to Yield a New Ge(II) Oxo-cluster $[Ge_6(\mu_3\text{-}O)_4(\mu_2\text{-}OC_6H_2\text{-}2,4,6\text{-}Cy_3)_4](NH_3)_{0.5}$: Main Group Aryloxides of Ge(II), Sn(II), and Pb(II) $[M(OC_6H_2\text{-}2,4,6\text{-}Cy_3)_2]_2$ (Cy = cyclohexyl). *Dalton Trans*., **2023**, *52*, 9582–9589.

[38] McLoughlin, C. P.; Fettinger, J. C.; Power, P. P. Mn(II), Fe(II), and Co(II) Aryloxides: Steric and Dispersion Effects and the Thermal Rearrangement of a Cobalt Aryloxide to a Co(II) Semiquinone Complex. *Inorg. Chem*., **2023**, *62*, 10131−10140.

[39] Hitchcock, P. B.; Jasim, H. A.; Kelly, R. E.; Lappert, M. F. Unusual Group 14 Metal Thiolates and Sulphides Derived from Tris(trimethylsilyl)methanethiol; X-ray Structures of $[Pb(NR_2)(\mu\text{-}SCR_3)]_2$ and cis-$[Ge(CH_2Ph)(NR_2)(\mu\text{-}S)]_2$, (R = $SiMe_3$). *J. Chem. Soc., Chem. Commun*., **1985**, *24*, 1776–1778.

[40] Weinert, C. S. An NMR (^1H and ^{77}Se) Investigation of the Reaction of $Ge[N(SiMe_3)_2]_2$ with Mesitylselenol: Formation of $(MesSe)_4Ge$. *Main Group Met. Chem*., **2007**, *30*, 93-100.

[41] Seligson, A. L.; Arnold, J. Synthesis, Structure, and Reactivity of Homoleptic Tin(II) and Lead(II) Chalcogenolates and Their Conversion to Metal Chalcogenides. X-ray Crystal Structures of $\{Sn[TeSi(SiMe_3)_3]_2\}_2$ and $(PMe_3)Sn[TeSi(SiMe_3)_3]_2$. *J. Am. Chem. Soc*., **1993**, *115*, 8214−8220.

[42] Wojnowski, W.; Wojnowski, M.; Peters, K.; Peters, E.-M.; von Schnering, H. G. Beiträge zur Chemie der Silicium-Schwefel-Verbindungen. XXXIX. Blei(II)-bis-tri-tert-butoxysilanthiolat. *Z. Anorg. Allg. Chem*., **1986**, *535*, 56–62.

[43] Lorbach, A.; Hübner, A.; Wagner, M. Aryl(hydro)boranes: Versatile Building Blocks for Boron-doped π-electron Materials. *Dalton Trans*., **2012**, *41*, 6048-6063.

[44] Samuel, P. P.; Kundu, S.; Mohapatra, C.; George, A.; De, S.; Parameswaran, P.; Roesky, H. W. One-Pot Catalytic Synthesis of gem-Diazides and Their Direct Conversion into Safe Materials. *Eur. J. Org. Chem*., **2017**, *16*, 2327-2331.

[45] Salvi, L.; Davis, N. R.; Ali, S. Z.; Buchwald, S. L. A New Biarylphosphine Ligand for the Pd-catalyzed Synthesis of Diaryl Ethers under Mild Conditions. *Org. Lett*., **2012**, *14*, 170–173.

[46] Pangborn, A. B.; Giardello, M. A.; Grubbs, R. H.; Rosen, R. K.; Timmers, F. J. Safe and Convenient Procedure for Solvent Purification. *Organometallics*, **1996**, *15*, 1518−1520.

[47] Sheldrick, G. M. SADABS, Siemens Area Detector Absorption Correction; Göttingen Universitat: Göttingen, Germany, **2008**, 33.

[48] Blessing, R. H. An Empirical Correction for Absorption Anisotropy. *Acta Cryst. Sect. A: Found. Cryst*., **1995**, *51*, 33−38.

[49] Sheldrick, G. M. SHELXTL, Ver. 6.1; Bruker AXS: Madison, WI, **2002**.

[50] Dolomanov, O. V.; Bourhis, L. J.; Gildea, R. J.; Howard, J. A. K.; Puschmann, H. OLEX2: A Complete Structure Solution, Refinement and Analysis Program. *J. Appl. Crystallogr.*, **2009**, *42*, 339−341.

[51] Marenich, A. V.; Cramer, C. J.; Truhlar, D. G. Universal Solvation Model Based on Solute Electron Density and on a Continuum Model of the Solvent Defined by the Bulk Dielectric Constant and Atomic Surface Tensions. *J. Phys. Chem. B*, **2009**, *113*, 6378–6396.

[52] Perdew, J. P.; Burke, K.; Ernzerhof, M. Generalized Gradient Approximation Made Simple. *Phys. Rev. Lett.*, **1996**, *77*, 3865–3868.

[53] Perdew, J. P.; Burke, K.; Ernzerhof, M. Erratum: Generalized Gradient Approximation Made Simple [Phys. Rev. Lett. 77, 3865 (1996)]. *Phys. Rev. Lett.*, **1996**, *78*, 1396.

[54] Adamo, C.; Barone, V. Toward reliable density functional methods without adjustable parameters: The PBE0 model. *J. Chem. Phys.*, **1999**, *110*, 6158–6170.

[55] Ernzerhof, M.; Scuseria, G. E. Assessment of the Perdew-Burke-Ernzerhof Exchange-Correlation Functional. *J. Chem. Phys.*, **1999**, *110*, 5029–5036.

[56] Weigend, F.; Ahlrichs, R. Balanced Basis Sets of Split Valence, Triple Zeta Valence and Quadruple Zeta Valence Quality for H to Rn: Design and Assessment of Accuracy. *Phys. Chem. Chem. Phys.*, **2005**, *7*, 3297–3305.

[57] Grimme, S.; Antony, J.; Ehrlich, S.; Krieg, H. A Consistent and Accurate Ab Initio Parametrization of Density Functional Dispersion Correction (DFT-D) for the 94 Elements H-Pu. *J. Chem. Phys.*, **2010**, *132*, 154104.

[58] Grimme, S.; Ehrlich, S.; Goerigk, L. Effect of the Damping Function in Dispersion Corrected Density Functional Theory. *J. Comput. Chem.*, **2011**, *32*, 1456–1465.

[59] Gaussian 16, Revision C.01, Frisch, M. J.; Trucks, G. W.; Schlegel, H. B.; Scuseria, G. E.; Robb, M. A.; Cheeseman, J. R.; Scalmani, G.; Barone, V.; Petersson, G. A.; Nakatsuji, H.; Li, X.; Caricato, M.; Marenich, A. V.; Bloino, J.; Janesko, B. G.; Gomperts, R.; Mennucci, B.; Hratchian, H. P.; Ortiz, J. V.; Izmaylov, A. F.; Sonnenberg, J. L.; Williams-Young, D.; Ding, F.; Lipparini, F.; Egidi, F.; Goings, J.; Peng, B.; Petrone, A.; Henderson, T.; Ranasinghe, D.; Zakrzewski, V. G.; Gao, J.; Rega, N.; Zheng, G.; Liang, W.; Hada, M.; Ehara, M.; Toyota, K.; Fukuda, R.; Hasegawa, J.; Ishida, M.; Nakajima, T.; Honda, Y.; Kitao, O.; Nakai, H.; Vreven, T.; Throssell, K.; Montgomery, Jr., J. A.; Peralta, J. E.; Ogliaro, F.; Bearpark, M. J.; Heyd, J. J.; Brothers, E. N.; Kudin, K. N.; Staroverov, V. N.; Keith, T. A.; Kobayashi, R.; Normand, J.; Raghavachari, K.; Rendell, A. P.; Burant, J. C.; Iyengar, S. S.; Tomasi, J.; Cossi, M.; Millam, J. M.; Klene, M.; Adamo, C.; Cammi, R.; Ochterski, J. W.; Martin, R. L.; Morokuma, K.; Farkas, O.; Foresman, J. B.; Fox, D. J. Gaussian, Inc.: Wallingford Connecticut, USA, **2016**.

Ni(I) and Ni(II) Bis(trimethylsilyl)amides Obtained in Pursuit of the Elusive Structure of Ni{N(SiMe$_3$)$_2$}$_2$

Citation: C.P. McLoughlin, A.J. Witt, P.P. Power. *Inorg. Chem.* **2024**, *Article ASAP*, doi.org/10.1021/acs.inorgchem.3c04483.

5.1. ABSTRACT

Salt metathesis routes to five new -N(SiMe$_3$)$_2$ nickel derivatives were studied to illuminate their mode of formation, structures, and spectroscopy. The reaction between NiI_2 and K{N(SiMe$_3$)$_2$} afforded the Ni(II) and Ni(I) complexes [K][Ni{N(SiMe$_3$)$_2$}$_3$] (**1**) and [K][Ni{N(SiMe$_3$)$_2$}$_2$] (**2**). Dissolving **1** in THF gave the Ni(II) species [K(THF)$_2$][Ni{N(SiMe$_3$)$_2$}$_3$] (**3**). The Ni(I) salt [K(DME)][Ni$_2$N(SiMe$_3$)$_2$}$_3$] (**4**) was obtained by using $NiCl_2$(DME) (DME = 1,2-dimethoxyethane) as the nickel source rather than NiI_2. The isolation of the Ni(I) complexes **2** and **4** highlights the tendency for K{N(SiMe$_3$)$_2$} to function as a reducing agent. Introduction of adventitious O_2 to solutions of [K][Ni{N(SiMe$_3$)$_2$}$_2$] (**2**) gave the nickel inverse crown ether (ICE) species [K$_2$][O(Ni{N(SiMe$_3$)$_2$}$_2$)$_2$] (**5**). Complex **5** is the first ICE complex of nickel and is one of 4 known ICE complexes for the 3d metals. The experimental results indicate that the reduced Ni(I) bis(trimethylsilyl)amides are relatively easily generated, whereas Ni(III) derivatives that might be expected from a disproportionation of a Ni(II) derivative are apparently not isolable by the above routes. Overall, the new species

crystallize readily from the reaction mixtures, but under ambient conditions they begin to decompose as solids within ca. 24 h. which hinders their characterization.

5.2. INTRODUCTION

In 2015 it was shown that the earlier report of the synthesis of $Ni\{N(SiMe_3)_2\}_2$ in THF solvent by Bürger and Wannagat[1] actually described its THF complex $Ni\{N(SiMe_3)_2\}_2(THF)$ instead of THF free, uncomplexed $Ni\{N(SiMe_3)_2\}_2$.[2] This finding was consistent with the formation of the corresponding Mn(II), Fe(II), and Co(II) THF complexes in THF solvent.[3] While several homoleptic Ni(II) amides are known,[4-12] the structure of the silylamide species $Ni\{N(SiMe_3)_2\}_2$ has remained elusive and its usefulness as a synthon is limited by its apparent instability.[2] The number of currently known neutral Lewis base complexes of $Ni\{N(SiMe_3)_2\}_2$ is limited,[13*a*] and the isolation of such complexes is strongly dependent upon the solvent employed. The other types of $Ni\{N(SiMe_3)_2\}_2$ derivatives are either Ni(II) or Ni(I) nickelate salts.[*b*] For example, $Ni\{N(SiMe_3)_2\}_2(dmap)_2$ (dmap = 4-dimethylaminopyridine) and $Ni\{N(SiMe_3)_2\}_2$ (2,2′-bipy) (2,2′-bipy = 2,2′-bipyridine) were isolated by Werncke and coworkers via the addition of dmap or 2,2′-bipy in toluene to the nickelate $[Li(THF)_{4.5\text{-}5.5'}][Ni\{N(SiMe_3)_2\}_3]$.[14] Reduction of $[Li(THF)_{4.5\text{-}5.5'}][Ni\{N(SiMe_3)_2\}_3]$[14] with KC_8 (KC_8 = potassium graphite) in Et_2O and 18-crown-6 (18-crown-6 = 1,4,7,10,13,16-hexaoxacyclooctadecane) gave the Ni(I) complex [K(18-crown-6)][$Ni\{N(SiMe_3)_2\}_2$] while reduction in toluene gave trace amounts of the Ni-Ni bonded species [K(toluene)][$Ni_2\{N(SiMe_3)_2\}_3$].[14] Additionally, attempts to isolate [Na][$Ni\{N(SiMe_3)_2\}_3$] were unsuccessful in the absence of donor ligands.[15] It was suggested that the nature of the donor ligand is critical for the initial formation of the nickelate.[15] The dependence of the formation of these Ni(II) silylamides on solvent effects and the use of chelating agents to form separated ion

pairs prompted us to investigate further the isolation of donor ligand-free derivatives of $Ni\{N(SiMe_3)_2\}_2$. Herein we report the syntheses of four new Ni(II) and Ni(I) complexes of the $-N(SiMe_3)_2$ ligand that do not require the use of complexing agents and whose isolations are determined solely by the reaction conditions. The complex **5** was obtained from the reaction of $[K][Ni\{N(SiMe_3)_2\}_2]$ (**2**) with molecular O_2.

Scheme 2. Reaction summary for the synthesis of complexes **1**-**5**.

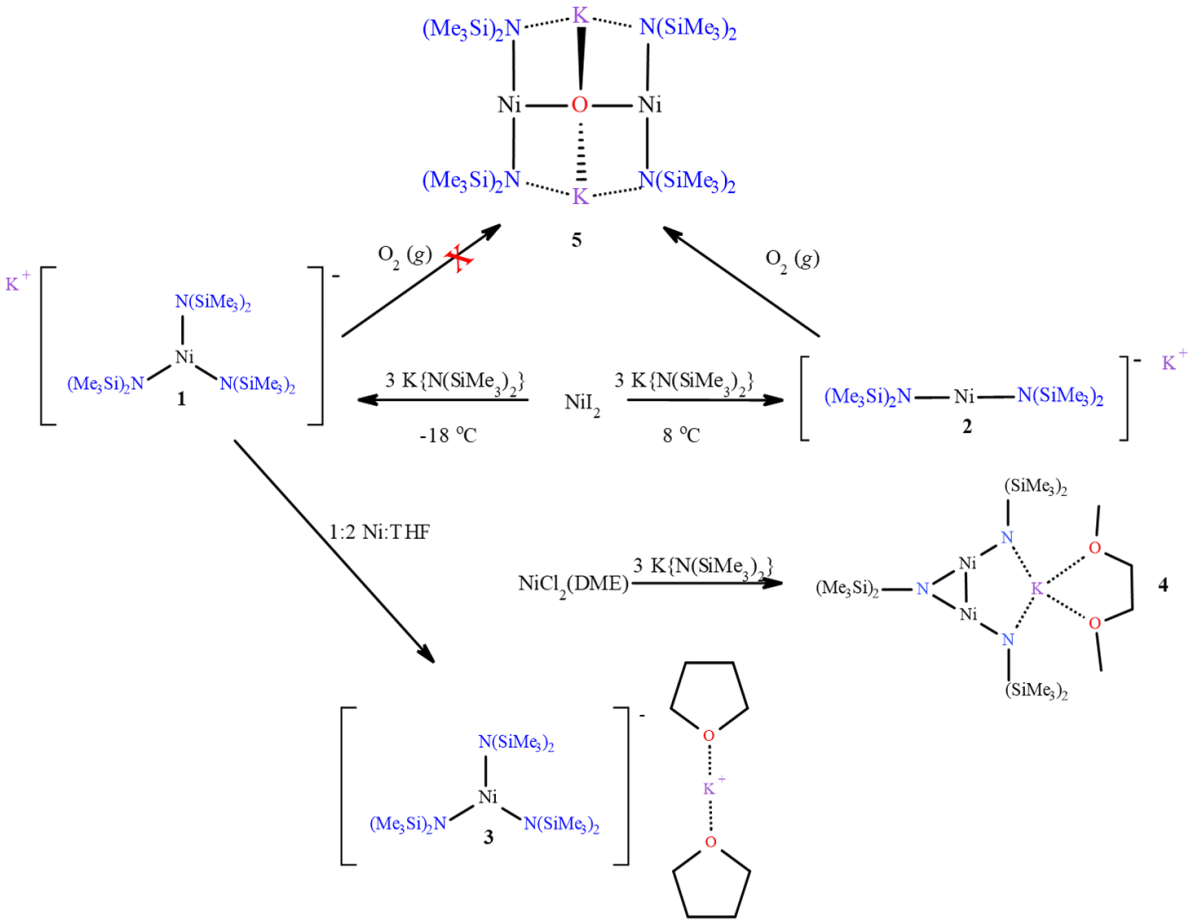

5.3. EXPERIMENTAL SECTION

[a]Although less common then the +2 oxidation state, Ni(I) complexes are now numerous
[b]For example, $[Li(dmap)_4][Ni(II)\{N(SiMe_3)_2\}_3]$[14] and $[Na(pmdeta)_2][Ni(II)\{N(SiMe_3)_2\}_3]$[15]

General Considerations

All manipulations were carried out under anaerobic and anhydrous conditions by using standard Schlenk techniques or in a Vacuum Atmospheres OMNI-Lab drybox under an atmosphere of dry argon or nitrogen. Solvents were dried by the method of Grubbs and co-workers,[16] stored over potassium or sodium, and then degassed by the freeze−pump−thaw method. All physical measurements were made under strictly anaerobic and anhydrous conditions. Melting points of samples in flame-sealed capillaries were determined using a Meltemp II apparatus equipped with a partial immersion thermometer and a device limit of 250 ^{o}C. IR spectra were recorded as Nujol mulls between CsI plates on a PerkinElmer 1430 spectrometer. UV−vis spectra were recorded as dilute toluene solutions in 3.5 mL quartz cuvettes using an Olis 17 modernized Cary 14 UV−Vis−near-IR spectrophotometer. NiI_2 and $K\{N(SiMe_3)_2\}$ were obtained from commercial sources and used as received. The purity of the $K\{N(SiMe_3)_2\}$, which was found to resonate at ca. 0.14 ppm in C_6D_6, was confirmed by ^{1}H NMR spectroscopy. $NiCl_2$(DME) was prepared according to a literature procedure.[17] NMR spectra were recorded on a Bruker 400 MHz AVANCE III HD Nanobay spectrometer, and the ^{1}H NMR spectra were referenced to the residual solvent signals in deuterated benzene or deuterated toluene. Magnetic susceptibility data were collected at room temperature by the Evans' method[18] and were corrected using the appropriate diamagnetic constants.[19] Powder X-ray diffraction (PXRD) patterns for **1** and **2** were collected on a Bruker D8 Advance diffractometer using Cu Kα radiation operated at 40 kV and 25 mA at room temperature.

Synthesis

$[K][Ni(N(SiMe_3)_2)_3]$ (**1**): 0.295 g NiI_2 (0.944 mmol) and 0.529 g $K\{N(SiMe_3)_2\}$ (2.65 mmol) were combined in a 100 mL Schlenk flask with cooling to ca. 0 ^{o}C. A ca. 35 mL solution of

chilled (ca. 0 ^{o}C) Et_2O was added via cannula to the reaction flask to give a grey suspension. This suspension was stirred for 15 minutes at ca. 0 ^{o}C and was then warmed to room temperature and stirred for a further ca. 18 h. The solvent was removed under reduced pressure (ca. 0.01 torr) to leave a dark green solid. The residue was washed with ca. 10 mL hexane and dried under reduced pressure for 1 h. Extraction of the dark green solids with ca. 40 mL hexane produced a red solution that was filtered via a filter-tipped cannula. The filtrate was concentrated to ca. 25 mL whereupon microcrystalline material precipitated onto the walls of the flask. This was redissolved at room temperature, and the solution was stored overnight at ca. -18 ^{o}C to give yellow needles of **1** that were suitable for X-ray crystallographic studies. Solutions of **1** begin to decompose above ca. -10 ^{o}C. In the absence of solvent the crystals slowly decompose over ca. 12 h. Yield: 0.086 g (16 %) mp 85-87 ^{o}C (dec). μ_{eff}: 2.37 μ_B. ^{1}H NMR (400 MHz, C_7D_8, 25 ^{o}C) 10.74 ppm ^{1}H NMR (400 MHz, C_6D_6, 25 ^{o}C) 10.75 ppm. UV-vis λ/nm (ε/$M^{-1}cm^{-1}$): 225 nm (6,800), 408 nm (3,000), 489 nm (2,300). IR (Nujol; $\tilde{\nu}$/cm^{-1}) 2900 (s), 2720 (m), 1450 (s), 1375 (s), 1255 (s), 1240 (s), 1210 (s), 970 (s), 830 (s), 780 (s), 755 (s), 740 (s), 705 (s), 670 (s), 655 (s), 620 (m), 610 (m), 395 (w), 370 (m).

[K][Ni(N(SiMe$_3$)$_2$)$_2$] (**2**): 0.299 g NiI_2 (0.956 mmol) and 0.572 g K{$N(SiMe_3)_2$} (2.868 mmol) were combined in a 100 mL Schlenk flask with cooling to ca. 0 ^{o}C. A ca. 35 mL solution of chilled (ca. 0 ^{o}C) Et_2O was added via cannula to the reaction flask to give a grey suspension. This suspension was stirred for 15 minutes at ca. 0 ^{o}C and warmed to room temperature. After ca. 1 h., the suspension became green and was stirred for a further 18 h. at room temperature. The solvent was removed under reduced pressure (ca. 0.01 torr) to leave a dark green solid. The residue was washed with ca. 10 mL of hexane and dried under reduced pressure for 1 h. Extraction of the dark green solid with ca. 40 mL of hexane produced a red solution that was

filtered via a filter-tipped cannula. This red solution was stored overnight in a ca. 8 °C fridge to give teal blocks of **2** that were suitable for X-ray crystallographic studies. Redissolving the crystals of **2** at room temperature in hexane, benzene, or toluene yields the slow decomposition of **2**. Crystalline **2** is stable for ca. 24 h. at room temperature. mp 183-185 °C (dec.) 0.026 g (7 %). μ_{eff}: 1.7 μ_B ^{1}H NMR (400 MHz, C_6D_6, 25 °C, ppm) 0.77, 0.04, -0.36. UV-vis λ/nm (ε/$M^{-1}cm^{-1}$): 225 nm (1,400). IR (Nujol; $\tilde{\nu}$/cm^{-1}) 2900 (s), 1470 (s), 1380 (s), 1250 (s), 1185 (m), 1050 (s), 985 (s), 940 (s), 835 (s), 785 (s), 755 (s), 715 (m), 670 (s), 620 (m), 380 (m).

[K(THF)$_2$][Ni(N(SiMe$_3$)$_2$)$_3$] (**3**): A solution of **1** was synthesized from 0.303 g NiI_2 (0.970 mmol) and 0.581 g K{$N(SiMe_3)_2$} (2.91 mmol). Then 0.039 g of crystalline **1** was dissolved in ca. 50 mL of hexane, and a 1:2 stoichiometric (Ni:THF) quantity of THF (0.01 mL) was added to the solution via syringe and stirred for ca. 2 h. The solvent was concentrated to ca. 15 mL which afforded a deposit of yellow microcrystalline material on the walls of the Schlenk flask. The solution was stored overnight in a ca. -35 °C freezer to give yellow, feather-like plates of **3** that were suitable for X-ray crystallography. Crystalline **3** is stable at room temperature for ca. 48 h., but ^{1}H NMR spectroscopy shows partial decomposition at ca. 25 °C. 0.024 g (48 %) mp 51-53 °C (dec.). μ_{eff}: 2.24 μ_B. ^{1}H NMR (400 MHz, C_6D_6, 25 °C, ppm) 10.70. UV-vis λ/nm (ε/$M^{-1}cm^{-1}$): 223 (3,400), 402 (650), 487 (660). IR (Nujol; $\tilde{\nu}$/cm^{-1}) 2900 (s), 2840 (s), 1455 (s), 1370 (s), 1255 (s), 1170 (m), 1085 (s), 1010 (s), 975 (m), 925 (m), 795 (s), 715 (m), 610 (w), 365 (w).

[K(DME)][Ni$_2$(N(SiMe$_3$)$_2$)$_3$] (**4**). 0.203 g (0.924 mmol) of $NiCl_2$(DME)[17] and 0.515 g (2.58 mmol) of K{$N(SiMe_3)_2$} were combined in a 100 mL Schlenk flask with cooling to ca. 0 °C. Chilled (ca. 0 °C) Et_2O (ca. 35 mL) was added via cannula to the reaction flask to give a pale green suspension. The suspension was stirred for 15 minutes at ca. 0 °C and warmed to room temperature whereupon stirring was continued for ca. 12 h. The solvent was removed under

reduced pressure (ca. 0.01 torr) to leave a green solid. This residue was washed with ca. 10 mL hexane and dried under reduced pressure for 1 h. Extraction of the dark green solids with ca. 40 mL of hexane produced a red solution that was filtered via a filter-tipped cannula. Storage of the red solution in a ca. 8 ^{o}C fridge for two days, followed by storage in a ca. -18 ^{o}C freezer for three weeks gave bright red crystals of **4** that were suitable for X-ray crystallography. Crystalline **4** is stable in solution at -18 ^{o}C, but as a room temperature solid it begins to decompose to black after ca. 24 h. Yield 0.033 g (10 %, calculated from $NiCl_2(DME)$) of **4**, mp 111-113 ^{o}C. ^{1}H NMR (400 MHz, C_6D_6, 25 ^{o}C, ppm) 3.03, 2.87, 1.39, 0.98, 0.92. μ_{eff}: 1.20 μ_B. UV-vis λ/nm (ε/$M^{-1}cm^{-1}$): 226 (1,400). IR (Nujol; $\tilde{\nu}$/cm^{-1}) 2900 (s), 1450 (s), 1370 (s), 1250 (s), 1085 (s), 1000 (s, broad) 975 (s), 880 (s), 830 (s, broad), 750 (m), 720 (m), 700 (m), 670 (m), 610 (w), 440 (w), 360 (w).

$[K_2][O(Ni\{N(SiMe_3)_2\}_2)_2]$ (**5**): The synthesis of **2** (see above) was repeated with 0.304 g (0.971 mmol) of NiI_2 and 0.503 g (2.52 mmol) $K\{N(SiMe_3)_2\}$. The hexane solution of *in situ* synthesized **2** was placed in a ca. -18 ^{o}C freezer for three weeks, after which the silicone grease seal had become eroded. Colorless crystals that were suitable for X-ray crystallography were recovered from this solution to yield 0.018 g (4 %, calculated from NiI_2) of **5**, mp 70-71 ^{o}C. μ_{eff}: 1.46 μ_B. ^{1}H NMR (400 MHz, C_6D_6, 25 ^{o}C, ppm) 0.38. UV-vis λ/nm (ε/$M^{-1}cm^{-1}$): 225 nm (5,800). IR (Nujol; $\tilde{\nu}$/cm^{-1}) 2920 (s), 2840 (s), 1460 (s), 1375 (s), 1260 (s), 1180 (m), 1015 (s), 930 (s), 840 (s), 800 (s), 385 (w).

X-Ray Crystallographic Studies

Crystals of **1**-**5** suitable for X-ray crystallographic studies were obtained from saturated hexane solutions at various temperatures (see above). The crystals were removed from the Schlenk tubes and immediately covered with a layer of hydrocarbon oil. Suitable crystals were selected, mounted on a nylon cryoloop, and then placed in the cold nitrogen stream of the diffractometer.

Data for **3** and **5** were collected at 100(2) K, and data for **1**, **2**, and **4** were collected at 190(2) K. Data for **3** were collected with Cu $K\alpha_1$ radiation (λ = 1.5418 A) while data for **1**, **2**, and **4-5** were collected with Mo $K\alpha_1$ radiation (λ = 0.71073 Å) using a Bruker D8 Venture dual source diffractometer in conjunction with a CCD detector. The collected reflections were corrected for Lorentz and polarization effects and for absorption by using Blessing's method as incorporated into the program SADABS.[20,21] The structures were solved by direct methods and refined with the SHELXTL (2012, version 6.1) or SHELXTL (2013) software packages.[22] Refinement was by full-matrix least-squares procedures, with all carbon-bound hydrogen atoms included in calculated positions and treated as riding atoms. The thermal ellipsoid plots were drawn using OLEX2 software.[23]

5.4. RESULTS AND DISCUSSION

Synthesis and Structures

The complex $[K][Ni\{N(SiMe_3)_2\}_3]$ (**1**) is readily isolated (see above) as bright yellow needles upon cooling a hexane solution of **1** to ca. -18 ^oC (Figure 1). These yellow needles can be removed under a counter-flow of the working gas (Ar or N_2) at room temperature for X-ray crystallographic analysis without noticeable decomposition. However, the stability of **1** in the Paratone oil used in the protection of the crystals is limited to ca. 30 min. at room temperature. Nonetheless, this stability is remarkable considering that the analogous species $[Na][Ni\{N(SiMe_3)_2\}_3]$ cannot be isolated without Lewis-base complexation of the sodium cation.[15] Complex **1** is the first isolable Ni(II) bis(trimethylsilyl)amide salt free of complexation by neutral donor solvent molecules bound to the Ni atom or donor-sequestered alkali metal cations. The isolation of **1** as a solid updates previous reports of donor-free Ni(II) and Ni(I) complexes which were reported to exist as oils at room temperature or to decompose readily in

the absence of solvent or under reduced pressure.[2,14,15] Hexane solutions of [K][Ni{N(SiMe$_3$)$_2$}$_3$] (**1**) retain a red hue for more than 1 week at temperatures less than ca. -10 ^{o}C. Benzene solutions of **1** decompose after ca. 12 h. at room temperature and toluene solutions of **1** decompose after ca. 12 h. at or above 0 ^{o}C. In further contrast to previous reports, the synthesis of other 3-coordinate Ni(II) nickelate salts required the use of THF[14] or pmdeta[15] as a solvent or the use of other base-stabilized Ni(II) species, such as Ni{N(SiMe$_3$)$_2$}$_2$(dmap)$_2$, as starting materials.[14]

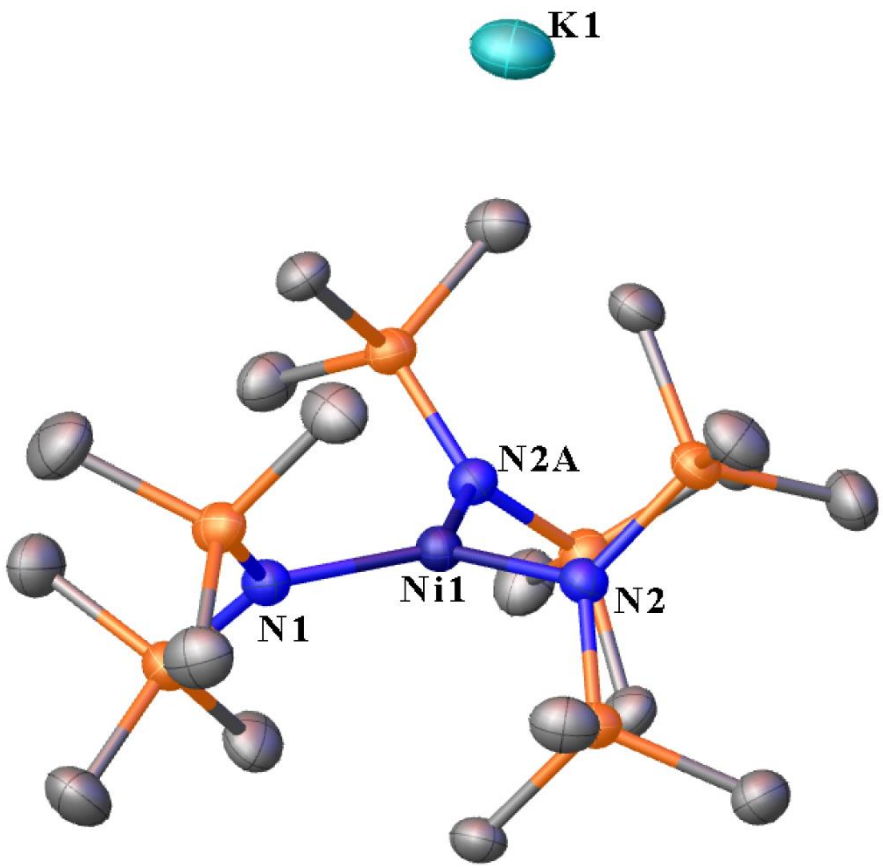

Figure 3. A 50% thermal ellipsoid plot of [K][Ni{N(SiMe$_3$)$_2$}$_3$] (**1**). Hydrogen atoms are not shown for clarity. Selected distances (Å) and angles (^{o}): Ni1-N1 1.934(2), Ni1-N2 1.9299(16), Ni1-N2A 1.9299(16), N1-Ni1-N2 121.13(5), N1-Ni1-N2A 121.12(5), N2-Ni1-N2A 117.75(9). Σ_{angles} Ni1 = 360.00(11).

After a solution of **1** was stored for ca. 1 week in a benzene-d_6 solution, teal crystals were recovered from the J. Young NMR tube. Analysis of the crystals by X-ray crystallography gave a structure of the Ni(I) species [K][Ni{N(SiMe$_3$)$_2$}$_2$] (**2**) (Figure 2). The complex [K][Ni{N(SiMe$_3$)$_2$}$_2$] (**2**) is a Ni(I) nickelate that is not stabilized by the coordination of donor solvents or sequestered cations. The initial isolation of **2** from the NMR tube gave crystals in a quantity that only permitted an X-ray crystallographic characterization. Investigations of the intentional formation of the Ni(I) complex [K][Ni{N(SiMe$_3$)$_2$}$_2$] (**2**) in higher yield revealed that at temperatures below ca. -10 ^{o}C, a 3:1 ligand to metal ratio gives complex **1** with no observable formation of teal-colored crystals. However, repeating this reaction with the same 3:1 ligand to metal salt ratio, followed by storage at ca. 8 ^{o}C gave pale, teal-colored blocks of [K][Ni{N(SiMe$_3$)$_2$}$_2$] (**2**) as the only crystalline product (Scheme 2). Storing solutions of **1** at room temperature also gave crystalline **2**, consistent with its initial isolation, but in lower crystalline yield.

Scheme 3. Synthesis of compounds **1** and **2**.

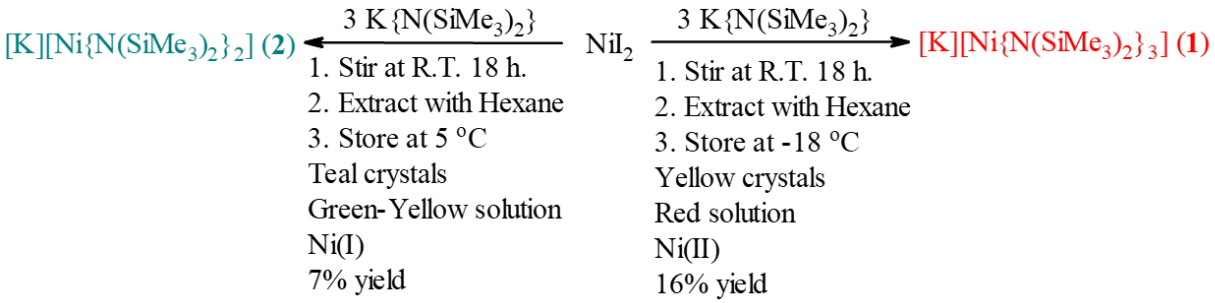

Thus, the formation of **2** from solutions of **1** is likely the result of a one-electron reduction of an *in situ* generated Ni{N(SiMe$_3$)$_2$}$_2$ by the excess equivalent of K{N(SiMe$_3$)$_2$}, rather than by the degradation of Ni{N(SiMe$_3$)$_2$}$_2$ or other intermediates, with the rate of reduction being temperature dependent. Potassium salts of organic nucleophiles have been shown to reduce similar species[24] but the Ni(I) tetramer[2] [Ni{N(SiMe$_3$)$_2$}]$_4$ was not observed as a side product in

this case. The reported investigations into other potential mechanisms of formation revealed that the use of the powerful reducing agent KC_8 with $[Li(THF)_{4.5\text{-}5.5}][Ni\{N(SiMe_3)_2\}_3]$[14] in toluene gave a Ni(I) complex $[K(toluene)][Ni_2\{N(SiMe_3)_2\}_3]$.[14] It was suggested that this complex could be viewed as an intermediate in the decomposition pathway to the Ni(I) tetramer $[Ni\{N(SiMe_3)_2\}]_4$.[2,14] While there are some structural similarities between **2** and $[K(toluene)][Ni_2\{N(SiMe_3)_2\}_3]$,[14] such as the sub-180° N-Ni-N angles and the sub-1.9 Å Ni-N distances, the solution behavior of interest cannot be compared at present due to the difficulty in isolating $[K(toluene)][Ni_2\{N(SiMe_3)_2\}_3]$ in quantities suitable for thorough spectroscopic characterization.[14]

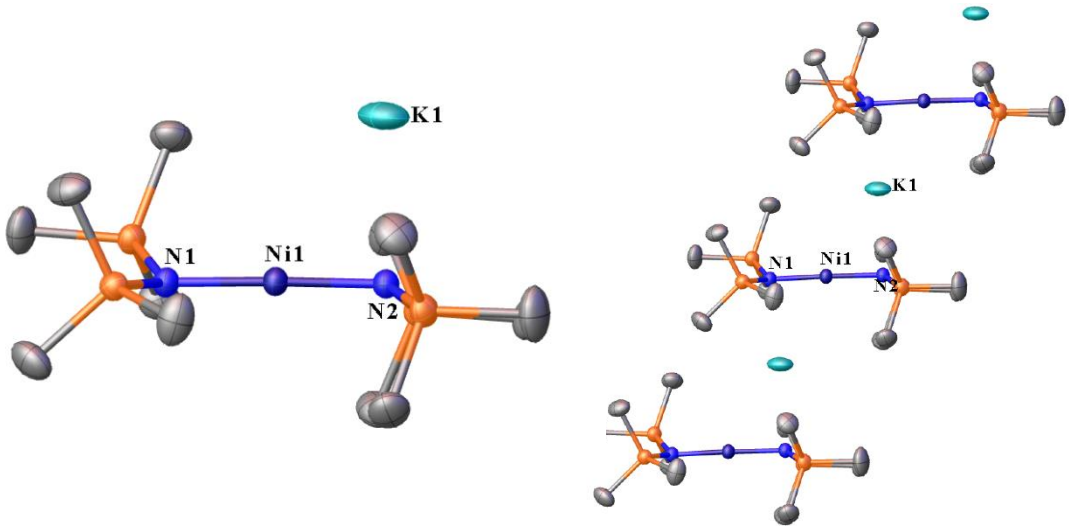

Figure 4. Left: 50% thermal ellipsoid plot of $[K][Ni\{N(SiMe_3)_2\}_2]$ (**2**). Right: Side view of a 50% thermal ellipsoid plot of $[K][Ni\{N(SiMe_3)_2\}_2]$ (**2**) showing the connectivity between each molecule in their discrete asymmetric units. Hydrogen atoms are not shown for clarity. Selected distances (Å) and angles (°): Ni1-N1 1.8559(9), Ni1-N2 1.8711(9), K1···N2 2.8370(9). N1-Ni1-N2 176.81(4).

To determine if coordinating solvents prevent the formation of a 3-coordinate Ni(II) nickelate species, a stoichiometric amount of THF (Scheme 1) was added to a hexane solution of **1**.

Storage of this solution at ca. -35 °C gave yellow, feather-like crystals. Analysis of these crystals via X-ray crystallography revealed them to be $[K(THF)_2][Ni\{N(SiMe_3)_2\}_3]$ (**3**). The structure of the $[Ni\{N(SiMe_3)_2\}_3]^-$ anion in **3** (Figure 3) is nearly identical to that of **1**, but the counter cation features THF coordination to the K^+ ion. This result is surprising, as we expected that the coordination of THF to the Ni^{2+} ion would occur rapidly in solution and give the known compound $Ni\{N(SiMe_3)_2\}_2(THF)$.[2] This further emphasizes the significance of the transfer agent cation and the solvent type in the isolation of new complexes.

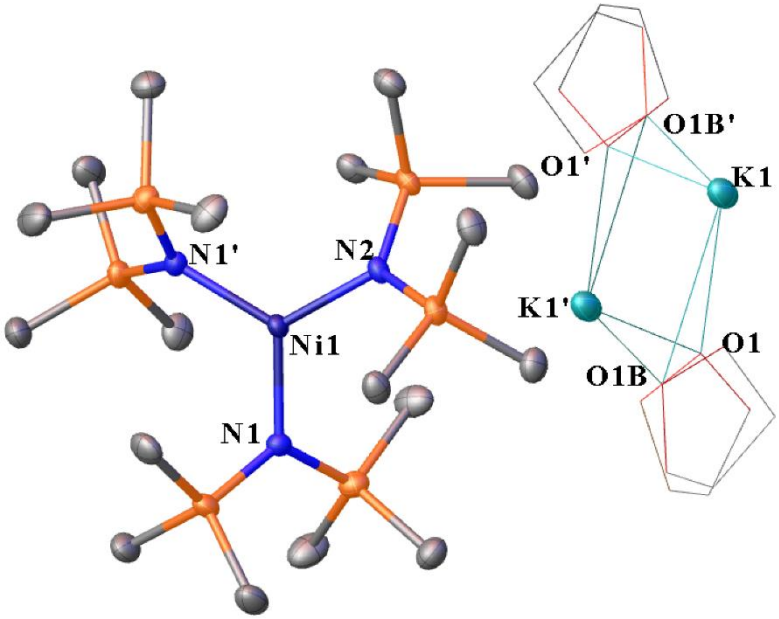

Figure 5. Thermal ellipsoid plot (50%) of $[K(THF)_2][Ni\{N(SiMe_3)_2\}_3]$ (**3**) with solvent molecules (THF) shown in their disordered positions as wireframe structures. Hydrogen atoms are not shown for clarity, K1 (light blue) is disordered over two positions (K1 and K1′), each with 50% occupancy. Selected distances (Å) and angles (°): Ni1-N1 1.9339(16), Ni1-N2 1.927(2), Ni1-N1′ 1.9339(16), Ni1···K1 6.4053(11), Ni1···K1′ 7.5809(10), N1-Ni1-N2 119.96(5), N1-Ni1-N1′ 120.07(10), N2-Ni1-N1′ 119.96(5), ΣNi1 359.99(12). O1-K1′ 2.595(8), O1-K1 3.279(8), O1B-K1 2.609(9), O1B-K1′ 3.302(8).

While a previous attempt to synthesize $Ni\{N(SiMe_3)_2\}_2$ using $NiCl_2$ and $K\{N(SiMe_3)_2\}$ as the transfer agent in a 3:1 ligand to metal ratio gave intractable brown solids,[14] addition of $K\{N(SiMe_3)_2\}$ to $NiCl_2$(DME) in a 3:1 ligand to metal ratio followed by extraction of the resultant residue with hexanes gave red crystals of $[K(DME)][Ni_2\{N(SiMe_3)_2\}_3]$ (**4**, Figure 4) in low yield. No other crystalline compounds were isolated from this reaction. The structure of **4** is analogous to that of $[K(toluene)][Ni_2\{N(SiMe_3)_2\}_3]$[14] reported by Werncke and coworkers. Where the complex $[K(toluene)][Ni_2\{N(SiMe_3)_2\}_3]\}$ was isolated from the KC_8 reduction of $[Li(THF)_{4.5\text{-}5.5'}][Ni\{N(SiMe_3)_2\}_3]$ in toluene.[14] The propensity for $K\{N(SiMe_3)_2\}$ to function as a reducing agent is further demonstrated in the isolation of **4**, given that its toluene congener is only observed upon reduction with the potent reducing agent KC_8.[14]

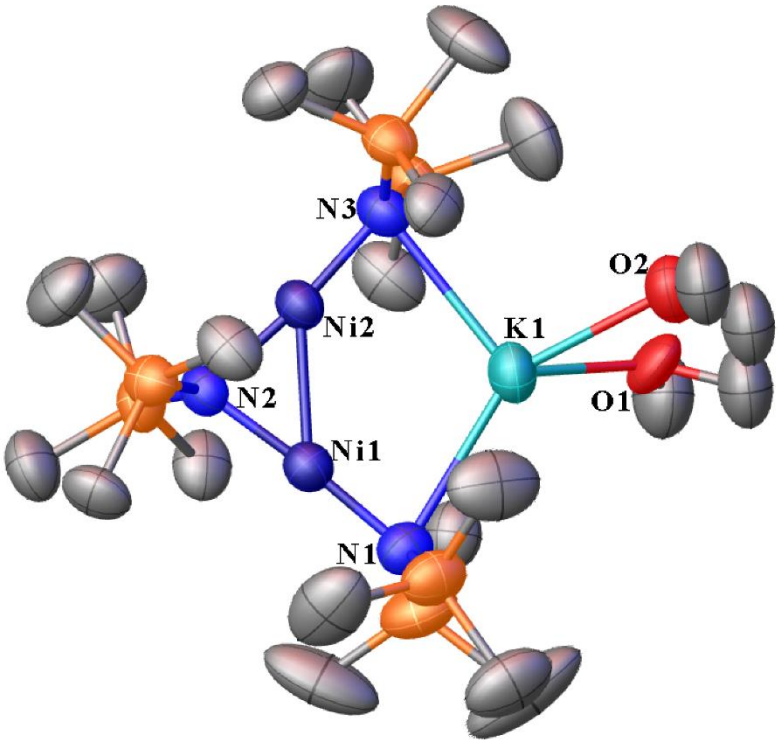

Figure 4. Thermal ellipsoid plot (50%) of [K(DME)][Ni_2{$N(SiMe_3)_2$}$_3$] (**4**). Hydrogen atoms and minor occupancy positions of the -$SiMe_3$ groups and DME atoms are not shown for clarity. Selected distances (Å) and angles (°): Ni1···K1 3.3051(7), Ni2···K1 3.2759(8). Ni1-Ni2 2.4109(5), Ni1-N1 1.8660(19), Ni1-N2 1.8921(17), Ni2-N2 1.9005(15), Ni2-N3 1.8607(17), N1-K1 3.052(2), N3-K1 3.0539(19), N1-Ni1-N2 175.83(8), N2-Ni2-N3 174.00(8), N3-Ni2-Ni1 135.62(6), N1-Ni1-Ni2 133.48(6), Ni1-N2-Ni2 78.94(6), N2-Ni2-Ni1 50.38(5), N2-Ni1-Ni2 50.68(5), N1-K1-N3 110.77(5).

During attempts to repeat the synthesis of [K][Ni{$N(SiMe_3)_2$}$_2$] (**2**), a flask containing 3 equivalents of K{$N(SiMe_3)_2$} and 1 equivalent of NiI_2 was stored in a ca. -18 °C freezer for three weeks. After this period, it was removed from the freezer, and it was observed that the silicone grease of the glass stopper had become “streaky” and partially eroded. Removal of the supernatant liquid via cannula revealed a cluster of colorless crystals that had been deposited on

the wall of the flask that were suitable for characterization via X-ray crystallography. These crystals allowed the structure of the new Ni(II) complex $[K_2][O(Ni\{N(SiMe_3)_2\}_2)_2]$ (**5**) to be determined. The formation of complex **5** (Figure 5) is likely due to adventitious amounts of oxygen or moisture that arose during storage of the Schlenk flask in the freezer produced an imperfect silicone grease seal at the glass stopper. In the 'inverse-crown' ether (ICE) structure, the metals in the 'crown' act as Lewis acids for the O^{2-} anion.[25,26] To date, the principal isolation routes of all ICE complexes of the first-row transition metals have been reported to involve the introduction of 'adventitious' amounts of oxygen, similar to the isolation route for complex **5**.[27,28] Furthermore, the syntheses designed to isolate pure ICE complexes of the 3d metals give impure products for Mn(II) and Co(II), but pure ICE complexes of Zn(II) can be isolated.[27-29] For Ni(II), storage of three separate hexane solutions of $[K][Ni\{N(SiMe_3)_2\}_2]$ (**2**) in a -18 ^{o}C freezer with an imperfect silicone grease seal reliably gave colorless crystals of **5**.

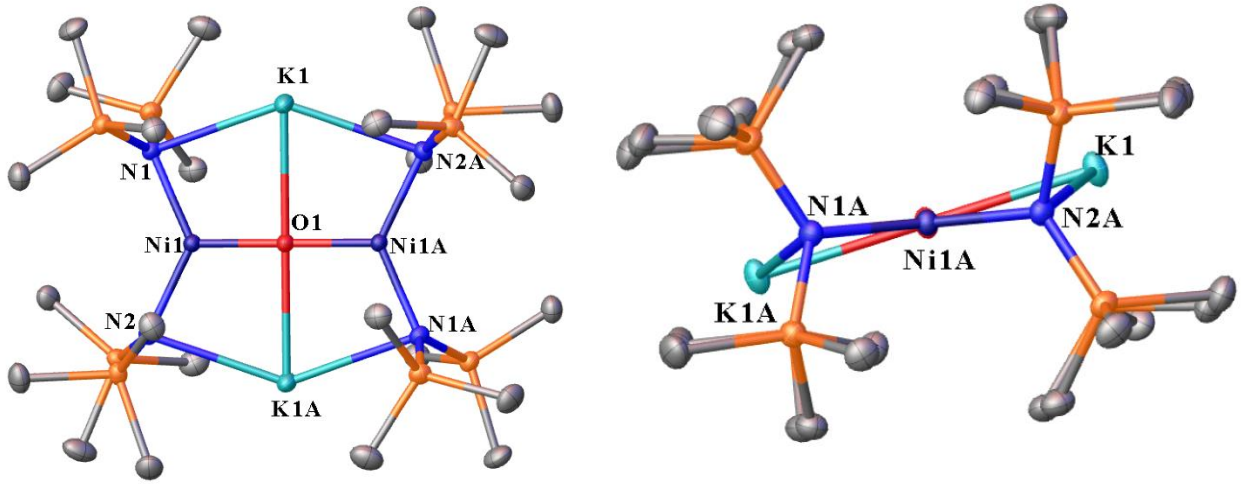

Figure 5. Thermal ellipsoid plot (50%) of $[K_2][O(Ni\{N(SiMe_3)_2\}_2)_2]$ (**5**) with hydrogen atoms not shown for clarity. Selected distances (Å) and angles (°): Ni1-O1 1.80152(19), Ni1-N2 1.9330(11) Ni1-N1 1.9362(11), K1-O1 2.6873(3), K1-N2A 2.7923(11), K1-N1 2.8381(11), Ni1⋯K1 3.2675(4), Ni1-K1A ⋯3.2028(4), O1-Ni1-N2 115.90(3), O1-Ni1-N1 113.92(3), N2-Ni1-N1 130.18(5), Ni1-O1-Ni1A 180.00, Ni1A-O1-K1 88.761(8), Ni1-O1-K1 91.238(9), Ni1A-O1-K1A 91.239(8), Ni1-O1-K1A 88.762(9), K1-O1-K1A 180.00.

The structure of **5** resembles those of the rare 3d metal inverse crown-ether (ICE) complexes of Mn(II),[27] Co(II),[28] and Zn(II) reported by Mulvey and coworkers.[29] The bis(trimethylsilyl)amido ICE complexes are limited to a Mn(II) complex with Na^+ cations,[27] a Co(II) complex with Na^+ cations,[28] and two Zn(II) complexes.[29] A further Mn(II) ICE complex was isolated using 2,2,6,6-tetramethylpiperidide to give an amido anion.[27] A few other ICE complexes exist for s- and p-block[30-34] metals and one f-block ytterbium ICE complex.[35] The complex **5**, however, is the first example for nickel.

Structural Analysis

In complex **1**, the K^+ ion is associated with the anion via C-H···K^+ contacts. The sum of the interligand bond angles at the Ni(II) atom in [K][Ni{N(SiMe$_3$)$_2$}$_3$] (**1**) are within a standard deviation of 360^o and are indicative of a trigonal planar geometry. The Ni-N distances (av. 1.931(2) Å) in **1** are similar to those reported for neutral and anionic Ni(II) complexes.[2,14,15] However, the distances are near the upper end of the range of Ni-N(SiMe$_3$)$_2$ distances of ca. 1.86-1.95 Å (Table 1). The K^+ ions are 'solvated' by 12 adjacent (K···H < 3.1 Å) hydrogens from 6 of the ligand methyl groups. Two of the three bis(trimethylsilyl)amido ligands at each Ni(II) atom participate in this solvation of K^+ ions by the discrete [Ni{N(SiMe$_3$)$_2$}$_3$]$^-$ units.

Only one 2-coordinate Ni(I) amido anion stabilized exclusively by bis(trimethylsilyl)amido ligands has been isolated to date and this features either 18-crown-6 or [2.2.2]cryptand sequestered K^+ countercations for a [Ni{N(SiMe$_3$)$_2$}$_2$]$^-$ anion. Notably, the previously reported Ni(I) complex K{(18-crown-6)}[Ni{N(SiMe$_3$)$_2$}$_2$][14] (or K{[2.2.2]cryptand}[Ni{N(SiMe$_3$)$_2$}$_2$][14]) has the only strictly linear coordinated Ni(I) anion with a 180^o N-Ni-N angle (Table 1). The N-Ni-N angle between the bis(trimethylsilyl)amido ligands in [K][Ni{N(SiMe$_3$)$_2$}$_2$] (**2**) is 176.81(6)^o and its deviation from linearity, although slight, is the largest of the related 2-coordinate complexes (Table 1). The Ni-N distances of 1.8559(9) and 1.8711(9) Å differ slightly. The solvation of the K^+ ion in **2** by the ligands and the K^+···N distance of ca. 2.86 Å implicates the coordination of the K^+ ion by the lone-pair electrons of the nitrogen atom (N2, Figure 2) as the cause of the deviation from linearity. This close contact between the nitrogen atom and K cation cause a slight pyramidalization of the geometry at the N atoms, which is not observed in other 2-coordinate Ni(I) species. Unexpectedly, the Ni-N distances in **2** are shorter than those reported for other Ni(I) amido species and just two Ni(II) species have shorter Ni-N distances (cf. Table 1).

Table 1. Selected distances (Å) and angles (°) in Ni(I) and Ni(II) bis(trimethylsilyl)amides.

Compound	Ni-N	Ni-Donor	N-Ni-N	Coord. No. and Structure Type	Σ_{angles} Ni
$[K][Ni\{N(SiMe_3)_2\}_3]$ (**1**)	1.931(2)[a]	N/A	120(2)[a]	3, ion pair	359.999(8)
$[K][Ni\{N(SiMe_3)_2\}_2]$ (**2**)	1.86(1)[a]	N/A	176.81(6)	2, ion pair	176.81(6)
$[K(THF)_2][Ni\{N(SiMe_3)_2\}_3]$ (**3**)	1.932(4)	N/A	120.00(6)	3, ion pair	359.99(12)
$[K(DME)][Ni_2\{N(SiMe_3)_2\}_3]$ (**4**)	1.88(2)[a]	K-Donor	175(1)	3, monomer	360.00(12)
$[K_2][O(Ni\{N(SiMe_3)_2\}_2)_2]$ (**5**)*	1.935(2)[a]	N/A	130.18(5)	3, monomer	360.00(6)
$Ni\{N(SiMe_3)_2\}_2(THF)^2$	1.861(3)[a]	2.0143(2)	140.664(5)	3, monomer	359.86(27)
$Ni\{N(SiMe_3)_2\}_2(py)_2^2$	1.942(4)[a]	1.9310(6)[a]	179.2607(3)	4, monomer	358.3599(4)
$[Ni\{N(SiMe_3)_2\}]_4^2$	1.916(3)[a]	N/A	168.85(7)[a]	2, tetramer	168.85(7)[a]
$Ni\{\overline{N(SiMe_2)_2(SiMe_2CH_2)}\}(py)_2^2$	1.9197(14)	1.96(6)[a]	N/A	4, monomer	360.07
$[Na(pmdeta)_2][Ni\{N(SiMe_3)_2\}_3]$[15]	1.929(2)[a]	Na-Donor	120.0(7)[a]	3, ion pair	359.9(2)
$[Li(dmap)_4][Ni\{N(SiMe_3)_2\}_3]$[14]	1.930(2)[a]	Li-Donor	120(2)[a]	3, ion pair	360.00(8)
$Ni\{N(SiMe_3)_2\}_2(dmap)_2$[14]	1.949(1)[a]	1.917(1)[a]	179.08(6)	4, monomer	356.64(8)
$[Ni\{N(SiMe_3)_2\}(bipy)]$[14]	1.898(3)	1.947(4)[a]	N/A	3, monomer	360.01(31)
$Ni\{N(SiMe_3)_2\}_2(bipy)$[14]	1.860(1)	2.030(1)	136.05(6)	4, monomer	415.05(10)
[K(18-crown-6)][$Ni\{N(SiMe_3)_2\}_2$][14]	1.866(1)	K-Donor	180	2, ion pair	180
[K(toluene)][$Ni_2\{N(SiMe_3)_2\}_3$][14]	1.881(16)	K-Donor	174.74(5)	3, monomer	359.91(7)

[a]Average value *triclinic data. dmap = 4-dimethylaminopyridine; bipy = 2,2′-bipyridine; pmdeta = N,N,N′,N″,N″-pentamethyldiethylenetriamine.

$[K(THF)_2][Ni\{N(SiMe_3)_2\}_3]$ (**3**) is the only nickel bis(trimethylsilyl)amido complex featuring a donor solvent (in this case THF) coordinating to an atom other than nickel. The K^+ ions are disordered over two 50% occupancy positions. The solvent molecules reflect the split occupancy of the K^+ ions in the lattice and are also disordered over 51% (Figure 3, top) and 49% (Figure 3, bottom) occupancy positions. The sum of the interligand angles at the Ni(II) atom of 359.99(12)° confirm a trigonal planar geometry. This sum of angles is identical to that observed in **1** and is within a standard deviation to those observed in Ni(II) nickelate anions featuring donor-sequestered cations (Table 1). Two of the three Ni-N distances are identical at 1.9339(16) Å,

while one is slightly shorter at 1.927(2) Å to give an average Ni-N distance of 1.932(4) Å. These Ni-N distances are within the expected range[2,14,15] of ca. 1.86-1.95 Å (Table 1) for Ni(II) species and are identical within standard deviations to those observed in complex **1**.

For [K(DME)][Ni_2{$N(SiMe_3)_2$}$_3$] (**4**), the Ni1-Ni2 distance of 2.4108(6) Å is shorter than that observed in [K(toluene)][Ni{$N(SiMe_3)_2$}$_3$][14] by ca. 0.03 Å. This Ni1-Ni2 distance is also shorter than those observed in the Ni(I) tetramer [Ni{$N(SiMe_3)_2$}]$_4$[2] by ca. 0.02 Å. The Ni-N distances are comparable to those in [K(toluene)][Ni{$N(SiMe_3)_2$}$_3$],[14] but shorter than those in [Ni{$N(SiMe_3)_2$}]$_4$.[2] Given that the structure of [K(toluene)][Ni{$N(SiMe_3)_2$}$_3$][14] and [K(DME)][Ni_2{$N(SiMe_3)_2$}$_3$] (**4**) can be viewed as intermediate structures between neutral Ni{$N(SiMe_3)_2$}$_2$ and [Ni{$N(SiMe_3)_2$}]$_4$,[2,14] the shorter Ni-N distances are expected due to a decrease in steric repulsion of the -$SiMe_3$ groups compared to those in the Ni(I) tetramer [Ni{$N(SiMe_3)_2$}]$_4$.[2] The effective magnetic moment of 1.20 μ_B for [K(DME)][Ni_2{$N(SiMe_3)_2$}$_3$] (**4**) indicates a strong anti-ferromagnetic coupling between the two Ni(I) ions, since the spin-only value for two distinct, non-interacting Ni(I) nuclei is 2.45 μ_B.[36] Crystallographic data for **4** were collected at 190(2)K and at this temperature, **4** crystallizes in the orthorhombic space group Pbca. Slowly cooling the crystal on the goniometer to 100(2)K results in a temperature dependent phase transition from orthorhombic Pbca to monoclinic $P2_1/c$. The beta angle shifts from 90^o at 190(2) K to 90.285(4)^o at 100(2) K. A temperature dependent phase transition was not reported for [K(toluene)][Ni{$N(SiMe_3)_2$}$_3$][14] and further investigation is required to determine if this observation is unique to complex **4**.

The complex [K_2][O(Ni{$N(SiMe_3)_2$}$_2$)$_2$] (**5**) features a planar coordinated μ_4-O atom that occupies a center of symmetry and affords a half-molecule per unit cell. Examination of the crystals under a microscope reveal two distinct morphologies for crystalline **5**. The first form

involves colorless rectangular plates in which **5** crystallizes in the triclinic space group $P\bar{1}$ (Figure 5). The second involves rectangular blocks that crystallize in the monoclinic space group $P2_1/n$. In the triclinic crystal system, the average Ni-N distance of 1.935(2) Å is comparable to those in the Ni(II) complexes **1** and **3** within standard deviations (Table 1). The sum of the angles in **5** for the Ni and O atoms is 360.00(6)°. The K^+ ions and the nitrogen atoms of the bis(trimethylsilyl)amido ligands in **5** are not coplanar. A planar configuration is likely unfavorable due to electrostatic and steric repulsion of the bis(trimethylsilyl)amido ligands. The average Ni···K geometrical distance for **5** in the space group $P\bar{1}$ is 3.24(5) Å and this distance is between the geometrical distance observed in the Ni(I) complexes **2** and **4**.

Spectroscopy

The solution phase ^{1}H NMR spectrum of **1** is of interest, since the chemical shifts of the resonances observed (Table 2) for **1** are remarkably similar to those given in the 2015 report for the synthesis of $Ni\{N(SiMe_3)_2\}_2$.[2] The ^{1}H NMR signal in C_7D_8 assigned to $Ni\{N(SiMe_3)_2\}_2$ appeared at 10.7 ppm,[2] while the chemical shift for $[K][Ni\{N(SiMe_3)_2\}_3]$ (**1**) in the same solvent resonated at 10.74 ppm. A signal at 0.09 ppm which was assigned to $HN(SiMe_3)_2$ is also observed for **1**, but there is no signal in the spectrum that indicated the formation of the Ni(I) decomposition product $[Ni\{N(SiMe_3)_2\}]_4$, whose ^{1}H NMR signal appears at 0.03 ppm. It was suggested[15] that the donor ligands (pmdeta, dmap, (18-crown-6), [2.2.2]cryptand) were crucial for the formation of the reported nickelates,[14,15] and that their solution phase equilibria with $Ni\{N(SiMe_3)_2\}_2$[15] can be tuned by the presence of these donor ligands, depending on the solvents and chelating agents used.

Table 2. Solution-phase ^{1}H NMR chemical shifts (ppm) at room temperature for **1**-**5** and ^{1}H NMR $SiMe_3$ resonances for known Ni(I) and Ni(II) bis(trimethylsilyl)amides.

Compound	Solvent	^{1}H NMR Chemical Shift (ppm)
$[K][Ni\{N(SiMe_3)_2\}_3]$ (**1**)[a]	C_7D_8	10.74
	C_6D_6	10.74
$[K][Ni\{N(SiMe_3)_2\}_2]$ (**2**)[a]	C_6D_6	0.77, 0.04, -0.36
$[K(THF)_2][Ni(\{N(SiMe_3)_2\}_3]$ (**3**)[a]	C_6D_6	10.70
$[K(DME)][Ni_2\{N(SiMe_3)_2\}_3]$ (**4**)[a]	C_6D_6	3.03, 2.87, 1.39, 0.98, 0.92
$[K_2][O(Ni\{N(SiMe_3)_2\}_2)_2]$ (**5**)[a]	C_6D_6	0.38
$Ni\{N(SiMe_3)_2\}_2$[2]	C_7D_8	10.70
$Ni\{N(SiMe_3)_2\}_2(THF)$[2]	C_7D_8	9.79
$Ni\{N(SiMe_3)_2\}_2(py)_2$[2]	N/A	N/A
$[Ni\{N(SiMe_3)_2\}]_4$[2]	C_6D_6	0.3
$Ni\{N(SiMe_2)_2(SiMe_2CH_2)\}(py)_2$[2]	N/A	N/A
$[Na(pmdeta)_2][Ni\{N(SiMe_3)_2\}_3]$[15]	THF-d_8	1.17
$[Li(dmap)_4][Ni\{N(SiMe_3)_2\}_3]$[14]	THF-d_8	1.18
$Ni\{N(SiMe_3)_2\}_2(dmap)_2$[14]	C_7D_8	4.24
$[Ni\{N(SiMe_3)_2\}(bipy)]$[14]	N/A	N/A
$Ni\{N(SiMe_3)_2\}_2(bipy)$[14]	THF-d_8	9.74
	C_7D_8	10.62
$[K(18\text{-crown-6})][Ni\{N(SiMe_3)_2\}_2]$[14]	THF-d_8	0.25

[a]This work

The solid-state structure of $[K][Ni\{N(SiMe_3)_2\}_3]$ (**1**) is unlikely to be completely maintained in solution as indicated by the large change in color from yellow to red upon its dissolution in hexane. Additionally, the similarity of the chemical shift of the ^{1}H NMR resonance at 10.74 ppm to that of $Ni\{N(SiMe_3)_2\}_2$, and the presence of an $HN(SiMe_3)_2$ signal at 0.09 ppm, suggests that partial dissolution has occurred with concomitant formation of $Ni\{N(SiMe_3)_2\}_2$. However, no transformation to the Ni(I) species $[Ni\{N(SiMe_3)_2\}]_4$ was observed. This is inconsistent with the conclusions in previous reports.[14,15] It also demonstrates that the formation of a nickelate species is not necessarily dependent upon the presence of donor solvents,[14,15] since none is needed to

initially form or stabilize [K][Ni{N(SiMe$_3$)$_2$}$_3$] (**1**). No signal was observed in the solution phase ^{1}H NMR spectrum of the species [Ni{N(SiMe$_3$)$_2$}]$_4$ and no black crystals were recovered from the dark, decomposed solutions of [K][Ni{N(SiMe$_3$)$_2$}$_3$] (**1**).

The ground state term symbol for a d^8 Ni(II) ion is ^{3}F$_4$.[37] In the D$_{3h}$ point group, the free ion term symbol is further split into E″, A$_1$′, and E′ levels, in order of increasing energy.[37] As such, a minimum of three absorptions are expected to be observed in the electronic spectrum. Accordingly, three maxima appear in the UV-vis spectrum of **1** at 225 nm (6,800 M^{-1}cm^{-1}), 408 nm (3,000 M^{-1}cm^{-1}), and 489 nm (2,300 M^{-1}cm^{-1}). The related Ni(II) species [K(THF)$_2$][Ni{N(SiMe$_3$)$_2$}$_3$] (**3**) displays very similar absorption maxima at 223 nm (3,400 M^{-1}cm^{-1}), 402 nm (650 M^{-1}cm^{-1}), and 487 nm (660 M^{-1}cm^{-1}). However, the extinction coefficients for **3** are significantly lower than those in **1** for all of the observable transitions. The ^{1}H NMR spectrum of **3** reflects this significantly different solution phase behavior compared to **1**, as the ^{1}H NMR signal for **3** is shifted somewhat to 10.70 ppm (Table 2). Notably, this is essentially the same as the ^{1}H NMR resonance reported for neutral Ni{N(SiMe$_3$)$_2$}$_2$.[2] The differences in the electronic spectra and ^{1}H NMR spectra of **1** and **3**, despite their common anionic [Ni{N(SiMe$_3$)$_2$}$_3$]$^-$ moieties, is likely indicative of the nearly complete dissociation in hydrocarbon solution of [K(THF)$_2$][Ni{N(SiMe$_3$)$_2$}$_3$] (**3**) to Ni{N(SiMe$_3$)$_2$}$_2$ and probably K(THF)$_2${N(SiMe$_3$)$_2$}. Unfortunately, the extinction coefficients in the electronic spectrum of Ni{N(SiMe$_3$)$_2$}$_2$ were not reported, and further study will be needed to determine the extent to which complexes **1** and **3** dissociate in solution to form Ni{N(SiMe$_3$)$_2$}$_2$. These results indicate that the reactions between the Ni(II) halides and alkali metal bis(trimethylsilyl)amides are a complex process that can result in several different products. The type of product obtained depends mainly on the Ni(II) halide used, the counter-cation of the bis(trimethylsilyl)amide

ligand, and the solvent used. In this respect, the nickel system differs drastically from the corresponding Mn(II), Fe(II), and Co(II) systems.

5.5. CONCLUSIONS

Five new nickel derivatives of -$N(SiMe_3)_2$ were synthesized via a salt metathesis of NiI_2 or $NiCl_2$(DME) and K{$N(SiMe_3)_2$} in varying stoichiometric ratios. [K][Ni{$N(SiMe_3)_2$}$_3$] (**1**) and [K][Ni{$N(SiMe_3)_2$}$_2$] (**2**) are the first Lewis base free ionic bis(trimethylsilyl)amido nickel complexes. Similarly, the complex [$K(THF)_2$][Ni{$N(SiMe_3)_2$}$_3$] (**3**) is the first to feature THF coordinating to the K+ ion rather than the Ni(II) atom. The formation of [K][Ni{$N(SiMe_3)_2$}$_2$] (**2**) and [K(DME)][Ni_2{$N(SiMe_3)_2$}$_3$] (**4**) via K{$N(SiMe_3)_2$} reduction emphasize the importance of the -$N(SiMe_3)_2$ group counter-cation used as the transfer agent in these reactions. The propensity for Ni{$N(SiMe_3)_2$}$_2$ derivatives to undergo reactions with small molecules like O_2 is realized in the formation of the complex [K_2][O(Ni{$N(SiMe_3)_2$}$_2$)$_2$] (**5**). Complex **5** is one of just 4 characterized ICE complexes for the 3d metals.

ASSOCIATED CONTENT

Supporting Information

Spectroscopic (^{1}H NMR, IR, and UV-Vis) data of **1**-**5**, crystallographic tables for **1**-**5** (PDF). CCDC Accession numbers: 2315574-2315576, 2315578-2315579.

AUTHOR INFORMATION

Corresponding Author

*Philip P. Power, Department of Chemistry, University of California, Davis, California 95616, USA. orcid.org/0000-0002-6262-3209

E-mail: pppower@ucdavis.edu

Authors

Connor P. McLoughlin, Department of Chemistry, University of California, Davis, California 95616, USA. orcid.org/0000-0002-4707-1135

Anthony J. Witt, Department of Chemistry, University of California, Davis, California 95616, USA

ACKNOWLEDGMENT

C.P.M. would like to thank James C. Fettinger for his guidance with crystallographic modeling and the U.S. National Science Foundation for funding (Grant No. CHE-2152760). C.P.M. would also like to thank Luis J. Garay and Tanner Q. Kimberly from the S.M. Kauzlarich lab at U.C. Davis for their invaluable assistance with PXRD.

DECLARATION OF INTEREST

There are no competing interests to declare.

REFERENCES

[1] Bürger, H.; Wannagat, U. Silylamido-Verbindungen von Chrom, Mangan, Nickel und Kupfer. *Monatsh. Chem.* **1964**, *95*, 1099–1102.

[2] Faust, M.; Bryan, A.M.; Mansikkamäki, A.; Vasko, P.; Olmstead, M.M.; Tuononen, H.M.; Grandjean, F.; Long, G.J.; Power, P.P. The Instability of $Ni\{N(SiMe_3)_2\}_2$: A Fifty Year Old Transition Metal Silylamide Mystery. *Angew. Chem. Int. Ed*. **2015**, *54*, 12914–12917.

[3] Andersen, R.A.; Bryan, A.M.; Faust, M.; Power, P. P. Divalent Manganese, Iron, and Cobalt Bis(trimethylsilyl)amido Derivatives and Their Tetrahydrofuran Complexes. *Inorg. Synth*. **2018**, 37, 1st edn, ch. 1, pp. 1–14.

[4] Hope, H.; Olmstead, M.M.; Murray, B.D.; Power, P.P. Syntheses and X-ray Structures of $[Li(THF)_4][Ni(NPh_2)_3]\cdot 0.5C_7H_8$, $[\{Ni(NPh_2)_2\}_2]$, and $[\{Co(NPh_2)_2\}_2]$: Structural Characterization of Three Coordinate First-Row d^7 and d^8 Complexes *J. Am. Chem. Soc*. **1985**, *107*, 712–713.

[5] Bartlett, R.A.; Chen, H.; Power, P.P. $[M(NMesBMes_2)_2]$ (M = Cr, Ni): Stable, Distorted, Two-Coordinate d^4 and d^8 Complexes**. *Angew. Chem. Int. Ed. Engl*. **1989**, *28*, 316–317.

[6] Chen, H.; Bartlett, R.A.; Olmstead, M.M.; Power, P.P.; Shoner, S.C. Series of Two-Coordinate and Quasi-Two-Coordinate Transition-Metal Complexes: Synthesis, Structural, and Spectroscopic Studies of Sterically Demanding Borylamide Ligands -$NRBR'_2$ (R = Ph, R′ = Mes, Xyl; R = R′ = Mes), Their Lithium Salts $Li(Et_2O)_2NRBR'_2$, and Their Transition-Metal Derivatives $M(NPhBMes_2)_2$ (M = Cr, Co, Ni), $Co(NPhBXyl_2)_2$, and $M(NMesBMes_2)_2$ (M = Cr→Ni). *J. Am. Chem. Soc*. **1990**, *112*, 1048–1055.

[7] Bryan, A.M.; Merrill, W.A.; Reiff, W.M.; Fettinger, J.C.; Power, P.P. Synthesis, Structural, and Magnetic Characterization of Linear and Bent Geometry Cobalt(II) and Nickel(II) Amido Complexes: Evidence of Very Large Spin−Orbit Coupling Effects in Rigorously Linear Coordinated Co^{2+}. *Inorg. Chem*. **2012**, *51*, 3366–3373.

[8] Li, J.; Song, H.; Cui, C.; Cheng, J.-P. Synthesis and Characterization of Linear and Square-Planar Nickel Complexes with Primary Amido Ligands. *Inorg. Chem*. **2008**, *47*, 3468–3470.

[9] Lipschutz, M.I.; Tilley, T.D. Synthesis and Reactivity of a Conveniently Prepared Two-Coordinate Bis(amido) Nickel(II) Complex. *Chem. Commun*. **2012**, *48*, 7146–7148.

[10] Power, P.P. Stable Two-Coordinate, Open-Shell (d^1−d^9) Transition Metal Complexes *Chem. Rev*. **2012**, *112*, 3482–3507.

[11] Lappert, M.F.; Power, P.P.; Sanger, A.R.; Srivastava, R.C. *Metal and Metalloid Amides: Syntheses, Structures, and Physical and Chemical Properties*, Ellis Horwood Limited, **1980**.

[12] Lappert, M.F.; Power, P.P.; Protchenko, A.; Seeber, A. *Metal Amide Chemistry*. John Wiley & Sons, Ltd. **2009**.

[13] Lin, C.-Y.; Power, P.P. Complexes of Ni(I): A "Rare" Oxidation State of Growing Importance. *Chem. Soc. Rev.*, **2017**, *46*, 5347-5399.

[14] Reckziegel, A.; Battistella, B.; Schmidt, A.; Werncke, C.G. Intricate Road to Linear Anionic Nickel(I) Hexamethyldisilazanide $[Ni(N(SiMe_3)_2)_2]^-$. *Inorg. Chem*. **2022**, *61*, 7794-7803.

[15] Borys, A.M.; Hevia. E. Beyond $Ni\{N(SiMe_3)_2\}_2$: Synthesis of a Stable Solvated Sodium Tris-Amido Nickelate. *Organometallics*, **2021**, *40*, 442-447.

[16] Pangborn, A.B.; Giardello, M.A.; Grubbs, R.H.; Rosen, R.K.; Timmers, F.J. Safe and Convenient Procedure for Solvent Purification. *Organometallics*, **1996**, *15*, 1518−1520.

[17] Ward, L.G.L. Anhydrous Nickel(II) Halides and their Tetrakis(ethanol) and 1,2-Dimethoxyethane Complexes. *Inorg. Synth*. **1972**, *13*, 154-164.

[18] Evans, D. F. 400. The Determination of the Paramagnetic Susceptibility of Substances in Solution by Nuclear Magnetic Resonance. *J. Chem. Soc*., **1959**, 2003−2005.

[19] Bain, G.A.; Berry, J.F. Diamagnetic Corrections and Pascal's Constants. *J. Chem. Educ*., **2008**, *85*, 532-536.

[20] Sheldrick, G.M. *SADABS, Siemens Area Detector Absorption Correction*; Göttingen Universitat: Göttingen, Germany, **2008**, 33.

[21] Blessing, R.H. An Empirical Correction for Absorption Anisotropy. *Acta Cryst. Sect. A: Found. Cryst*., **1995**, *51*, 33−38.

[22] Sheldrick, G.M. *SHELXTL*, Ver. 6.1; Bruker AXS: Madison, WI, **2002**.

[23] Dolomanov, O.V.; Bourhis, L.J.; Gildea, R.J.; Howard, J.A.K.; Puschmann, H. OLEX2: A Complete Structure Solution, Refinement and Analysis Program. *J. Appl. Crystallogr.*, **2009**, *42*, 339−341.

[24] Reckziegel, A.; Battistella, B.; Werncke, C.G. On the Synthesis of a T-Shaped Imido Nickel Complex and Trigonal Amido Nickel Complexes. *Eur. J. Inorg. Chem*. **2022**, *10*, No. e202101102.

[25] Haiduc, I. Inverse Coordination-The Janus Face of Coordination Chemistry. *Ann. Chem. Sci. Res.*, **2021**, *2*, 1-2.

[26] Haiduc, I. in *Comprehensive Coordination Chemistry III*., Elsevier, **2021**, pp. 66-120.

[27] Kennedy, A.R.; Klett, J.; Mulvey, R.E.; Newton, S.; Wright, D.S. Manganese(II)–Lithium and –Sodium Inverse Crown Ether (ICE) Complexes. *Chem. Commun.*, **2008**, *3*, 308-310.

[28] C.B. Hansen, A.S. Filatov, G.L. Hillhouse. Crystal Structure of the Inverse Crown Ether Tetrakis[μ_2-bis(trimethylsilyl)amido]-μ_4-oxido-dicobalt(II)disodium, [$Co_2Na_2\{\mu_2$-$N(SiMe_3)_2\}_4$]-(μ_4-O). *Acta Cryst.*, 2016, E72, 780–784.

[29] Forbes, G.C.; Kennedy, A.R.; Mulvey, R.E.; Rowlings, R.B.; Clegg, W.; Liddle, S.T.; Wilson, C.C. 'Inverse Crown Ether' Complexes Extended to Group 12 through the Syntheses of [$Na_2Zn_2(HMDS)_4(O)$] and [$\{K_2Zn_2(HMDS)_4(O_2)_x(O)_y\}_\infty$]. *Chem. Commun.*, **2000**, *18*, 1759-1760.

[30] Kennedy, A.R.; Mulvey, R.E.; Raston, C.L.; Roberts, B.A.; Rowlings. R.B. 'Inverse Crown Ether' Complexes: Extension to Potassium through the Synthesis of [$\{[(Me_3Si)_2N]_4K_2Mg_2(O_2)\}_\infty$], a Peroxo-Centred Macrocycle Linked into Infinite Chains by Intermolecular K···$CH_3(SiMe_2)$ Interactions. *Chem. Commun.*, **1999**, *4*, 353-354.

[31] Clark, N.M.; García-Álvarez, P.; Kennedy, A.R.; O'Hara, C.T.; Robertson, G.M. Reactions of (−)-sparteine with alkali metal HMDS complexes: conventional meets the unconventional. *Chem. Commun.*, **2009**, *39*, 5835-5837.

[32] Kennedy, A.R.; Mulvey, R.E.; Rowlings, R.B. Intermetallic Lithium−Magnesium Hexamethyldisilazide: Synthesis and Structure, Discovery of an Oxygen-Centered Variant, and a Reaction with Benzonitrile That Produces a Novel Amidinate Cage Compound with a Trigonal Bipyramidal Li_4MgO Core. *J. Am. Chem. Soc*. **1998**, *120*, 7816-7824.

[33] Kennedy, A.R.; Mulvey, R.E.; Rowlings, R.B. Remarkable Reaction of Hetero-S-Block-Metal Amides with Molecular Oxygen: Cationic $(NMNMg)_2$ Ring Products (M=Li or Na) with Anionic Oxo or Peroxo Cores. *Angew. Chem. Int. Ed*. **1998**, *37*, 3180-3183.

[34] Wu, J.; Pan, X.; Tang, N.; Lin, C.-C. Bulky Bisphenol Ligand-Supported Aluminum−Sodium Inverse Crown Ether Complex. *Inorg. Chem.*, **2010**, *49*, 5362-5364.

[35] Lu, X.-H.; Ma, M.-T.; Yao, Y.-M.; Zhang, Y.; Shen, Q. Controlled Synthesis of Lanthanide–Lithium Inverse Crown Ether Complexes. *Inorg. Chem. Commun.* **2010**, *13*, 1566-1568.

[36] Kahn, O. *Molecular Magnetism.* VCH Publishers, **1993**, p. 10.

[37] Figgis, B.N.; Hitchman, M.A. *Ligand Field Theory and Its Applications*. Wiley-VCH, **2000**.